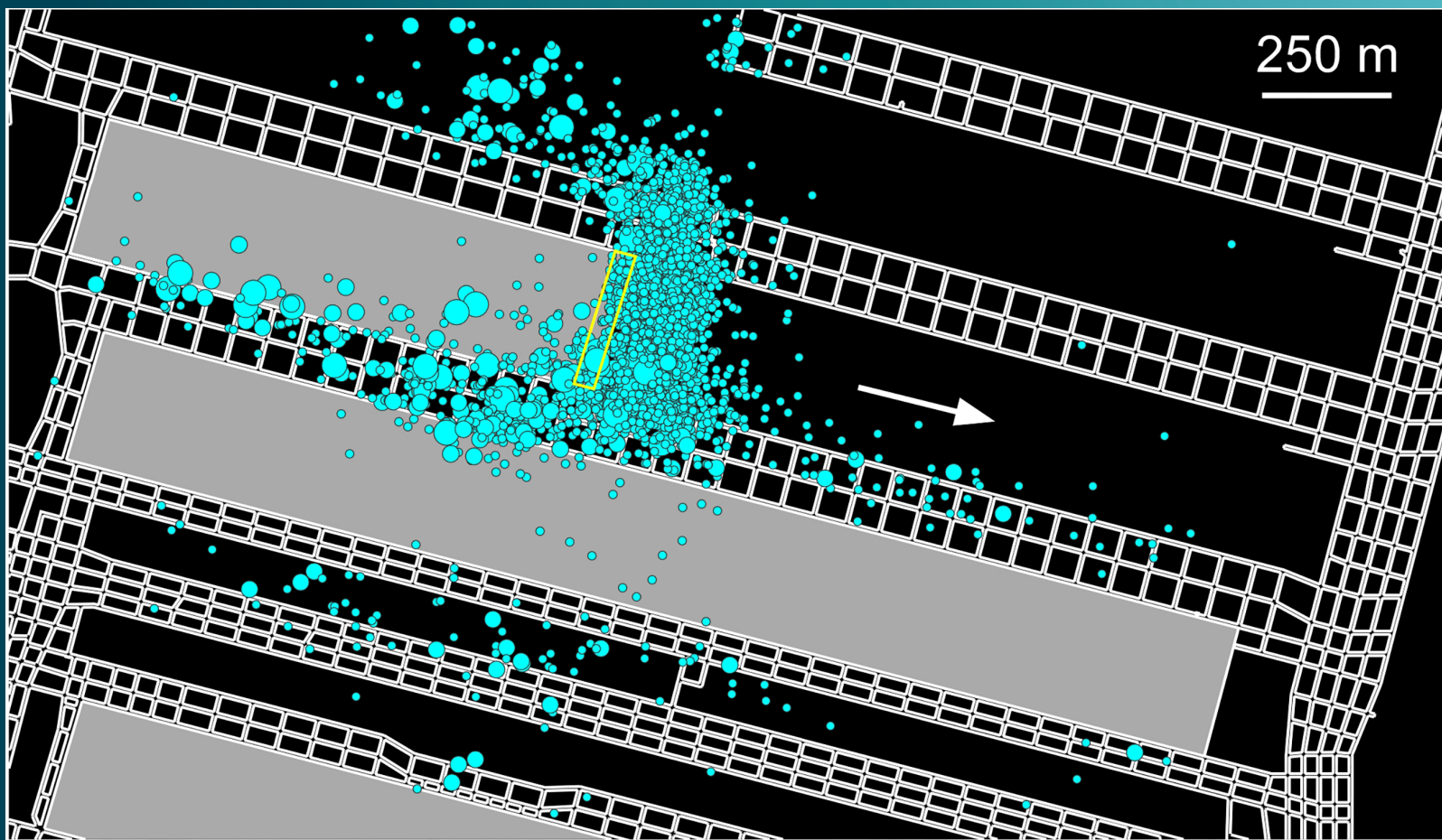


Seismic Monitoring Strategies for Deep Longwall Coal Mines



Report of Investigations 9700

Seismic Monitoring Strategies for Deep Longwall Coal Mines

Peter Swanson, M. Shawn Boltz, and Derrick Chambers

DEPARTMENT OF HEALTH AND HUMAN SERVICES
Centers for Disease Control and Prevention
National Institute for Occupational Safety and Health
Office of Mine Safety and Health Research
Pittsburgh, PA • Spokane, WA

October 2016

This document is in the public domain and may be freely copied or reprinted.

Disclaimer

Mention of any company or product does not constitute endorsement by the National Institute for Occupational Safety and Health (NIOSH). In addition, citations to Web sites external to NIOSH do not constitute NIOSH endorsement of the sponsoring organizations or their programs or products. Furthermore, NIOSH is not responsible for the content of these Web sites. All Web addresses referenced in this document were accessible as of the publication date.

Ordering Information

To receive NIOSH documents or more information about occupational safety and health topics, please contact NIOSH:

Telephone: **1-800-CDC-INFO** (1-800-232-4636)

TTY: 1-888-232-6348

CDC INFO: **www.cdc.gov/info**

or visit the NIOSH Web site at **www.cdc.gov/niosh**.

For a monthly update on news at NIOSH, subscribe to *NIOSH eNews* by visiting **www.cdc.gov/niosh/eNews**.

Suggested Citation

NIOSH [2016]. Seismic monitoring strategies for deep longwall coal mines. By Swanson P, Boltz MS, and Chambers D. Spokane WA: U.S. Department of Health and Human Services, Centers for Disease Control and Prevention, National Institute for Occupational Safety and Health, DHHS (NIOSH) Publication No. 2017-102, RI 9700.

DHHS (NIOSH) Publication No. 2017-102

October 2016

Cover photo by NIOSH.

Contents

Abstract.....	1
Introduction	2
Background.....	2
Evolution of Technology in Hardrock Mines.....	3
Bump Hazard in Coal Mines.....	3
Seismic Monitoring Objectives	4
Need for Documentation	5
Ground Vibration Measurements.....	6
Rockburst Risk Management	7
Experience in Coal Mine Seismic Monitoring	8
Seismic Monitoring in the United States	8
Examples of International Seismic Monitoring	9
Challenges of Adapting Monitoring Technology in Deep Coal Mines.....	10
Rapid Excavation of Large Longwall Panels.....	10
Accessibility	12
Permissibility and Intrinsic Safety	13
Wave Propagation Medium Effects	13
Seismic Source Characteristics from Waveform Measurements	14
Characteristics of Different Seismic Monitoring Systems.....	17
Five Seismic Monitoring Strategies for Deep Coal	18
Single-station Option.....	18
Regional Seismic Network Augmentation Option	29
Temporary Network Deployment Option	33
District- and Mine-wide Networks Option.....	37
Microseismic Monitoring Network Option	46
Discussion	53
Factors Guiding Strategy Selection	53
Pre-installation Estimates of Event Location Accuracy	54
Effects of Heterogeneous Velocity Structure	55
Hazard Assessment and Risk Management for Rockbursts	56
Implementation	57
Conclusion	58
Acknowledgments.....	59
References	59

Appendix A: Wave Propagation Medium Effects	67
Layer-specific Properties.....	67
Waveform Character	69
Velocity-model Development.....	70
Appendix B: Seismic Source Characteristics Derived from Waveform Measurements	75
Waveform Measurements	75
Appendix C: Single-Station Monitoring Implementation Options.....	79
Appendix D: Station Corrections and Multi-event Location Techniques.....	81
Travel-time Station Corrections	81
Multi-event Location Techniques.....	82
Glossary of Seismic Terms	85

Figures

Figure 1. Spatial domains of seismic monitoring	5
Figure 2. Large longwall panel size and high excavation rate provide a challenge to maintaining high-density seismic monitoring network	12
Figure 3. Large angular coverage gaps in longwall coal mines due to inaccessible gob areas..	13
Figure 4. Relationships between magnitude, seismic moment, corner frequency, and rupture dimension. Plotted data are from the studies listed below the graph	16
Figure 5. Frequency range of six different types of seismic monitoring systems.....	18
Figure 6. Helicorder-style plot of 12 hours duration from a 1-Hz short-period vertical seismometer	19
Figure 7. Unfiltered (A) and low-pass filtered (B) helicorder records near active longwall.....	20
Figure 8. Multiseam extraction helicorder record showing large-magnitude seismic events	20
Figure 9. Seismic body-wave particle motions.....	21
Figure 10. Two sets of three-component seismograms with P and S arrivals.....	22
Figure 11. Increasing S-P times with propagation distance	23
Figure 12. Observed S-P times exhibit discrete values (A, B, C).....	24
Figure 13. Comparison between range estimates based on S-P times and longwall locations..	24
Figure 14. Seismograms from north- and east-oriented components (red and blue traces in first two panels) used to construct a hodogram plot (third panel) illustrating P-wave polarization for back-azimuth measurements	25
Figure 15. Map showing outline of a longwall coal mine with a single-station location based on range and back-azimuth measurements	27
Figure 16. Comparison of single-station location estimates from multiple stations	28
Figure 17. Multiple range estimates based on S-P times constrains possible event locations ...	28
Figure 18. Seismic stations of the Nation's backbone network	30
Figure 19. Locations of active U.S. underground coal mines.....	31
Figure 20. Seismic stations currently operating in the eastern and central United States	32
Figure 21. Temporary exploration seismic array (magenta lines on left panel) captures diverse seismic response at two mine sites (right panel).....	35
Figure 22. Temporary array of surface geophones tracks seismic response of longwall shearer motion.....	36
Figure 23. Seismic activity recorded during temporary deployment of broadband stations (red triangles) above active longwall	37
Figure 24. Seismic stations of the North Fork Valley district network (triangle symbols).....	38
Figure 25. Seismometer, remote power, and telemetry infrastructure of a typical district-wide network station.....	39
Figure 26. Software-automated event locations from district-wide network over 60-day period.....	41

Figure 27. Seismic response to progressive failure. (A) number of events per day with $M \geq 1$, (B) helicorder plot from day with four events with $M \geq 2$, (C) cumulative number of events during progressive failure, (D) map view of manually processed event locations	43
Figure 28. Map showing a five-panel longwall section traversed by several steeply dipping faults (blue lines).....	44
Figure 29. Cumulative number of seismic events with $M \geq 1.0$ during a 5-panel extraction sequence, showing a significant increase in activity during mining of the fifth panel.....	45
Figure 30. Seismic event locations during mining of fifth panel in 5-panel sequence.....	45
Figure 31. Surface and underground geophone stations of microseismic array covering one or more adjacent longwall panels	46
Figure 32. Surface station of microseismic network, showing: (a) triaxial surface geophone prior to burial and (b) station infrastructure platform	47
Figure 33. Seven days of seismic activity (red circles) located by the microseismic network during 42 m (137 ft) of longwall retreat (yellow rectangle). Completed longwall panels are shaded gray and unmined panels are white	49
Figure 34. Large magnitude events during 42 m (137 ft) of longwall retreat ($0 \leq M < 1.5$, blue; $1.5 \leq M \leq 2.7$, yellow)	50
Figure 35. Microseismic activity observed during 30-day period of no mining	50
Figure 36. Number of seismic events detected during each hour of the day during a 30-day period with longwall production on both day and swing shifts. Peak activity occurs between 9 and 10 p.m. (hours 21 and 22)	51
Figure 37. Seismic activity per day detected by microseismic-scale (panel-scale) and district-wide networks and daily longwall retreat distances.....	52
Figure A1. Snell's law governing seismic wave refraction in layered media.....	67
Figure A2. Reflection at layer boundaries controlled by acoustic impedance	68
Figure A3. Conversion of incident P-wave into reflected P- and S-waves in the upper layer and refracted P- and S-waves in the lower layer	68
Figure A4. Effect of propagation path on waveform character as observed at ten seismic stations at increasing distance	69
Figure A5. Two sets of three-component seismograms (vertical Z, north N, and east E) recorded on a common station comparing signals generated from a mining-induced event (top) and a natural earthquake (bottom)	70
Figure A6. Sonic log in strata above the coal seam with model velocity values and layer thicknesses assigned to individual layers (red horizontal bars)	71
Figure A7. Comparison of velocity structures in two nearby boreholes.....	72
Figure A8. Variation of P-wave velocity with overburden.....	73
Figure A9. Shift in calculated event locations when seismic velocity model fails to match actual velocity. Frame A shows raypath lengths calculated for an unmined coal panel with known seismic velocity. Frame B shows the effect of a modest 10% reduction in seismic velocity. Frame C shows the resultant change of the calculated event location where travel-time observations from both sensors can be satisfied simultaneously	74
Figure B1. Theoretical displacement amplitude spectrum (graph on left) for shear slip on circular crack (illustration on right).....	75

Figure D1. Velocity model errors partially compensated by travel-time station correction factors. Raypaths from mine B are affected by topographic features unaccounted for in the velocity model	81
Figure D2. Raypaths between stations (red triangles) and event clusters (black dots) affect suitability of double-difference location scheme. (a) suitable array configuration, (b) unsuitable array configuration	83

Tables

Table 1. Back azimuths and predicted back azimuths from particle motion analysis for temporary deployment.....	26
Table 2. Distances between underground coal mines and existing seismic stations.....	33
Table 3. Seismic monitoring objectives matched to monitoring strategies.....	53
Table 4. Minimum sensor densities for different scale networks.....	54
Table 5. Velocity model requirements for specific monitoring objectives.....	55
Table 6. Levels of complexity, staff time, and expense for different seismic monitoring strategies.....	58
Table B1. Relations between seismic magnitude, moment, radiated energy, rupture dimension, and potential energy equivalent.....	78

Acronyms and Abbreviations

ANSS	Advanced National Seismic System
CDC	Centers for Disease Control and Prevention
CISN	California Integrated Seismic Network
CMI	Central Mining Institute
DOE	Department of Energy
EI	energy index
GPS	global positioning system
IP	Internet protocol
M	Magnitude
MSHA	Mine Safety and Health Administration
NAP	National Academies Press
NIOSH	National Institute for Occupational Safety and Health
NRC	National Research Council
NSF	National Science Foundation
PC	personal computer
PC-SUDS	Personal Computer Seismic Unified Data Structures
PSN	public seismic network
P-wave	compressional wave
SHA	short-term hazard assessment
S-wave	shear wave
S-P	S-wave minus P-wave
USBM	United States Bureau of Mines
USGS	United States Geological Survey
UUSS	University of Utah Seismic Stations

Unit of Measure Abbreviations

cm	centimeter
deg	degree
ft	foot
GJ	gigajoule
Hz	hertz
J	joule
kg	kilogram
kg/m ³	kilogram/cubic meter
kHz	kilohertz
kJ	kilojoule
km	kilometer
km ²	square kilometer
km/s	kilometers/second
m	meter
m ²	square meter
m ³	cubic meter
m/s	meters/second
mi	mile
mi ²	square mile
min	minute
MHz	megahertz
MJ	megajoule
μm	micrometer
mm	millimeter
MPa	megapascal
N	newton
Nm	newton-meter
%	percent
s	second
TJ	terajoule

Seismic Monitoring Strategies for Deep Longwall Coal Mines

Peter Swanson¹, M. Shawn Boltz², and Derrick Chambers³

Abstract

This report presents five strategies for detecting and recording seismic activity associated with deep longwall coal mining:

1. Single-station monitoring
2. Augmentation of an existing regional seismic network
3. Temporary network deployment
4. Implementation of a mine-wide or district-wide network
5. Installation of a dense microseismic network

These strategies take into consideration: (1) the variety of potential objectives for seismic monitoring, (2) the notable contrast of coal mining environments with conditions in hardrock mines, where these techniques were originally developed, (3) the enormous range in magnitude and physical size of seismic events, and (4) the significant variation in expense and complexity of the different approaches. The strategies range from simple and inexpensive methods that can be implemented on the surface by a mining engineer to complex and expensive endeavors requiring involvement by underground mine personnel and monitoring-system suppliers. This report provides example monitoring results from deep longwall coal mines, and describes the capabilities and limitations of each of the five suggested approaches.

¹ Geophysicist, Mine Stability Ground Control, NIOSH Spokane Mining Research Division (SMRD), Spokane, WA.

² Mining Engineer, Mine Stability Ground Control, NIOSH SMRD, Spokane, WA.

³ Mining Engineer, Mine Stability Ground Control, NIOSH SMRD, Spokane, WA.

Introduction

Background

Following the Crandall Canyon Mine (Utah) collapse in 2007 with nine fatalities [Gates et al. 2008], questions were raised about the potential benefits of applying seismic/microseismic monitoring technology to improve mine safety in deep underground coal mines, where deep is defined as several hundred meters or more of overburden. The underground mining industry's widespread use of seismic monitoring in deep rockburst-prone hardrock mines [Durrheim et al. 2007] indicates that it has been beneficial in these applications, suggesting that it may also prove useful in addressing the problem of coal bumps (also known as coal bursts or rockbursts) and other large-scale ground instabilities such as mine collapse. A total of 13 workers in U.S. coal mines were killed by such ground failures in the ten-year period 2006–2015.

Prompted by Crandall Canyon and other earlier coal mine accidents, Congress directed the National Institute for Occupational Safety and Health (NIOSH) to conduct studies related to the safety implications of retreat room-and-pillar mining practices in underground coal mines at depths greater than 1,500 feet (450 m). In its report to Congress [NIOSH 2010], NIOSH recommended “further seismic monitoring research be conducted at demonstration sites where the technology and interpretation techniques can be tested and refined to advance the state of practice of seismic monitoring for hazard assessment in deep underground coal mines.” The work presented in this report represents part of that effort.

As part of a NIOSH contract, the University of Utah convened an international panel of mine seismicity experts in 2008 to evaluate the potential benefits of seismic monitoring in U.S. coal mines. The purpose of the panel was to assess the current state of seismic monitoring in U.S. coal mines and to evaluate the costs and practical benefits of seismic monitoring at various magnitude scales. The panel reported on ways that routine mine seismic monitoring is being used internationally, particularly in hardrock mines in South Africa, Canada, and Australia, but also in coal mines in Germany, Poland, and China [Arabasz and McCarter 2009]. The panel concluded that seismic monitoring is one of the few techniques able to provide a three-dimensional assessment of strata conditions surrounding mining excavations. To be useful, the panel suggested, seismic monitoring needs to be integrated with geotechnical observations and modeling. The capabilities of a seismic system must enable the system to locate seismic events to within at least a few tens of meters, allowing the system to associate the seismic events with identifiable geological or mining features. A seismic system should also have the sensitivity to detect small events, as these can reveal the seismic character of the ground reaction to excavation before the mine encounters more serious problems.

Deploying and operating a seismic network capable of locating events to the accuracy recommended by the panel, however, requires a significant investment of resources and labor. Also, seismic monitoring in coal mines is more difficult than monitoring in hardrock mines because of the larger scale of mines, much faster rate of mining, and highly variable properties of sedimentary layering. For these reasons, seismic systems that meet the panel's requirements are rarely implemented in coal mines. For example, in the decade before the international panel convened, there was only one instance of a temporary in-mine system with the resolution to meet these objectives in an underground U.S. coal mine [Ellenberger et al. 2001]. While we acknowledge the need for high accuracy of event locations in order to integrate seismic

monitoring into geotechnical modeling, we also present methods that allow less accurate, more cost-effective monitoring systems to satisfy other objectives.

Evolution of Technology in Hardrock Mines

The evaluation conducted by NIOSH's international mine seismicity expert panel leaned heavily on experience from the application of seismic monitoring to deep hardrock mines, where monitoring has evolved to a much higher level of operational practice than in other types of mines. South African mines have led this effort with a 120-year historical progression of the development and application of seismic monitoring in ground control practices in the Witwatersrand Basin gold mines [Riemer and Durrheim 2011]. A brief history of seismic monitoring in South African mines is provided here to underscore the vast difference in the application of seismic monitoring in U.S. coal mines compared to that in deep hardrock mines.

Seismic events associated with mining in South Africa were recognized as far back as 1908 from recordings made on a single, standalone seismometer. Complete synchronized seismic networks, deployed on the surface but specifically focused on rockburst areas of mining, were first described in 1939, followed by underground networks in the 1960s, and real-time digital systems starting in the 1970s. In the 1970s, mining companies began using seismic systems, which were primarily developed for research, as management tools to assist in rescue operations and safety procedures following rockbursts. With the anticipation that rockbursts may possibly be predicted, real-time monitoring systems were introduced on a mine-wide basis. By the early 1990s, digital monitoring was considered the standard; mines started hiring their own seismologists, and monitoring networks ultimately became fully owned by the mining companies [Durrheim 2010]. There are now a total of 25 systems in the Witwatersrand gold mines that encompass about 430 underground sensor sites, and they are estimated to locate approximately 125,000 events each month. A similar widespread deployment of commercial systems is in place in deep hardrock mines in Canada and Australia, along with deployments in the rockburst-prone hardrock mines in the United States, where the first mine-owned digital system supplied by a commercial vendor was installed in 2002 [Dehn and Knoll 2013]. By the year 2000, research and monitoring efforts moved away from prediction and more toward hazard assessment and risk management. Recognizing that high-quality data are needed for these applications and that maintenance of a mine-wide seismic network poses significant challenges, many mining companies are now choosing to outsource some or all of their monitoring operations [Durrheim et al. 2007].

Bump Hazard in Coal Mines

One important question associated with seismic monitoring in coal mines is whether the approach taken in applying seismic monitoring to burst-prone hardrock mines is the same approach that should be taken for bump-prone deep coal mines. Only a few mining regions of the United States have the necessary conditions for coal bursting, and of those mines experiencing bumps, there are often long periods of mining where bumping is not a problem. A useful strategy for mitigating bumps is to minimize exposure, where possible, by avoiding areas where the conditions for coal bumping are prevalent. For example, high stresses produced by thick overburden cover are one of the prime ingredients for bumps [Iannacchione and Zelanko 1995], and, in many coal mines, exposure to such areas can be avoided or minimized. In deep hardrock

mining there is not as much flexibility to mine in alternate areas; the deep cover and strong host rocks are typically omnipresent.

Because the coal bump hazard is not pervasive, there has not been an industry-wide imperative to engage in an aggressive campaign to develop and apply technology to manage coal bumps as has been the case in deep metal mining districts. The potential benefits of applying seismic monitoring to ground control issues in coal will only come about through wider demonstration trials and research showing its value in mitigating hazards; this is the path taken in the hardrock mines (e.g. [Riemer and Durrheim 2011]). Additionally, seismic monitoring is just one tool of many that can be used in addressing geostructural challenges.

As the bump hazard is not uniformly distributed throughout a coal mine property, and the value of the monitoring in terms of mitigating hazards has not been amply demonstrated (in coal), it is impractical to deploy a dense microseismic network, of the kind used in hardrock, to cover the entire mine. With the variability in the coal bump hazard, and the diversity of possible objectives for seismic monitoring, including those that go beyond the narrow coal bursting issue, it is recognized that no single monitoring system is suitable for satisfying all requirements. In this report, five strategic approaches to seismic monitoring are presented which, with a variety of implementation options, can be tailored to specific objectives. These five strategies, which encompass a wide range of cost and complexity, provide flexibility in using seismic monitoring to better understand and address ground control problems in coal mines.

First, potential objectives for seismic monitoring in coal mines are described. Then, a review of coal mine seismic monitoring applications, used for research in the United States and for industry use in international mines, is presented. Challenges to adapting seismic-monitoring technology from hardrock to deep longwall coal are then described, followed by a brief review of quantitative measures of seismic source parameters, which place constraints on monitoring systems' hardware specifications. Descriptions and applications of the five strategies are then presented. This report aims to identify flexible options to achieve a monitoring objective while minimizing cost and complexity.

Seismic Monitoring Objectives

Seismic monitoring allows for the detection, location, and estimation of the strength, or size, of dynamic ground movements from remote measurements. Potential objectives for seismic monitoring are varied and can entail measurement of “seismic events” with magnitudes (M) of zero (0) and above, and/or “microseismic events” with $M < 0$ (later in this report, the concept of magnitude and the various magnitude scales are discussed in more detail). Unless otherwise noted, the term “seismic” is used to describe both seismic and microseismic⁴ events and monitoring systems. One of the most basic objectives of monitoring is to provide an awareness of the dynamic rock mass response to mining. A certain amount of seismic activity is expected

⁴ The term “microseismic” is used throughout the document to refer to small-scale seismic events. It is not to be confused with the term “microseism” which, in conventional earthquake seismology literature, refers to small amplitude ambient seismic noise generated largely by wave action in the oceans.

with some types of mining, such as longwalling under strata with at least modest competence. In such mining conditions, where seismicity is extremely common and rarely problematic, seismic monitoring may not provide any safety benefit. Pillar and strata deformation processes associated with subsidence produce seismic activity and its presence can, in part, be taken as a sign that the mine design is working as intended. Thus, the presence of seismic activity is not evidence of the need to develop a monitoring program; seismic activity occurs at all mining operations to some extent. If unusual conditions are experienced or anticipated, however, seismic monitoring can be used to obtain useful information on rock-mass response.

An overview of the different spatial domains for the monitoring objectives discussed in this report is given in Figure 1. Areas of concern vary from regions outside of a mining district down to specific areas in an individual mine. Potential objectives range from providing simple awareness to more quantitative rockburst hazard assessments.

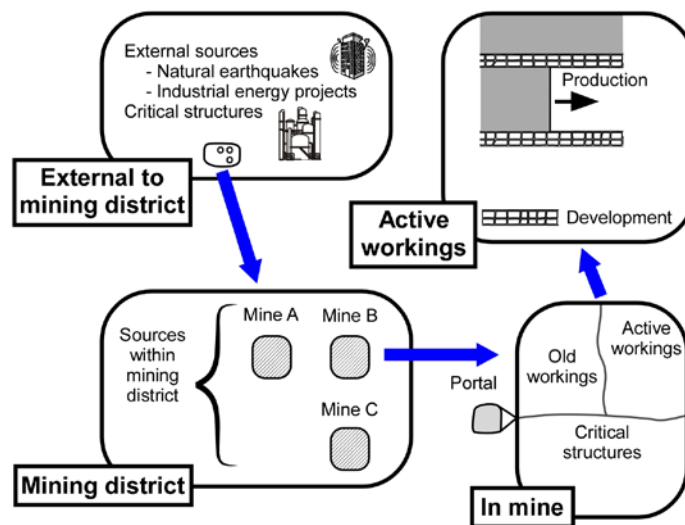


Figure 1. Spatial domains of seismic monitoring.

Need for Documentation

External and Mining-district Activity Sources

Responsibility for documenting seismic activity on the national scale falls to the U.S. Geological Survey (USGS). The earthquake location resolution across much of the United States, outside of areas of major earthquake hazard, is the smallest locatable event of magnitude 3 and location uncertainties of 10 km (6.2 mi) horizontally and 10 km (6.2 mi) in depth [ANSS 2014]. As a result of this large uncertainty, an event's possible location could include multiple mining operations as well as sources of tectonic earthquakes [Swanson et al. 2008]. As discussed in the Regional Seismic Network Augmentation Option section of this report, most coal mine monitoring objectives cannot be achieved with the Advanced National Seismic System (ANSS) network.

A basic objective for documentation purposes would be to discriminate between seismic activities induced by mining activities at different closely spaced mines. Another is to characterize nonmining related seismic activity. The presence of unusual levels of in situ stress,

derived from tectonic or gravitational forces, can have a major impact on ground control [Mark and Gadde 2008], and a determination of the background level of local seismicity may aid in assessing regional stresses for mine design evaluations.

Activity along major geologic structures is of special concern as the largest seismic events associated with mining are reported to be triggered along fault systems [Gibowicz and Kijko 1994]. A distinction is made between seismic events that are induced and triggered [e.g., McGarr et al. 2002]. “Induced” events result from human activities that contribute most of the local stress involved in a rock mass failure. Induced events typically occur in the immediate vicinity of the active workings and show a strong relationship to the mining cycle. “Triggered” events result from much smaller incremental changes in the stress state on natural earth structures (i.e. pre-existing faults) that were already close to failure. Triggered events are reported to be less dependent on the daily mining cycles and occur after large expanses of ground have been excavated. The extraction causes small changes in stress to pre-existing faults, at some distance from the current workings, which triggers dynamic slip. Documentation of activity near faults is an important objective prior to, and during, mining in the vicinity of such structures.

Another source of seismic activity that is becoming more commonplace in a number of coal mining states is that introduced by industrial/civil projects, such as deep borehole liquid waste injections [NRC 2012]. Such projects have created a tremendous interest in, and scrutiny of, seismic activity attending their operation. As a result, it may be important for some mines to distinguish between seismic events generated by oil and gas hydraulic fracturing operations and those induced by mining.

For all of these reasons, it may be desirable to provide documentation of seismic activity in the vicinity of mining operations with higher spatial resolution and magnitude sensitivity than that available through the USGS.

Internal Activity Sources

Another possible monitoring objective is to document seismic activity within a mine. Mines are designed with standup times (the length of time before ground failure is expected to begin) that are considerably shorter than most civil structures [e.g., Brady and Brown 1985]; degradation of old mine workings may gradually occur while mining takes place in virgin ground. Mature longwall coal mines result in large areas of old workings that slowly succumb to the effect of gravity, often producing seismic events long after mining has progressed to other areas. Seismic monitoring can be used to identify events in older areas and to detect and track any unusual degradation in active workings or other critical areas of the mine.

Ground Vibration Measurements

Measurement of ground vibration levels is another possible objective for mines generating large magnitude seismic events. There may be critical mine structures such as portals, steep slopes, waste impoundment ponds, etc., or resources in the community that could be negatively affected by excessive levels of ground vibration associated with mining-induced seismic activity. Recordings of blast vibration levels, long recognized as essential in the surface mining and construction communities [e.g., Siskind 1983], provide quantitative measurements to address these issues.

Rockburst Risk Management

Monitoring objectives directly related to reducing the impact of rockbursts have been established through decades of seismic monitoring in hardrock mines [e. g., Mendecki et al. 1999; Durrheim et al. 2007], and could be extended to coal mining. These objectives are described in the following subsections:

Rescue Response

A real-time online monitoring system alerts mine management of the occurrence of potentially damaging events. Locating these events within the mine enables rapid response by rescue personnel and/or mine staff seeking to quickly evaluate safety of mine personnel and the degree of damage to mine infrastructure with attendant hazards. Subsequent monitoring allows real-time stability evaluation in areas of concern and indicates when activity has returned to normal levels.

Post-event Analysis of Large and/or Damaging Seismic Events

Careful analyses of the mechanics behind and conditions leading up to large and/or damaging seismic events can help identify causative factors so that mitigation and preventative measures can be developed and implemented.

Evaluation and Verification of Mine Design Performance

Mine designs are based upon an expectation of how the rock mass should behave during the mining process. Seismic event data provide first-order information on the seismic rock mass response. Comparison of observations with expectations offers the opportunity to verify that the response is consistent with the design and to implement design changes in response to unexpected behavior. The effectiveness of adjustments in the design, or mitigation measures, can be evaluated in a similar manner.

Hazard Assessment (following [Durrheim et al. 2007])

Seismic monitoring data is used for hazard assessment over various time scales, including:

- **Long-term (months to years).** Seismicity data collected over long periods of time allows hazardous mine and geologic structures to be recognized and mitigated through long-term mine planning efforts, such as minimizing exposure to the problematic structures.
- **Medium-term (weeks to months).** Monthly seismic hazard assessments provide input to mine planning procedures and are based on quantitative seismicity measures such as spatial and temporal event distributions, seismic moments and energies, and derived parameters related to dynamic stresses and strains. These parameters are monitored to detect changes in seismic hazard associated with mining geometry, rate of mining, and geologic structures.
- **Short-term (days to weeks).** Analysis of various seismic parameters in relation to mining activity, such as face advance, can help to relate short-term changes in the parameters to emerging hazards.

A quantitative description of seismic events and seismicity is considered necessary, but not sufficient, to achieving the above rockburst hazard assessment and risk management objectives [Mendecki et al. 1999].

Experience in Coal Mine Seismic Monitoring

Seismic Monitoring in the United States

Early research applications of microseismic monitoring in U.S. underground coal mines focused on coal bumps and roof falls [Leighton and Steblay 1977]. In the late 1980s and early 1990s, the U.S. Bureau of Mines (USBM) was engaged in studies directed at coal mine bump prediction using small-scale arrays that followed the longwall face [e.g. Rowell 1989; Rowell and Lemons 1991; Wilson and Lemons 1992]. Attempts to directly apply hardware-automated microseismic techniques, which were developed for hardrock environments, were not entirely successful due to much lower signal frequencies and signal-to-noise ratios found in coal mines [Rowell 1989]. These differences were attributed to wave propagation effects, including greater attenuation and much larger propagation distances for events that were, on average, larger in magnitude than in the hardrock mines. Subsequent automation of the processing relied on picking P-wave arrivals, or the first arriving seismic energy, in software.

In face-centered networks, such as those in the early USBM work, geophones were placed in the gateroads on each side of a longwall face, and analog signals were transmitted via long cables to a central data acquisition and processing site in the main entries. The USBM was granted an experimental permit by the Mine Safety and Health Administration (MSHA) that allowed these sensors and preamplifiers to be operated in potentially explosive coal mine environments. Sensors were moved with the face as it retreated. This resulted in a two-dimensional coverage area in the seam ahead of the face with little to no constraint outside this immediate area. A homogeneous isotropic velocity model was used to calculate seismic event source locations in the plane of the seam. Throughout most of this work, a full-time geophysical engineer was stationed by the USBM at the mine sites to install, maintain, and operate the networks. Closure of the USBM in 1996 resulted in the loss of the staff and equipment that provided this capability for both coal and hardrock environments.

In the late 1990s, NIOSH development work focused on using the PC as a data acquisition and processing platform, making use of public domain PC-SUDS-based modular software [Swanson 2001]. A PC-networked adaptation of this method was developed and applied in a study of the mechanical deformation behavior of the overburden above a deep bump-prone longwall coal mine [Ellenberger et al. 2001]. Independent surface and underground networks using 4.5-Hz geophones were synchronized and, in both networks, long cables were used to transmit analog signals back to analog-to-digital converters.

NIOSH developed a simple, layered velocity model to locate events in the initial stages of mining prior to extensive gob and cave development. By the time a large fraction of the first panel had been developed, a shift in calculated event locations with respect to the panel outline was observed, indicating systematic location errors [Ellenberger et al. 2001]. Attempts to deal with the deviation of the velocity structure from the idealized model involved the implementation of “station corrections,” which added or subtracted a fixed travel-time delay or advance to arrival times at each station.

In a joint project between NIOSH and several deep western underground coal mines [Swanson et al. 2008], a surface seismic network was implemented to provide district-wide coverage and is covered later in the District- and Mine-wide Networks Option section in this document.

The University of Utah Seismograph Stations (UUSS) has studied seismicity associated with the underground coal mines of Utah because of their proximity to the UUSS regional seismic network. In operation since 1962, the 200+ station network houses 22 sites in the vicinity of the coal mining districts and provides the densest regional seismic coverage of any coal mining area in the United States. Such coverage allows smaller-magnitude events to be detected and then located more often than in most of the United States, other than in the major earthquake hazard areas. Arabasz et al. [1997] conducted an analysis of the UUSS catalog and determined that all events greater than or equal to magnitude 1.8 have been detected in the Utah coal mining districts since 1978. This threshold is considerably less than the magnitude 3 target established for minimum detection level across the U.S. [ANSS 2014].

The UUSS conducted detailed examinations of event locations, magnitude statistics, source mechanisms, and acceleration levels at coal mines in Utah, using data collected from temporary local surface networks. These included surface deployments surrounding multiple mines in the Eastern Wasatch Plateau in 1984 [Williams and Arabasz 1989; Wong et al. 1989], a 12-station network distributed above the Trail Mountain Mine (and one underground station) within a 6-km radius [Arabasz et al. 2005; Fletcher and McGarr 2005; Boltz et al. 2014], and an augmentation of the UUSS regional network with temporary stations deployed in the vicinity of the Crandall Canyon Mine [Pechmann et al. 2008; Kubacki et al. 2014].

There has also been limited microseismic monitoring conducted by the U.S. mining industry. An eastern U.S. coal mine has recently reported the operation of a 5–6 station surface network above deep cover longwall panels [Su et al. 2014]. Seismic data were used to provide feedback on mine design changes following the occurrence of several large seismic events. The stations covered 5 to 8 panels at a time and were moved with the panels as they were excavated. Mine design changes, including changing the panel width from 305 to 210 m (1,000 to 700 ft), were reported to have resulted in the reduction of one order of seismic magnitude for the largest events experienced in the narrower panels.

Examples of International Seismic Monitoring

Seismicity is currently being monitored at underground coal mines in Germany by 60 seismic stations [Fritschen 2015]. The stations are grouped into local networks surrounding two active underground coal mines, two abandoned coal mines, and one recently closed mine currently undergoing flooding. Sensors are three-component 4.5-Hz geophones sampled at 500 samples per second. All but one are installed on the surface. German coal mines are deep (~700 to 1,500 m, 2,300 to 4,900 ft), and longwall faces are preconditioned to reduce burst potential [Baltz and Hucke 2008]. While seismic monitoring was first developed in response to coal bursting activity, in more recent times emphasis is on large seismic events that produce vibrations which impact the dense population centers in the vicinity of the mines. Hardware, software, system operation, and data analysis are handled by a private company [Fritschen 2015].

Over the last 30 years, one of the German coal mining districts, the Ruhrgebiet, has been routinely monitored with a regional seismic network operated by Ruhr-University Bochum. Recent studies have made use of its short-period and broadband stations to investigate magnitude statistics (b-values), relationships to mining, and source mechanisms of longwall coal mining events, and the 4.5-Hz geophone station network has been used to establish empirical ground

motion relations [Bischoff et al. 2010a]. A temporary one-year deployment of 15 surface sensors above one of the Ruhr coal mines [Bischoff et al. 2010b] provided a data set used by Sen et al. [2013] to calculate full moment tensors using a software-automated process.

There are approximately 20 underground coal mines in Poland that monitor seismicity using in-mine systems developed at the Central Mining Institute (CMI) [Lurka 2015]. Mines are responsible for reporting events with energy of 10^5 joules and higher. As larger events often clip signals from the underground sensors, CMI operates the Upper Silesian Coal Basin regional seismic network, consisting of both conventional 1-Hz short period and broadband triaxial sensors, to provide independent confirmation of event energy. Of the ~20 underground sensors at a mine, two are placed on each gateroad ahead of the face, and are moved when the face is within 40 m (130 ft) distance, maintaining an average distance between the face and the first sensor of 150 m (500 ft). In recent years, CMI has moved from using 4.5-Hz geophones to accelerometers and now uses a current-modulation technique to transmit signals via long cables to the data acquisition computer providing built-in limits on current draw. Small onsite staffs maintain systems, analyze data, and develop hazard forecasts.

Microseismic monitoring systems in Australian coal mines have been deployed in a number of temporary research networks to delineate fracturing processes associated with longwall caving [e.g. Hatherly et al. 1997; Luo and Hatherly 1998]. Many of these short-term experiments utilized exploration-style triaxial geophone sensors grouted into surface-drilled boreholes in a tight array that straddled the face in one part of a longwall panel. Microseismic monitoring was also applied to a windblast problem produced by a thick resistant-to-cave conglomerate layer in the immediate roof above longwall panels [Hayes 2000]. Geophones were grouted into the ends of 10-m-long boreholes drilled into the conglomerate. The combination of hydraulic fracture preconditioning of the roof and warnings provided through real-time analysis of the microseismic data helped minimize the risk [Hayes 2000].

In a recent survey of 62 of the 142 rockburst-prone coal mines in China, approximately 80% of them use microseismic monitoring as one of the tools to “monitor and forewarn” the occurrence of rockbursts [Qi et al. 2015].

Challenges of Adapting Monitoring Technology in Deep Coal Mines

Due to inherent differences in the nature of hardrock and coal mining, a direct transfer of microseismic monitoring technology from hardrock to coal is met with some technical challenges. Issues that coal mines face in adopting these systems include: (1) rapid excavation of large longwall panels, (2) limited and restricted access for sensor placement, (3) hardware permissibility, and (4) presence of more complicated wave propagation effects.

Rapid Excavation of Large Longwall Panels

Individual longwall coal panels in the United States are larger than the footprint of many hardrock mines in which seismic monitoring takes place. Hudyma and Brummer [2007] tabulated basic seismic monitoring network characteristics from 24 different hardrock mines. Although it is difficult to make a straightforward comparison between a planar coal mine and a more three-dimensional hardrock ore body, the report shows that the cross-sectional footprint of

the area that was monitored in the surveyed hardrock mines was significantly smaller than the typical longwall coal mine. In fact, the areas are smaller than individual longwall panels. The median footprint of the monitored area of all 24 hardrock mines in this study was 600 by 400 m (2,000 by 1,300 ft) or 24 hectares (59 acres).

A single typical longwall panel (~2,300 by 300 m; ~7,500 by 1,000 ft), excluding gateroads, measures ~70 hectares (~172 acres). If one includes gateroad pillars, where large pillars (e.g., 58-m or 190-ft) are in use in deep U.S. coal mines, the area of a single longwall panel is 4–5 times the footprint of the average monitored area in the hardrock mines⁵. Furthermore, multiple adjacent longwall panels make up a section or district, and longwall coal mines consist of multiple sections. When the large size of the monitored area is combined with a rapid pace of excavation, there are significant challenges to installing and maintaining a geophone array with sufficient density to provide high-resolution details of fracture and deformation processes.

In a hardrock mine, a sensor array can be established and left in place while mining takes place within the array bounds for several years, if not for decades, with only minor periodic adjustments in the array geometry. At longwall coal mines, in contrast, a face that is 335 m (1,100 ft) wide may sweep through a section of panel that is 500 m (1,600 ft) long in just one month (> 16 hectares; > 40 acres) (shown in Figure 2). In less than six weeks, the typical longwall coal panel will have completely mined out the median footprint of the hardrock mines studied by Hudyma and Brummer. The effort required to continually move the array in a coal operation to maintain similar high-sensitivity event detections and high-resolution locations as mining progresses is significant. Nevertheless, while difficult to achieve, certain monitoring objectives may require continuous monitoring with an underground microseismic network.

⁵ South African hardrock mines targeting deep tabular deposits are much larger than the typical mines surveyed in Hudyma and Brummer [2007], but rates of excavation are still at least an order of magnitude slower than U.S. longwall coal mines. Multiple monitoring systems are also implemented within individual mines [Durrheim 2010] to maintain a smaller fixed footprint.

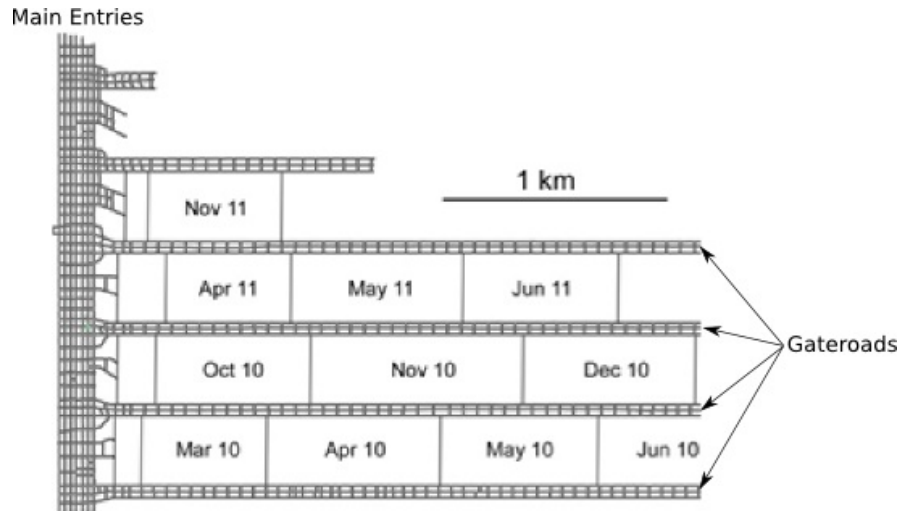


Figure 2. Large longwall panel size and high excavation rate provide a challenge to maintaining high-density seismic monitoring network.

Accessibility

One unique challenge of seismic monitoring in longwall coal mines is the difficulty in the placement and maintenance of sensors near the active face. In hardrock mines, sensors can be placed as near to the working face as protection from blast flyrock allows, or sensors can be placed on a different level above or below the working face. In longwall coal mines, there are typically no accessible levels above or below the active seam. The working face has a length of ~250–365 m (800–1,200 ft) and all of the available rock/coal surfaces make contact with moving parts of the longwall machinery, leaving no surface undisturbed for mounting sensors. Instead, sensors must be placed some distance away in the gateroads, along mains, or on the surface above the mine. Sensors along the tailgate do not survive long once the longwall face passes and the resultant caving produces gob, leaving a very large gap angle with no sensors at all (Figure 3). Such a large gap in coverage provides little constraint on event location solutions in the direction of the gap, resulting in systematic amplification of errors and biases in the calculated locations. Boreholes from the surface provide an option for placing sensors near the working face, and even for surrounding the seismic sources. However, this is an expensive and difficult option for deep coal mines and is only beneficial while the face is in the vicinity of the boreholes.

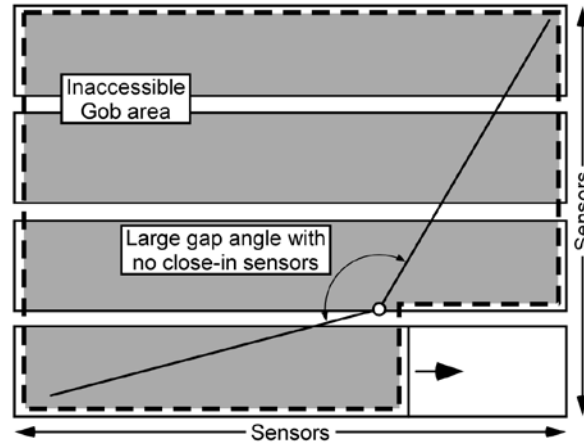


Figure 3. Large angular coverage gaps in longwall coal mines due to inaccessible gob areas.

Permissibility and Intrinsic Safety

A general strategy for measuring seismic deformation response is to place sensors as close as possible to areas of interest. In gassy mines, placing electronic equipment close to active mining areas is problematic unless the equipment is intrinsically safe or can be made permissible, or considered safe to operate in a potentially explosive environment. No microseismic monitoring system in use today is considered intrinsically safe under U.S. regulations, although some systems have achieved this rating in other countries. A permissible system can be developed through the use of electrical barriers and by housing digitizers and electronics in explosion-proof boxes. Before use in the United States, however, such a system must receive MSHA certification, which involves a lengthy approval process. Placing sensors and electronics in fresh-air entries, where permitted, may provide acceptable but more limited coverage.

Wave Propagation Medium Effects

Layered sedimentary structures in coal mines introduce wave propagation effects that are absent, or marginal, in hardrock mines. The geology in most hardrock mines is not necessarily uniform, but the spatial variation in the seismic velocity across the extent of a typical hardrock seismic network is small, on the order of 5%–10%. The small variation in seismic velocity allows for the use of a homogeneous isotropic velocity model to calculate reasonably accurate event locations. Periodic adjustment of the single P-wave velocity in the model for a hardrock mine is achieved with additional calibration or production blasts. A big advantage of a homogeneous isotropic velocity model, in terms of seismic event location schemes, is that seismic raypaths (paths the energy travels from the source to the sensors) closely approximate straight lines.

The sedimentary layers found at coal mines, in contrast, have large (10%–90%; [Jones 1994]), sudden changes in elastic properties, resulting in raypaths that are not straight but reflected, refracted, and mode converted. Seismic energy can also get trapped in low-velocity layers, such as coal seams. As the distance between the source and the sensor increases, the first arriving signal is no longer the direct, or straight, raypath from the source but is instead energy

that travels along longer paths through higher-velocity layers. Thus, in order to use arrival times of the first arriving phase to locate events, one must be able to reconstruct the path of the seismic wave. Determining the raypath is only possible with a realistic model of the seismic velocity structure. An additional important complication is the effect of the excavations and attendant longwall caving on the seismic velocity. The three-dimensional alterations of the seismic velocity from the excavation accumulate through time and result in the need for a continually updated seismic velocity model. Advancements in this area are needed to reduce systematic errors in event locations that arise when such complications are not accounted for in the velocity model. A summary of the effects of wave propagation in layered media, the influence of low-velocity gob regions on event locations, and the development of layered velocity models is provided in Appendix A.

Seismic Source Characteristics from Waveform Measurements

The approaches to seismic monitoring described in this report are designed to capture transient vibrations produced by dynamic adjustments in the rock mass. Such a rapid adjustment, termed a “seismic event,” produces elastic waves that originate at the “source location.” Analysis of the emitted seismic waves allows certain characteristics of the source to be identified. These seismic source parameters are briefly introduced in the paragraphs below with further elaboration in Appendix B.

Dynamic failures in the mining environment, ranging from minute rock fractures to large-scale triggered fault slip, cover an enormous span in magnitude and energy release. Seismic magnitudes, such as the Richter magnitude [Stein and Wyession 2009], are empirical instrumental measures of earthquake size based on maximum amplitudes of specific wave types. Although they are useful, and widely known through communications with the public about the relative sizes of earthquakes, such measures do not provide a direct link with the mechanical process that produced the seismic signals. As a more informative alternative, seismologists use seismic moment, or moment magnitude, to describe the size of an event [Stein and Wyession 2009]. Moment magnitude is the preferred magnitude for all earthquakes listed in the USGS earthquake catalogs [USGS 2016]. Instead of a single measurement, the current trend is to use two independent parameters that are measured on the seismic waveforms to describe the size of an earthquake: seismic moment and radiated seismic energy. Seismic moment provides a measure of the physical size, and radiated energy provides a measure of its capability to do damage to infrastructure.

Seismic moment, M_o , describes the forces required to produce a given amount of fault slip and is based on the physical attributes of rupture area, A , averaged shear slip, \bar{d} , and shear modulus, μ , of the source rocks,

$$M_o = \mu A \bar{d} \tag{1}$$

An advantage of M_o is that it gauges the mechanical energy needed to produce the seismic event, whereas earlier magnitude measures lack a one-to-one relationship with radiated earthquake energy, E_s . Both seismic moment and radiated energy are obtained through

independent measurements on the seismic waveforms. M_o and E_s , and their combinations, can be used to estimate source parameters, such as: stress drop, apparent stress, rupture area, average slip distance, orientation of the slip vector, etc. [e.g. Gibowicz and Kijko 1994].

The simple two-dimensional shear-slip source embodied in Equation 1, also known as a double-couple source, involves no volume change. It is a very good model to describe many natural earthquakes. The shear-slip model can be shown [Gibowicz and Kijko 1994] to be a special case of a more general moment tensor description of a seismic source that includes volumetric components. A source that contains a nonshear implosional component is often needed to describe mining-induced seismic events that accompany the closure of mine openings [Fletcher and McGarr 2005].

Another important parameter derived from seismic waveform measurements is the corner frequency, f_c , (Appendix B). The corner frequency is inversely proportional to seismic source dimension and is of particular importance to specification of monitoring system characteristics. Measurements of seismic moment and corner frequency for a number of cases of mining-induced seismicity in hardrock mines⁶ are shown in Figure 4. Event magnitude is the moment magnitude based on the logarithm of seismic moment (Appendix B). The events span a moment magnitude range of $-3 < M < +4$, which is the magnitude range pertinent to the monitoring strategies discussed herein.

⁶ Data from hardrock mines are shown because of insufficient measurements of suitable source parameters from coal mines to span a similar range in moment magnitude.

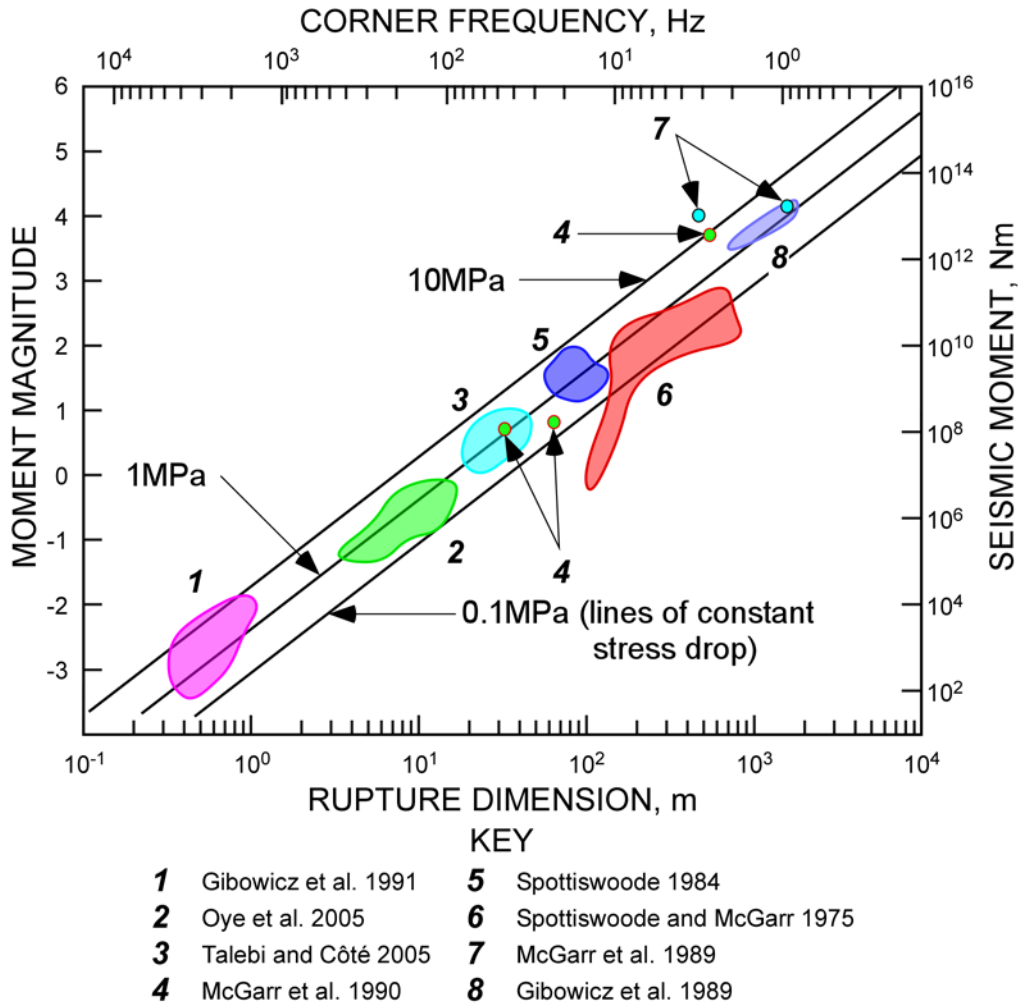


Figure 4. Relationships between magnitude, seismic moment, corner frequency, and rupture dimension. Plotted data are from the studies listed below the graph.

The largest mining-related seismic events ever recorded were produced by triggered slip on faults in deep South African mines [Durrheim et al. 2006] and large-scale mine collapse in evaporate deposits in Germany and the United States [Whyatt and Varley 2008]. These events are in the magnitude 5+ range with corner frequencies less than 1 Hz and would require characterization by a larger-scale network than those considered in this document. The smallest microseismic events reported from production-oriented, in-mine monitoring systems have magnitudes of approximately -3 with source dimensions of tens of centimeters and corner frequencies in the kilohertz range (Figure 4). Although not shown in Figure 4, this plot could have been extended to higher frequencies and smaller source dimensions. Quantitative analysis of laboratory rock fracture experiments with grain-scale and sub-grain scale fracturing produces magnitudes into the -8 to -6 range [McLaskey and Lockner 2014; Goodfellow and Young 2014]. “Acoustic emission” is often used to describe these events but ultrasonic, or “ultrasonic acoustic emission,” is more apt for these high-frequency events.

Characteristics of Different Seismic Monitoring Systems

A monitoring system must be selected such that the response characteristics of the system match the expected frequency range (or size) of the seismic events of interest. The system response includes the response of both sensor and recording system, as well as the propagation medium. In order to resolve corner frequencies from seismic waveforms, Mendecki et al. [1999] cite the necessity of measuring frequencies that are five times above and below the corner frequency. The span of four orders of magnitude in corner frequency in Figure 4 asserts that a single type of sensor is inadequate to accurately measure events over the size scale observed for mining-induced events.

Array configuration, especially station spacing, is another monitoring system feature that must be matched to the event size of interest. Station spacing becomes important because of attenuation—low frequencies propagate long distances, but high frequencies are quickly attenuated. This provides a type of spatial filtering in that small events with high frequencies may be detected when occurring in close proximity to sensors with high-frequency range but would not be detected by stations that are farther away. In order to detect and locate small events, it is necessary to install a dense network near the sources. For example, if the objective is to detect minute events (e.g. $M = -3$ to -4) associated with a developing roof fall, the network must be close by and of a sufficiently high-frequency range to capture small-scale events.

The different types of seismic systems needed to span nine orders of magnitude in frequency are shown in Figure 5. Piezoelectric sensors used in acoustic emission networks ($-8 \leq M \leq -3$) have a response in the tens of kHz to MHz range. Sensors in microseismic systems ($-4 \leq M \leq 3$) include piezoelectric-based accelerometers at the high end of the frequency range and moving-coil geophones (seismometers) for the remainder of the range. Inexpensive geophones are primarily developed for the exploration geophysics market and have a frequency range that is largely 5–10 Hz and above. Circuitry to boost the low-frequency range of geophones so that they help resolve the low corner frequencies of the largest mining-induced seismic events provide a low-cost alternative to the more expensive seismometers commonly used in earthquake seismology. Low-noise, strong-motion accelerometers (0 to 200 Hz response) or seismometers with responses down to 1 Hz provide suitable response for coal-mine-oriented district-wide ($0 \leq M \leq 4$) and mine-wide ($-1 \leq M \leq 4$) networks.

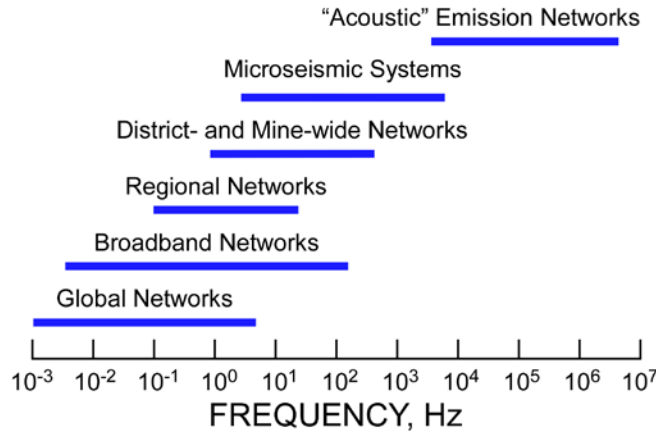


Figure 5. Frequency range of six different types of seismic monitoring systems.

Regional seismic networks ($M \geq 1.5$) have used the standard 1-Hz short-period velocity seismometers for decades, but are now gradually replacing them with broadband sensors. Broadband networks ($M \geq 1.0$) now cover the ranges that used to be covered by specialized ultra-low frequency sensors (down to a period of $\sim 1,000$ s) for worldwide earthquake monitoring ($M \geq 4$) and the short-period seismometers in regional networks.

Five Seismic Monitoring Strategies for Deep Coal

In this section, five strategies for monitoring seismicity in deep coal mines are presented: (1) a single station, (2) a regional seismic network augmentation, (3) a temporary network deployment, (4) a district-wide or mine-wide seismic network, and (5) a microseismic network. Examples of the use of each of these strategies are provided.

Single-station Option

The deployment of a single seismometer, with suitable data recording and display capability, offers an effective way to provide awareness and rudimentary documentation of local seismic activity. Of the various options for providing seismic monitoring coverage at an operating mine, the use of a single station is the simplest and least expensive method. Additionally, mining/geology engineering staff should have the technical skills (i.e., selecting a suitable site, connecting the electrical components, and running data collection software) to easily deploy a single station as a do-it-yourself project. One of the key features of deploying a single station is the ability to provide continually updated visual records of ground motions that come from all sources of vibration, including: local mining-related seismic events, earthquakes, local and regional blasting, and vehicular traffic and earthwork with heavy machinery. Rough constraint can, in many cases, be placed on the origin of the local mining-related seismic events with a little effort in manipulating and measuring waveforms recorded by a three-component, or triaxial, sensor. Such analysis provides estimates of the distance between the seismometer and the origin of typical mining-related seismic events, and estimates of the direction (bearing or back azimuth)

from which the seismic waves originated. Combining range and bearing measurements provides a method to estimate source locations using a single triaxial station.

Helicorder Display

A continually updated visual record of ground motion, or helicorder plot, is shown in Figure 6 for a vertically oriented short-period (1-Hz) uniaxial seismometer deployed in a coal mining district. A helicorder display is the digital equivalent of the old pen and ink, or smoked paper, drum recordings. They show vibration output from a single seismometer component as a function of time—typically a 12- or 24-hour duration.

Through daily examination of helicorder plots, the ability to identify different types of seismic sources is rapidly mastered, with suitable initial guidance, so that local mining-related events can be quickly recognized and separated from other sources. Sensors should be placed away from the immediate vicinity of large local noise sources (e.g., vehicle traffic, conveyor belts, wash plants, stockpiles) and closer to the workings of interest. The 12-hour display of Figure 6 provides examples of signals from a magnitude 3.3 coal burst at a distance of 12 km (7.3 mi), coal trains at a distance of 700 m (2,300 ft), a small local mining-related seismic event ($M \sim 0.4$) at a distance of 1 km (3,300 ft), and background noise from a coal mine wash plant at 700 m (2,300 ft).

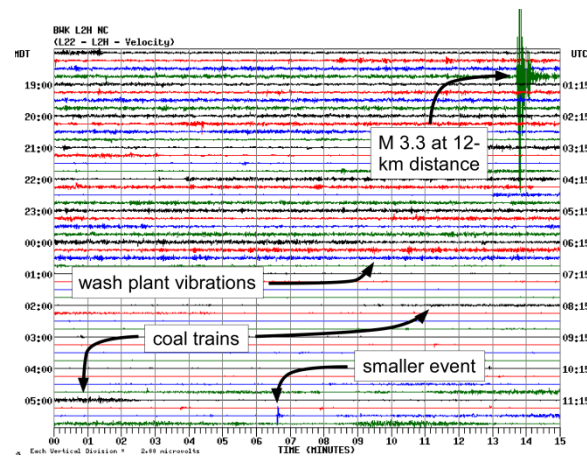


Figure 6. Helicorder-style plot of 12 hours duration from a 1-Hz short-period vertical seismometer.

A helicorder plot for a single station deployed away from the mine surface infrastructure and nearer to an active 270-m-wide (900-ft-wide) longwall panel is shown in Figure 7. A conventional short-period (1-Hz) seismometer was placed on the surface 460 m (1,500 ft) above the seam at a horizontal distance of 440 m (1,440 ft) from the tailgate edge of the face. Frequent, brief, spike-like signals associated with small seismic sources (fracturing) in the immediate vicinity of the panel are typical for a sensor this close to an active longwall at many western U.S. coal mines. The longwall face was actively cutting, accompanied by periods of elevated background noise, for approximately half of the time displayed in Figure 7A.

When background seismic event activity is elevated, it can be difficult to readily identify notable events. Applying a low-pass filter to the seismic signals before plotting allows larger seismic sources to be accentuated. For example, Figure 7B shows a low-pass filtered version of the record in Figure 7A. The low-pass filtered trace (Figure 7B) attenuates the numerous short

high-frequency spikes, and highlights the few lower-frequency signals from the largest mining events as well as regional and teleseismic earthquakes when present (signals from regional earthquakes are on blue and black traces at 9:36 am and 11:09 am local time, on the left axis).

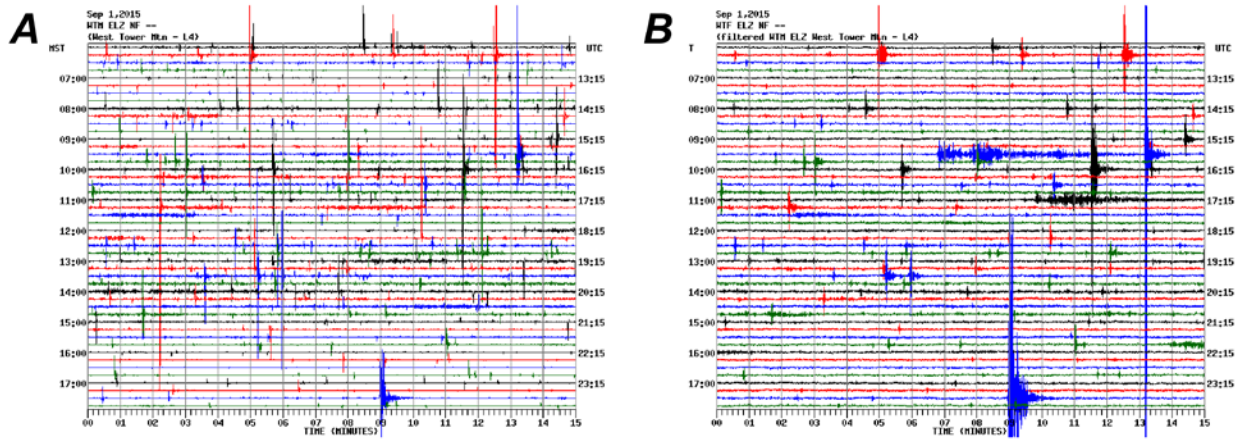


Figure 7. Unfiltered (A) and low-pass filtered (B) helicorder records near active longwall.

As a final example, Figure 8 shows frequent large-magnitude seismic events up to M2.8 recorded during multiseam panel extraction under 520 m (1,700 ft) of cover. The 200-m-wide (650-ft-wide) longwall panel retreated approximately 8.5 m (28 ft) per day at a level that was ~90 m (300 ft) beneath a previously mined seam. The panel, with gateroads that were offset from the overlying gateroads, was the fourth panel in a district that undermined the more extensive excavations of the upper seam. The single-station, low-pass filtered data was recorded with a 1-Hz, short-period seismometer that was positioned 3.3 km (2.1 mi) away from the panel. The elevated activity during this period indicates significant dynamic deformation of the strata in the vicinity of the active and overlying previously mined seams. Although elevated seismic activity does not always signal the onset of ground control problems, a damaging event did occur two days later, producing extensive floor heave ahead of the face along the tailgate. In this manner, the simple visual display of the helicorder record provides a quick assessment, and rudimentary documentation, of the seismic activity from that day.

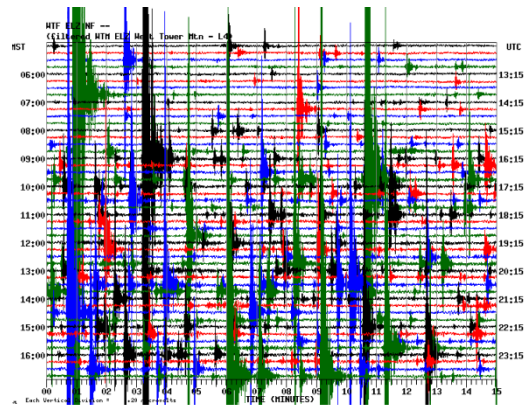


Figure 8. Multiseam extraction helicorder record showing large-magnitude seismic events.

Range Determination

There are two different types of waves that travel through a solid body (called body waves): P, or compressional, and S, or shear, waves. P-waves are the seismic equivalent of sound (acoustic) waves in air and propagate as an alternating sequence of compression and expansion pulses produced by particles in the ground vibrating in the direction of wave propagation (Figure 9). S-waves, which require a medium with rigidity to propagate, consist of an oscillating shear movement with particle motions perpendicular to the direction of wave propagation. A single station may be used to estimate the distance between a seismic source and a receiving seismometer by estimating the separation between these two body waves, because S-waves propagate at roughly 0.5 to 0.7 of the velocity of P-waves.

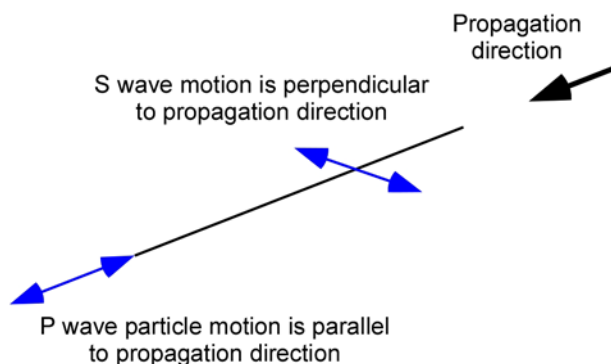


Figure 9. Seismic body-wave particle motions.

Examples of P and S phases, produced by an $M = -0.5$ event at seam level, are shown in Figure 10 for two different stations. The 4.5-Hz triaxial seismometers were located on the surface 600 m (2,000 ft) above the coal seam. Figure 10A shows a P arrival with abrupt onset and large amplitude on the Z (vertical) component, but with comparatively little energy at the time of the S-wave. Conversely, the two horizontal components (N, E) show higher amplitudes for the shear wave than the P-wave.

While the S-wave arrival can be estimated from Figure 10A by direct inspection, the arrival time in Figure 10B is not as clear. The difference is directly related to the influence of the propagation path of the seismic energy. While the straight-line path lengths between the source and the stations are similar at 834 m (2,736 ft) and 1,063 m (3,488 ft), respectively, for the stations in Figure 10A and 10B, the signal in Figure 10A traverses intact sedimentary strata, and that of Figure 10B traverses disrupted strata above the longwall gob. Several avenues are available for improving S-wave arrival time estimations. Instead of viewing the data in a coordinate system tied to the fixed E-W, N-S orientation of the sensor components, rotating the signal components into a coordinate system aligned with the incoming raypaths (radial and tangential components) maximizes separation of the signal into P- and S-waves to facilitate picking the S-wave arrival. Nongraphical techniques for estimating S-wave arrivals make use of quantitative wave polarization analyses [Cichowicz 1993].

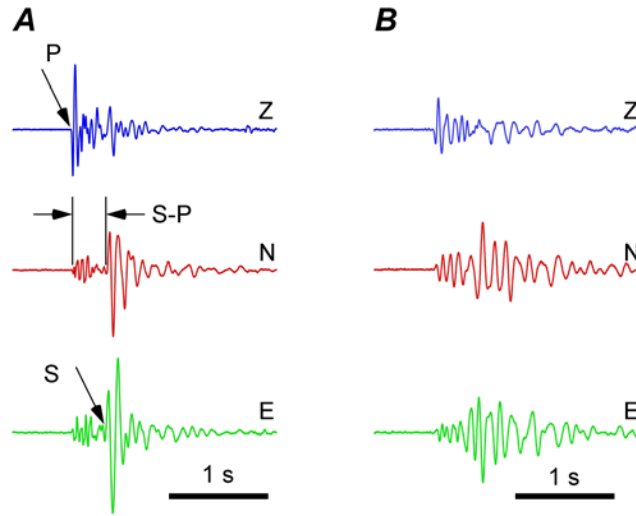


Figure 10. Two sets of three-component seismograms with P and S arrivals.

Because P- and S-waves travel at different velocities, the propagation distance is directly related to the difference in arrival times of these two phases. Assuming a homogeneous isotropic velocity structure and that the P- and S-velocities V_p , and V_s are known, then D , the range, or distance, in meters between the seismometer and the seismic source can be easily derived. Arrival times for P and S phases traveling a distance, D , are, respectively:

$$t_p = t_o + D/V_p \quad (2)$$

and

$$t_s = t_o + D/V_s \quad (3)$$

where event origin time is t_o .

Rearranging and substituting Equation 3 into Equation 2 yields:

$$D = (t_s - t_p)/(1/V_s - 1/V_p) \quad (4)$$

In most cases, independent measurements of both P and S velocities are not available, and the S velocity is estimated from an assumed ratio of V_p/V_s . While a common rule of thumb is $V_p/V_s = \sqrt{3}$ [Shearer 2011], values measured for specific sedimentary rock types range from 1.5 to greater than 2 [Castagna et al. 1985], with this ratio generally increasing to values of 2 and higher near the Earth's surface [Nicholson and Simpson 1985].

Folding the velocity dependent term in Equation 4 into a single parameter, c , yields:

$$D = (t_s - t_p) * c \quad (5)$$

where the assumption of a constant V_p / V_s ratio is implicit. The parameter c typically ranges from 2 to 8 km/s (6,000 to 26,000 ft/s) depending upon whether raypaths traverse short distances under shallow cover (low velocity, high P/S velocity ratio) or longer distances through deeper layers (high velocity, low P/S velocity ratio). For a particular situation, the value of c is best determined through calibration by observing seismic signals from a known source location. Equation 5 represents the distance to the seismic source regardless of the direction of wave propagation. A set of possible solutions to Equation 5 yields a sphere of radius D centered on the seismometer (assuming a homogeneous isotropic velocity). In cases where a two-dimensional geometry is appropriate, the solution is a circle of radius D centered on the seismometer (Figure 11).

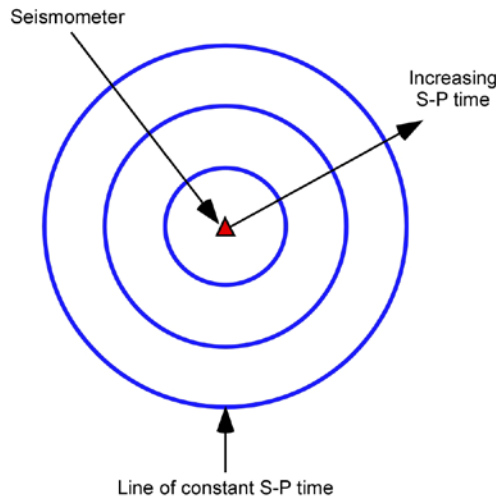


Figure 11. Increasing S-P times with propagation distance.

As an example of the single-station analysis (Equation 5), we present data collected at an isolated station as part of a data-gathering exercise performed prior to setting up a seismic network in a mining district. Both a triaxial, strong-motion accelerometer and a triaxial 2-Hz seismometer were deployed at the temporary station to collect baseline data over a two-month period. Helicorder plots were generated and used to identify the larger events, all of which had been saved in separate triggered-event files by the data acquisition software. Measurements of P- and S-wave arrival times were used to tabulate S-P times, which strongly clustered into three groups (Figure 12). As three different longwall coal mines were operating in the vicinity of this station, the tight groupings suggest that the events likely originated at the three different mines.

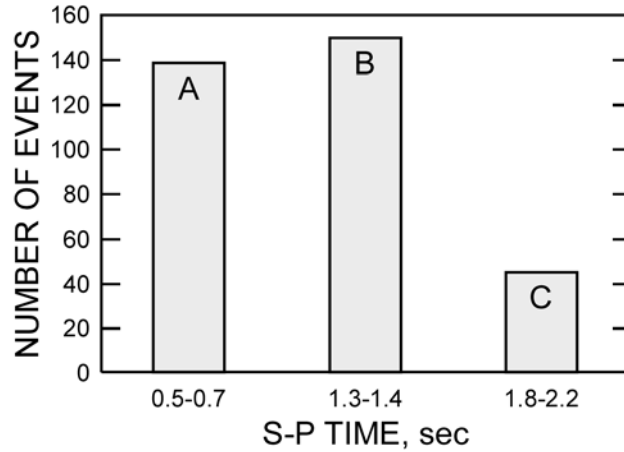


Figure 12. Observed S-P times exhibit discrete values (A, B, C).

Applying the S-P values to Equation 5 to estimate the distance to the events yielded unrealistically large distances when using standard values of c from earthquake seismology (8–10 km/s (e.g., [Stein and Wysession 2009])). As the location of one of the operating longwalls was known at the time these measurements were made, Equation 5 was used to solve for c for that specific distance, giving $c = 3.3$ km/s. Using this value of c produced range values, or circles of potential event locations, as shown in Figure 13. Locations of the longwalls in operation at the three mines at the time of the measurements are also shown, indicating fair agreement with range measurements estimated simply on the basis of S-P times.

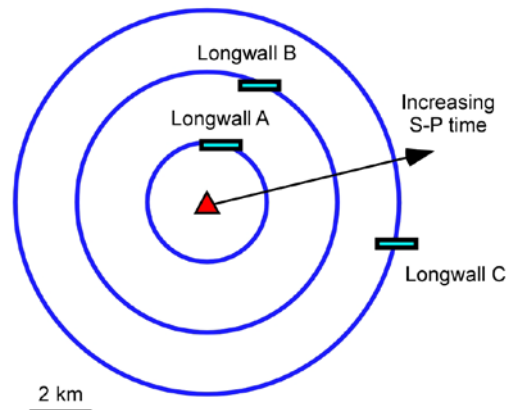


Figure 13. Comparison between range estimates based on S-P times and longwall locations.

Back-azimuth Determination

The back azimuth, or direction from which an event originates, is commonly estimated by measuring the recorded seismic waves along three perpendicular axes and fitting a line to the polarized P- and/or S-phases. A 180-degree ambiguity is inherent to this method, however, because the line conveys no information about propagation direction. Back azimuth can be estimated graphically using particle-motion diagrams (hodograms/Lissajou figures) or through more rigorous polarization analyses such as orthogonal regression and principal component analysis.

An example particle-motion diagram is provided in Figure 14. The left-most plots show the north (N) and east (E) outputs from a single 4.5-Hz triaxial geophone that recorded an M0.8 event. The middle figures show a magnified section of the dashed line segments in the first panel. The plot on the far right shows the output from the north component plotted against the output from the east component for the time period shaded in the middle panels. A NW-SE polarization of the initial P-wave is evident in the quasi-linear NW-SE trends of the plot. This orientation is consistent with the bearing between this station and the source location (black arrow) as determined through triangulation, using arrival times from a dense array of geophones. Later in the signal, beyond the initial P-wave arrival, energy starts arriving from various directions due to wave scattering, reflection, refraction, and general multipathing, which seriously degrades the linear polarization. Thus, this technique works best when the raypaths between the sources and the seismometer are devoid of complicated structures. Additionally, it is important to apply the analysis to only the beginning of the desired phase, and to filter out higher-frequency energy, which tends to be more sensitive to local variations in structure. Eisermann et al. [2015] found that it is also useful to apply several polarization methods and rate the quality of the predicted back azimuth by how well each of the methods agree.

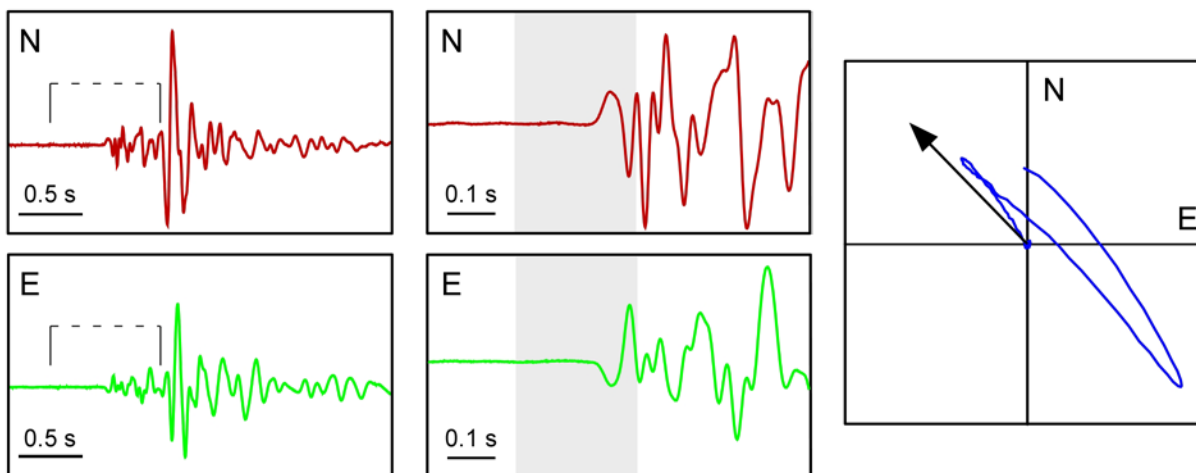


Figure 14. Seismograms from north- and east-oriented components (red and blue traces in first two panels) used to construct a hodogram plot (third panel) illustrating P-wave polarization for back-azimuth measurements.

In a temporary network deployment, NIOSH installed a number of broadband seismometers over an active longwall panel in the western United States. Triggered data were recorded on three channels at a 500-Hz sampling rate. Orthogonal regression was applied to estimate P-wave polarization on several events using the first 100 milliseconds of data after the onset of the P phase. The data were filtered between 1.0 to 2.0 Hz. Results for a typical event are shown in Table 1, where back azimuths predicted from orthogonal regression are compared to those calculated from arrival-time inversion. The predicted back azimuths are reasonably accurate, considering the instruments were manually oriented in the field with a hand-held compass.

Table 1. Back azimuths and predicted back azimuths from particle motion analysis for temporary deployment

Station	Back Azimuth (deg)	Predicted Back Azimuth (deg)	Residual (deg)
GS	155	157	2
GNW	335	344	9
GSW	190	205	15
GSE	111	119	8
GNE	75	67	-8
GRN	262	266	4
GN	40	56	16

Similar graphical and polarization analyses can be used for the more complex S-wave motion by searching for maximum particle motion perpendicular to the wave propagation direction [e.g., Cichowicz 1993].

Single-station Location

Combining range and back azimuth estimates results in two possible solutions due to the 180-degree ambiguity in the back azimuth. The ambiguity can be resolved with knowledge of existing workings or measurements with additional stations. In the example of Figure 15, range measurements based on S-P times indicate a distance of approximately 1 km (3,300 ft) from the underground 14-Hz triaxial geophone (red triangle). A N66°W back azimuth measurement from a particle-motion diagram intersects the circular line of constant S-P time at two widely separated locations. In this case, because one solution is in the current longwall panel and the other is in old workings, the event likely occurred in the current panel. However, events in old workings are commonplace, so the ambiguity remains unless additional measurements are available.

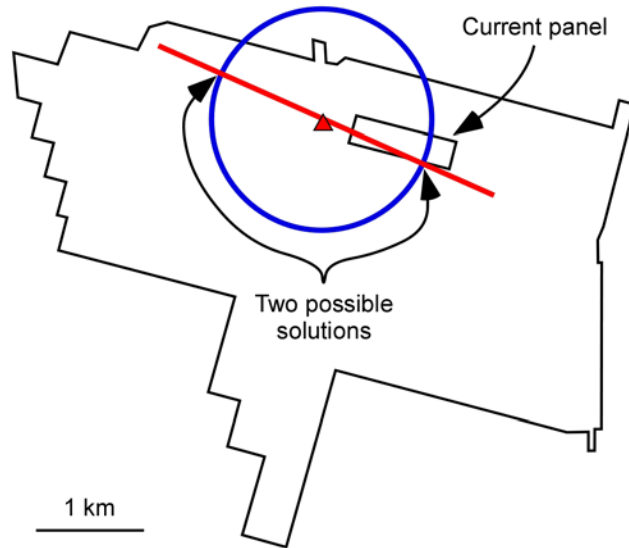


Figure 15. Map showing outline of a longwall coal mine with a single-station location based on range and back-azimuth measurements

Multiple Single Stations

Figure 16 illustrates how additional single-station measurements can constrain the location of the same event. Signals from three additional triaxial 14-Hz geophones (red triangles) deployed at the level of the coal seam were analyzed to estimate single-station locations using the combination of range and back azimuth measurements. An independent determination of the source location (cyan symbol) was made through triangulation using inversion of arrival-time measurements from 17 stations of a panel-scale microseismic network. A comparison of the four independent single-station event location estimates (yellow symbols) with the location constrained by the 17-station network (cyan symbol) shows that the level of error associated with any one single-station location estimate is, in this example, several hundred meters. Depending upon monitoring objectives, this error may be perfectly satisfactory for locating events within the confines of the overall 5–6 km (3.5 mi) dimensions of the mine.

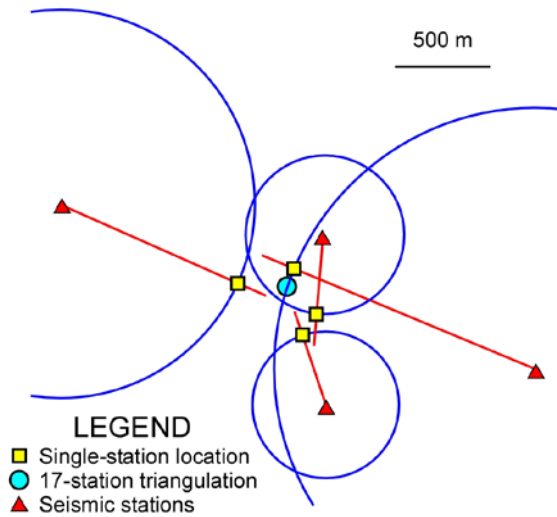


Figure 16. Comparison of single-station location estimates from multiple stations.

A common geoscience lesson is to apply Equation 5 to earthquake signals from multiple seismometers and then have students graphically solve for an earthquake's location. When S-P times from the same seismic source are measured at two different seismometers and circles of appropriate range (diameter) are plotted for each, the solution circles intersect at two different locations (assuming a two-dimensional problem). The addition of the second sensor reduces the number of possible source locations from infinity to just two. Addition of a third seismometer, with its circle of possible source location solutions, identifies the correct solution in the two-dimensional, error-free example in Figure 17.

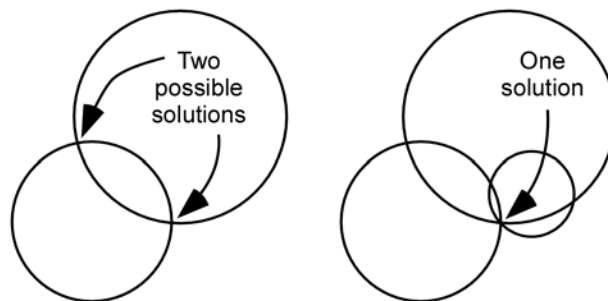


Figure 17. Multiple range estimates based on S-P times constrains possible event locations.

A few seismometers reporting S-P arrival-time differences can place significant constraint on a source location. In some applications, this may be sufficient to meet the monitoring objective. For example, this could be the case if the objective was to discriminate between events occurring in old workings versus current workings, at the longwall face versus development headings, or in adjacent mine properties, etc.

As shown in the above examples, the single-station seismic method offers a way to provide awareness of the seismic activity in the vicinity of the sensor at a range of distances from tens of meters to tens of kilometers. When paired with appropriate digitizing hardware and display software, it is a simple, low-cost method that can provide a continually updated visual record of ground motion. With a little extra analysis, through manipulation and measurement of the waveforms, arrival times of P- and S-phases and phase polarization directions can be used to estimate the distance to the seismic event, the back azimuth to the event and, when combined, an approximate location.

Another advantage of the single-station approach is that a synchronized timing device (e.g., GPS) is not required. Thus, estimation of range, back azimuth, or a single-station location may be possible through deployment of suitable blast-recorder type monitoring devices commonly available in many coal mining regions.

There are a variety of options for implementing single-station monitoring capability. These options range from user-assembled systems based on low-cost geophones, digitizing hardware, and open-source software, to high-quality fully digital broadband seismometers and proprietary software. Appendix C describes possible options for setting up single-station monitoring.

Regional Seismic Network Augmentation Option

The concept of network augmentation is to add one or more seismic stations to an existing network to improve coverage in the vicinity of mining operations. Instead of devoting resources and effort to develop the required expertise and monitoring network, a mining company could purchase the instrumentation, remote power, and telemetry hardware for any number of stations and partner with a participating network operator (typically a local university). A small amount of financial support may be required for telemetry and maintenance costs, but the additional station or stations would improve documentation of local seismic activity. The model for augmenting a regional network originates from the UUSS practice of placing strong-motion seismometers near underground coal mining operations in Utah and integrating the new stations with the rest of the network [Arabasz and Pechmann 2001]. However, there must be an existing network in the area to implement this option.

The USGS accomplishes its mission to monitor earthquakes across the country by supporting national and regional seismic networks. The Advanced National Seismic System (ANSS) consists of a backbone national network (Figure 18) along with additional coverage by 15 regional seismic networks [ANSS 2014]. The regional seismic networks are largely operated by university groups. The density of seismic network coverage across the country varies significantly, with a much higher density of seismometers in recognized areas of frequent earthquake occurrence. Much of the rest of the country is covered by the low-density ANSS backbone network. Both the epicentral location and depth uncertainty are ~10 km (6.3 mi) across much of the United States for events with $M \geq 3$, the minimum target magnitude for event detection and location in all areas [ANSS 2014]. Many significant mining ground control failures produce events below this magnitude threshold as well as nondamaging, but notable, dynamic adjustments of caving/subsiding ground, making the current ANSS backbone network insufficient for most mining operations.

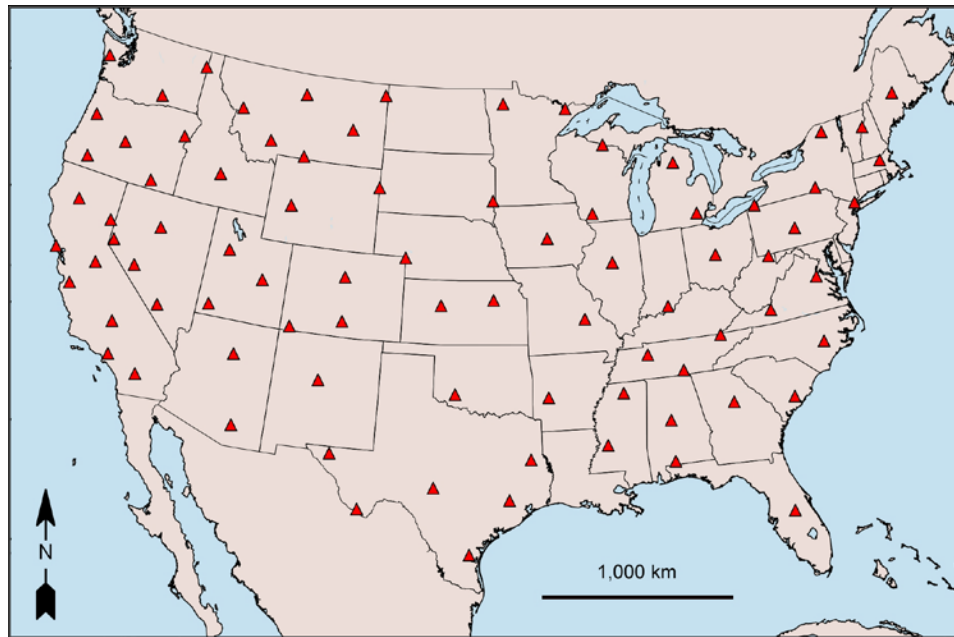


Figure 18. Seismic stations of the Nation's backbone network (after [ANSS 2016]).

The ANSS backbone network has recently been updated and expanded to a total of 95 stations [ANSS 2016]. The 15 regional networks under the ANSS umbrella are relied upon to provide additional coverage where earthquake hazards are of concern; in addition, there are other stations outside ANSS. In total, ANSS lists almost 50 network codes that have been assigned to seismic monitoring networks, ranging from individual stations and small networks hosted by universities to the major regional university/government networks of the Nation's monitoring capability.

Many U.S. coal mining regions (Figure 19) have never had very good coverage by seismic networks. However, improvements to the Nation's seismic monitoring capabilities, beyond the ANSS backbone, are occurring in and near some coal mining states because of an earth science initiative named Earthscope funded by the National Science Foundation (NSF). Earthscope is an NSF-funded "big science" experiment to characterize the geologic and geophysical structure of the North American continent, with a special emphasis on processes related to earthquakes and volcanoes [NAP 2001]. As part of this initiative, a temporary network of 400 high-quality broadband stations with ~70-km (~44-mi) spacing moved from west to east across the United States. Recognizing the benefit of a high-quality network, and the sparsity of station coverage across much of the eastern and central United States, a multi-agency collaboration (NSF, USGS, Nuclear Regulatory Commission, DOE) came together to keep 159 of the 400 stations in place as the Earthscope experiment continues on to Alaska [USARRAY 2015]. The 159 new stations are shown in Figure 20 as the N4 network. The addition of numerous seismic stations in this region increases the likelihood of detecting mining-related events in the area and locating them at the correct mine, but still only for the largest of events. As a standalone network, the ANSS is inadequate to achieve the main objectives of coal mine seismic monitoring in most coal mining regions.

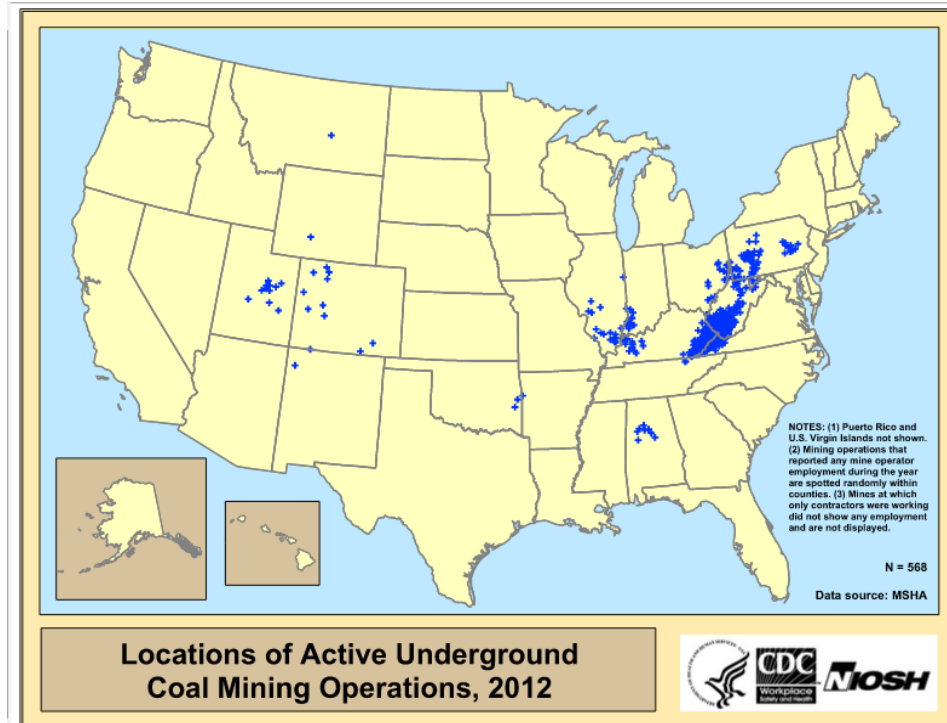


Figure 19. Locations of active U.S. underground coal mines (after [CDC 2012]).

One underground mine from each state with coal mining was randomly selected (sample coal mines black-outlined diamonds in Figure 20 for eastern-central U.S. mines), and the distance to the five nearest seismic stations was determined for each of the selected mines. Table 2 lists the distance to the closest station as well as the average distance to the nearest five stations. The mines with the best coverage are those in Utah, with a minimum source-receiver distance as low as 5 km and an average distance of 31 km for the selected mine. The source-station distances are much greater in other states with mines in the areas of West Virginia, Kentucky, and Virginia that have previously experienced bumps (polygon in Figure 20), having a closest station distance of 26–45 km (16–28 mi). However, there are a few seismic networks operated by universities near coal mining regions which are undergoing expansions in response to concerns related to waste disposal in deep boreholes and hydrofracking. Adding one or more stations in the vicinity of one of the mines, and feeding the data into a regional network covering the area, would enable smaller events to be detected and properly located. Additionally, there are nonconventional event detection methods (i.e., matched filters) that have been shown to increase the detection and location capabilities of regional networks that cover mining districts to the point of being comparable with deploying a local network over the district [Kubacki et al. 2014; Chambers et al. 2015].

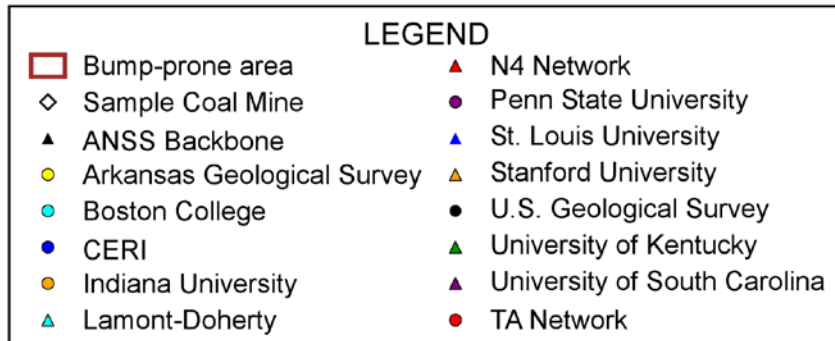
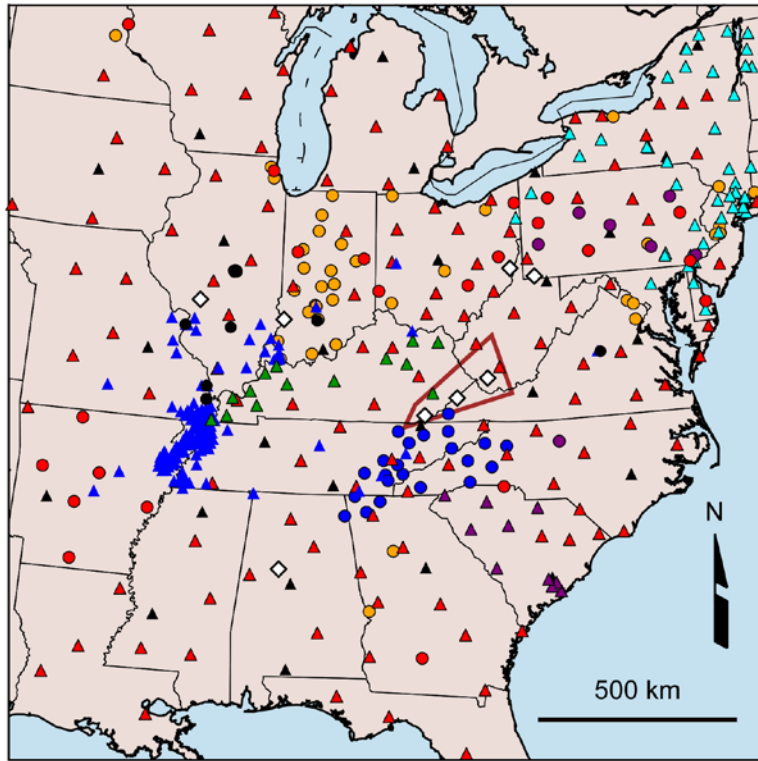


Figure 20. Seismic stations currently operating in the eastern and central United States (after [USARRAY 2015]).

Table 2. Distances between underground coal mines and existing seismic stations

Mine	State	Distance to Closest Station km (mi)	Average Distance to Nearest 5 Stations km (mi)
Mine A	Alabama	45 (28)	105 (65)
Mine B	Colorado	57 (35)	73 (46)
Mine C	Indiana	56 (35)	60 (37)
Mine D	Illinois	48 (30)	64 (40)
Mine E	Kentucky	26 (16)	52 (32)
Mine F	Ohio	49 (31)	77 (48)
Mine G	Oklahoma	70 (43)	119 (74)
Mine H	Pennsylvania	33 (20)	74 (46)
Mine I	Utah	5 (3)	31 (19)
Mine J	Virginia	45 (28)	79 (49)
Mine K	West Virginia	41 (25)	98 (61)
Mine L	Wyoming	91 (57)	133 (83)

Temporary Network Deployment Option

Temporary deployments have often been used to investigate seismicity associated with longwall coal mining at higher sensitivity and resolutions than are possible with regional seismic networks [Hatherly et al. 1997; Bischoff et al. 2010b; Arabasz et al. 2005]. Deployment of a temporary seismic network is an option that avoids the personnel and financial investments associated with a permanent system. With this method, the hardware and software of each of the four other types of monitoring options can be implemented on a temporary basis. Reasons to adopt this monitoring strategy include: (1) determination of whether or not the technique is suitable to the problem at hand, (2) monitoring a ground control issue that is not expected to be a recurring problem, or (3) a need to collect premining data as part of the permitting procedure or a company's exploration process.

Some specialized types of equipment that are well-suited to the rapid installation of temporary deployments include: certain conventional, cabled, exploration seismograph arrays; arrays of self-contained independent geophone recording systems used in exploration geophysics; and portable broadband seismometers used in earthquake aftershock studies.

A conventional engineering exploration seismograph system consists of one or more strings of geophones connected with spread cables to a small portable, battery-operated data acquisition unit (some specific exploration systems only record for a very short period of time for refraction work and require modification for continuous recording). A laptop receives and displays the waveform data and controls the data acquisition process. As an example, a 48-channel exploration seismograph was deployed on the surface directly above the longwall face at two separate coal mines. The deployments were similar at both mines with two 24-channel spread

cables with 14-Hz vertical geophones on 12-m (40-ft) spacing laid out along two perpendicular lines (Figure 21). One line was deployed parallel to the headgate, and the second line was perpendicular to the first and across the active panel. The second line was positioned ahead of the face so that, as mining progressed, the face would pass beneath it. Overburden was 275 m (900 ft) and 425 m (1,400 ft), respectively, for the two mines. The terrain above the first mine was flat with light vegetation, and the network was easily deployed by three people in a couple of hours. The terrain for the second mine was much steeper with heavy vegetation, requiring six hours to deploy the sensors.

This example illustrates not only the temporary network deployment concept but also the vast difference in possible longwall seismic response. A comparison of the signals recorded at each mine, while the shearer was actively cutting, is given in Figure 21. Nine geophone signals, out of a total of 48, are shown for each mine in 10-minute-long recordings. These signals are typical of those observed while the shearer was in operation at the two mines during the several-days test at each site. Traces from Mine A show very few transient seismic events, which is consistent with the general absence of the snapping and cracking sounds when underground in the vicinity of the longwall at Mine A. Although there are some sandstone channels in the roof at this mine, none were in the vicinity of the longwall face or excavated parts of the panel at the time of the measurements. Much of the overburden strata are comprised of layers that largely deform plastically, thereby producing very little seismicity. Mine B contains numerous modestly strong layers, including sandstones, in the roof and exhibits a steady stream of typical mining-induced transient seismic events; these signals coincide with the audible cracking sounds heard when underground in the vicinity of the active longwall at this mine. The maximum event magnitude during the day of monitoring at this mine was M2.3. Neither mine experienced any difficulties related to the seismicity accompanying extraction of these longwall panels.

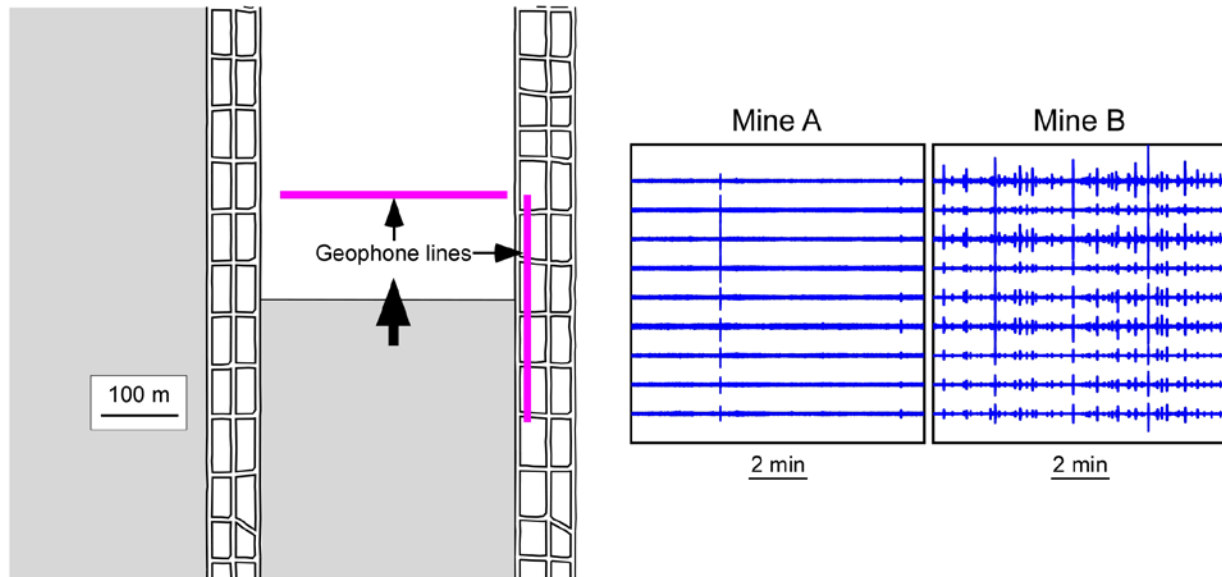


Figure 21. Temporary exploration seismic array (magenta lines on left panel) captures diverse seismic response at two mine sites (right panel).

The stark difference in seismic response for the two mines underscores the need for conducting preliminary measurements prior to the selection and design of a seismic monitoring approach at any given mine. A single-station measurement is the fastest, easiest way to gauge the type of seismic response to be expected.

While a temporary deployment can involve any combination of surface and underground sensors, a surface-only deployment is much simpler. It may seem that measurements from the surface would be much less sensitive than underground measurements, but this is not necessarily so. Longwall panels that are over 300 m (1,000 ft) wide, with large inaccessible gob areas, can result in shorter raypaths to surface stations than to available locations for underground stations. Because there is generally greater attenuation on longer paths, signals from underground sensors may have smaller signal-to-noise ratios. Also, the greatest motion from the closure of a horizontal tabular void created by longwall mining is in the vertical direction. Therefore, a vertical sensor on the surface will be most sensitive to motion parallel to the expected direction of movement, producing maximum signal amplitude. Another factor that degrades the signal-to-noise ratio underground is the greater noise in an underground environment. Direct mechanical excavation processes in the seam, ground vibrations in the entries from ventilation currents, and the waveguide effect of low-impedance coal seams—which traps vibrations and channels them through the medium where the underground sensors are deployed—all negatively impact the signal-to-noise ratio. For these reasons, surface sensors may be as effective as underground sensors, especially in cases where the distance to bedrock is small.

Evidence that surface sensors can detect seismicity associated with individual cuts of the longwall face is shown in Figure 22. Seismic activity was recorded on the surface by an array of eight 4.5-Hz vertically sensitive geophones distributed in a 425-m (1,400-ft) diameter circle above the face. Depth of cover under the array ranged from 180 to 300 m (600 to 1,000 ft).

Figure 22 shows clear evidence of the cycle of increasing and decreasing rates of seismic activity as the shearer moves back and forth across the face, with maximum seismicity rates attending cutting near the tailgate. Overburden strata in this area consists of interbedded layers of sandstones, mudstones (shales), and siltstones.

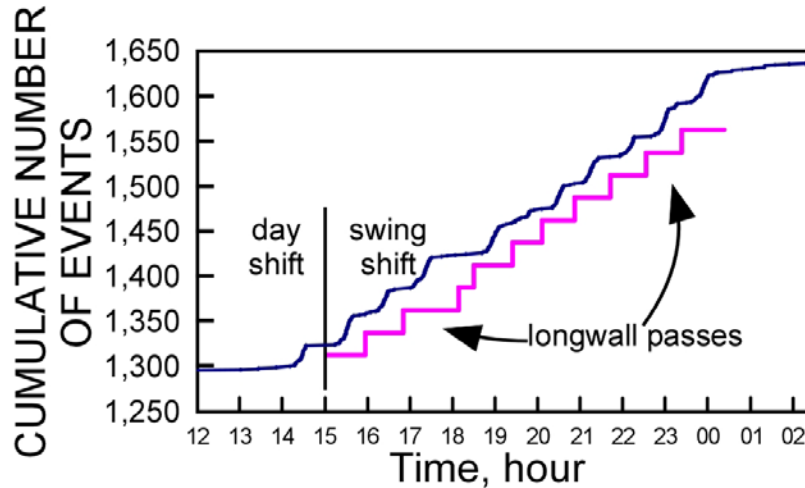


Figure 22. Temporary array of surface geophones tracks seismic response of longwall shearer motion.

Large-scale deployments of dense arrays of continuously recording, autonomous geophones are becoming commonplace in oil and gas exploration, as well as in research applications [Lin et al. 2013]. Up to several thousand self-contained, cordless geophone units incorporating GPS and digitizer hardware, measuring roughly 15 cm (6 in) in diameter and 20 cm (8 in) in length, can be deployed for continuous recordings of two weeks or longer while operating from an internal or external rechargeable battery. The instruments are housed in hardened plastic with spikes attached to the bottom of the units to facilitate coupling to the ground. Installation consists of simply scooping out a small pocket of dirt and pushing the spikes on the bottom of the unit into the ground. The internal GPS determines both the physical location coordinates and provides a data-synchronizing time stamp.

Another approach to temporary network deployments involves the use of high-quality broadband instruments. While broadband instruments require considerably more care in installation than geophones, they provide high signal-to-noise ratio signals over a frequency band necessary to extract source parameters of some of the larger events. A temporary deployment of broadband stations was described in the Single-station Option section. Each seismometer was placed in a 30-cm-deep (12-in-deep) hole, carefully leveled, covered, and powered with high-capacity batteries for one month of operation. Analysis of a 6-hour recording period from this data set is offered as an example of the temporary deployment of a network of broadband stations. Uninterrupted longwall cutting operations took place during this time period.

Continuous GPS-synchronized data streams were locally recorded on each unit and searched for time-coincident transient events that could be associated into separate event files. Event files were then processed to extract arrival times and event locations. Station locations (blue triangles), longwall infrastructure, and event locations for the 60 largest events that occurred

during this time interval are shown in Figure 23. All but one of these events were too small to be located by the district-wide network. While the majority of the events cluster about the retreating longwall front, three small groups of events fall outside the bounds of the longwall gateroads. The two northernmost groups coincide with continuous miner development in the north and east mains. Events from the southern group coincide with a steeply dipping, NW-trending fault structure (shown in Figure 23 as maroon lines).

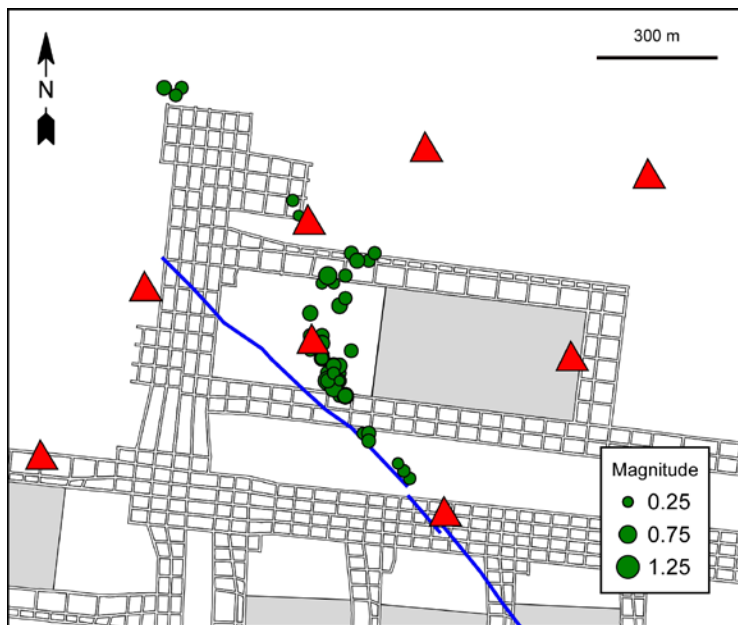


Figure 23. Seismic activity recorded during temporary deployment of broadband stations (red triangles) above active longwall.

District- and Mine-wide Networks Option

A mining district-wide network has dimensions large enough to encompass more than a single mining operation. The example described here is jointly owned and operated by coal mines of the North Fork Valley, Colorado, and NIOSH [Swanson et al. 2008]. As originally conceived, the network was designed to cover a single mine to investigate relative amounts of natural seismicity versus activity generated in the longwall caving process. Developing empirical relations between seismic event magnitude and levels of shaking measured at various distances was another research goal. Over time, the network grew to cover three separate operating longwall mines, all of which have a history of coal bursting [Mark et al. 2012]. Additional objectives were developed to implement a real-time event monitoring and notification tool, and to collect data for use in research studies aimed at quantifying impacts from mining-related seismicity. The potential impacts include dynamic rock mass failures, or bursts, as well as strong shaking in the vicinity of critical structures such as impoundment dams, reservoirs, mine seals, mine openings, and steep slopes.

Most longwall mining in this district takes place in three different coal seams under the variable topography of mountain-canyon terrain. Depth of cover extends up to 800 m (2,600 ft). Competent sandstone units are present with variable thickness and distance above and below the minable seams.

Stations

Historical reports of seismic activity in this district described events up to M3 and higher; therefore, strong-motion accelerometers were selected. Strong-motion seismographs are specifically designed to measure ground motions near seismic sources that are strong enough to potentially impact the integrity of engineered structures. An additional 1-Hz moving-coil seismometer was also included at the same location to provide higher sensitivity to smaller and/or more distant seismic events. The data recorders are configured to continuously stream data at 100 samples per second, and to trigger and save event data to local digital storage media. Time synchronization was provided by GPS receivers at each site.

A total of 17 stations was ultimately installed in the district (Figure 24), providing a coverage area of approximately 300 km² (120 mi²). Outlines in Figure 24 show lease boundaries for the three district mines. The average distance between seismic sources and the nearest five stations of the network is ~3.0 km (1.8 mi) with the largest distance averaging ~19 km (12 mi). This station spacing provides suitable coverage as a district-wide network. However, if only one mine was present and the array had fewer stations but similar station density, it could effectively serve as a coarse mine-wide network. In both district- and mine-wide networks, stations are confined to the surface because few places in an underground coal mine remain accessible for very long since longwall sections are continually excavated and subsequently sealed.

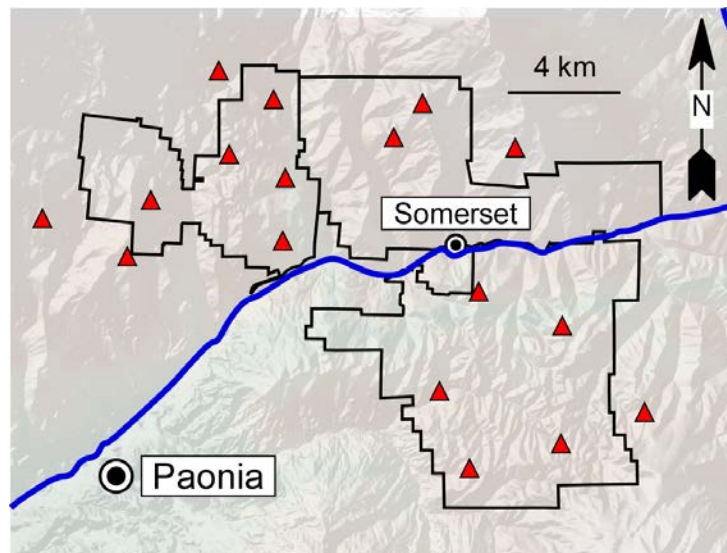


Figure 24. Seismic stations of the North Fork Valley district network (triangle symbols).

Station sites were selected to provide suitable azimuthal coverage of the mining areas, a workable telemetry path, concealment from view, and, wherever possible, access to bedrock. Separate instrument and power vaults were installed by digging shallow holes and installing vertically oriented, corrugated steel culverts with locking lids (Figure 25). A flat concrete floor was poured onto exposed bedrock in the instrument vault, onto which the strong-motion seismometer was bolted. Remote power sources were constructed with photovoltaic panels and deep-cycle batteries.



Figure 25. Seismometer, remote power, and telemetry infrastructure of a typical district-wide network station.

Data Communications

A variety of license-free radio networks are used to communicate with and transfer data from the seismic stations. Continuous digital seismic waveform data is sent from each station to a central site equipped with an Internet connection. The serial/IP data network allows complete control over the instruments from distant Internet-connected user locations.

Data Processing

A large portion of the data collection, processing, analysis, and display components uses the Earthworm software [Earle et al. 2003; Friberg et al. 2010]. The freely available, open-source software is configured to automatically detect, process, archive, and analyze seismic events from numerous types of seismic sensors and to make the raw data and processed results available over a computer network and the Internet. Earthworm has been in use since the late 1990s and, while initially receiving major support from the USGS, it is now supported and further developed through an active international network of users and operators of seismic networks, in addition to contractors hired by the USGS.

One of the powerful features of Earthworm is its distribution of data acquisition and processing across computers of mixed operating systems that are connected via a network. In the mining-district-wide network example described here, the main data acquisition, communications, and processing computers are located in a secure location with Internet access in the field. Further processing, data archiving, web access, and email notifications are handled by computers in the NIOSH Spokane office.

After arrival times are automatically picked for each station by Earthworm, event locations are calculated using the Hypoinverse software [Klein 2014] with a layered velocity model. Empirical station correction factors are developed to help counteract the effects of spatial variations in seismic velocity. A discussion of how both station correction factors and multiple-event location methods can be used to improve event locations is given in Appendix D.

Magnitude estimates are obtained from Earthworm modules using both the duration of seismic signals (coda magnitude) and their amplitudes (local/Richter magnitude). A moment magnitude Earthworm module is currently in beta testing.

Data Access

Raw and processed data are made available to users in several ways. Data can be accessed via a password-protected web page. The web page provides access to helicorder plots, triggered-event waveform files, event location and magnitude calculations from the automated processing, and summary peak ground motion data for each station. Time-critical information can also be distributed via email, pager, and/or text messages.

Event Location Display

Outside of Earthworm, a web server provides continuous reporting of seismic activity in the vicinity of the network. Client software provides near real-time maps of event locations, magnitudes, and times of occurrence based on the automated processing results with different audible notifications based on selected magnitude thresholds. Both server and client software use the Java-based California Integrated Seismic Network (CISN) model, designed for California earthquake monitoring and emergency management 24/7 operations centers (<http://www.cisn.org/>).

Custom modifications were made to the CISN software to provide additional control of the quality of the displayed events. Such quality control is desirable when results from wholly automated processing are accessed by non-seismologist users. Some event locations and magnitude assignments can be erroneously calculated because software currently cannot entirely replace the judgment of a human analyst. Such erroneous results occur, for example, with low signal-to-noise ratios or when multiple seismic events occur close together in time. These additional display control parameters increase the robustness of the event reporting and reduce the display of poorly constrained events when operating under the standard wholly automated processing conditions.

Email, Text, and Pager Notifications

Automated emails are used to notify users about the occurrence of events and high-acceleration levels using two separate Earthworm modules. Email recipients can tailor the conditions required for email issuance by specifying values for acceleration threshold, station names, minimum event magnitude, and distance to the event from individual stations. When strong ground shaking in the vicinity of critical structures is of concern, emails can be automatically issued to a list of users when threshold accelerations are met or exceeded. Emails may also be issued upon the occurrence of an event, independent of the observed acceleration levels, which include a map showing the event's location and waveforms with automated phase picks.

Example Results

The software-automated results can generally be used to identify the specific mine, or section of a mine, in which particular events ($M > 0$) occur. Figure 26 is based on the output from the CISN (also known as Quakewatch) client, showing a 60-day period in 2015 where all of the events ($0 \leq M \leq 3.0$) were processed in software without any human intervention. Three clusters of activity are apparent in the northern section. The westernmost cluster is associated with active

longwall mining in a panel with overburden ranging from 335 m to 600 m (1,100 to 2,000 ft). The two clusters to the east of this longwall originate in old mined-out areas where mining is no longer taking place. The middle cluster centers on an area where there was multi-seam longwall mining under 500 m (1,700 ft) of overburden; mining ceased in this area in 2010. The easternmost cluster is centered on a longwall district under cover ranging from 500 m to 800 m (1,700 to 2,600 ft) where mining stopped in 2012. The diffuse activity to the southeast occurs in areas containing both previous longwall mining under depths of cover up to 700 m (2,300 ft) and an active longwall mining under ~200 to 335 m (700 to 1,100 ft) of cover.

The distribution of general seismic activity across this district shows that there is a significant variety in the seismic response of both the active and formerly active mining areas. The awareness of the activity and the ability to discriminate between events occurring at the different mines, and within specific areas of the same mine, comes directly from the automatically processed results.

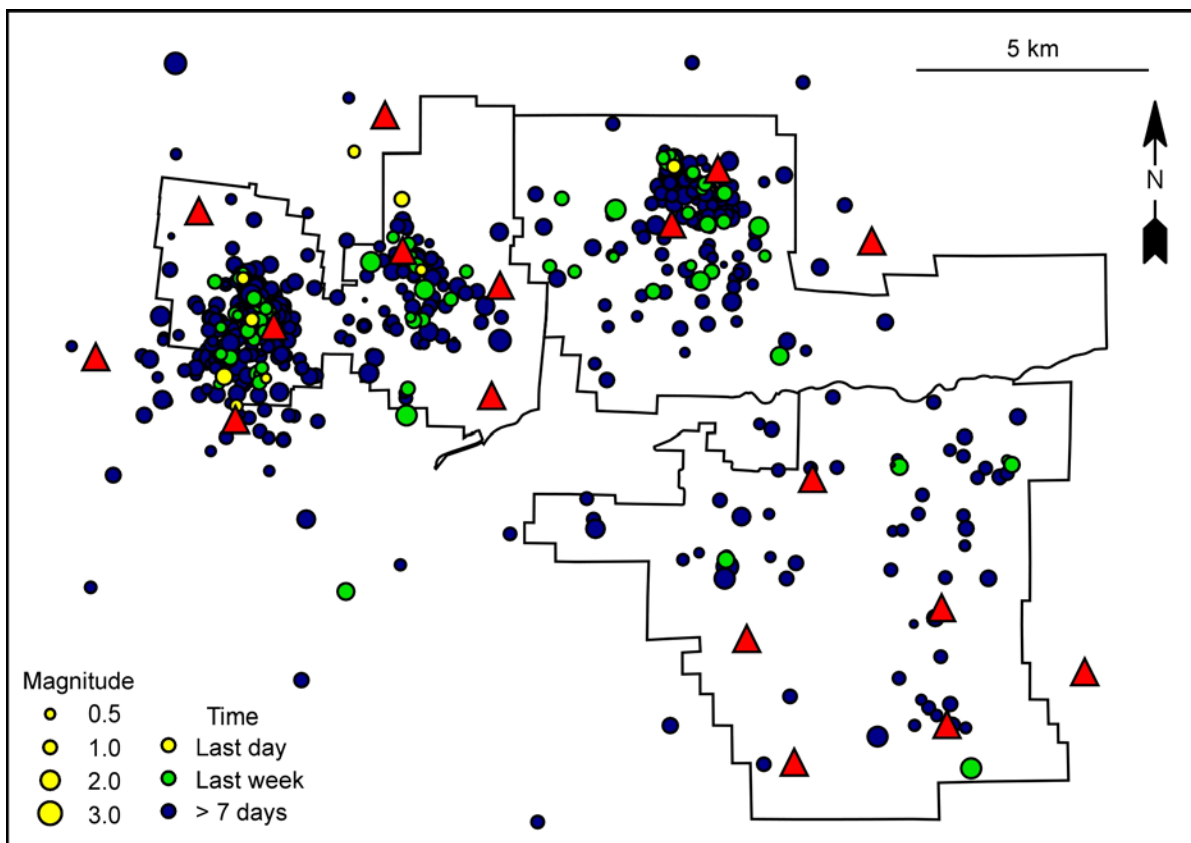


Figure 26. Software-automated event locations from district-wide network over 60-day period.

District-wide network data can, with the additional effort of making manual adjustments in arrival time picks and reprocessing, resolve further detail on deformation processes operating on the scale of individual longwall panels and smaller areas. Two examples are presented below to illustrate this point.

Seismic Event Sequence in a Working Area

A dynamic failure of pillars and floor occurred during room-and-pillar retreat operations under 150–210 m (500–700 ft) of cover. The progressive failure was accompanied in rapid succession by four seismic events with $M \geq 2.0$. Seismic activity ($M \geq 1$) as a function of time is shown in Figure 27A. A spike in seismic activity occurs on the first day with additional events tapering off with time. An unfiltered helicorder record from a station 3 km (2 mi) away is shown in Figure 27B. A closer look at the timing of the large-event seismic activity (large events on red trace) reveals that the period of increased seismic activity did not initiate with the occurrence of a large seismic event, as observed for some rockbursts, but rather the four large ($M \geq 2$) seismic events occurred over the span of 3.5 minutes approximately 8 hours after the start of the accelerating seismic activity. The large events were apparently more of a compounding effect than a cause of the initiation of the instability. An area of burnt coal was encountered adjacent to the workings, indicating possible enhancement of overburden loading in the area of mining due to volume reduction of the adjacent oxidized coal. Figures 27C and 27D illustrate the temporal and spatial progression of the seismic activity, which generally coincides with the damaged area. While the time history plot in Figure 27C includes events with $M \geq 1$ that were automatically processed, the plot in Figure 27D is limited to manually processed events with $M \geq 1.5$.

The unusual occurrence of four large seismic events within a few minutes presented some difficulty for the automated processing. As the software had difficulty recognizing where one event started and the next one ended, the system inferred fewer events but with larger magnitudes than obtained with manual processing.

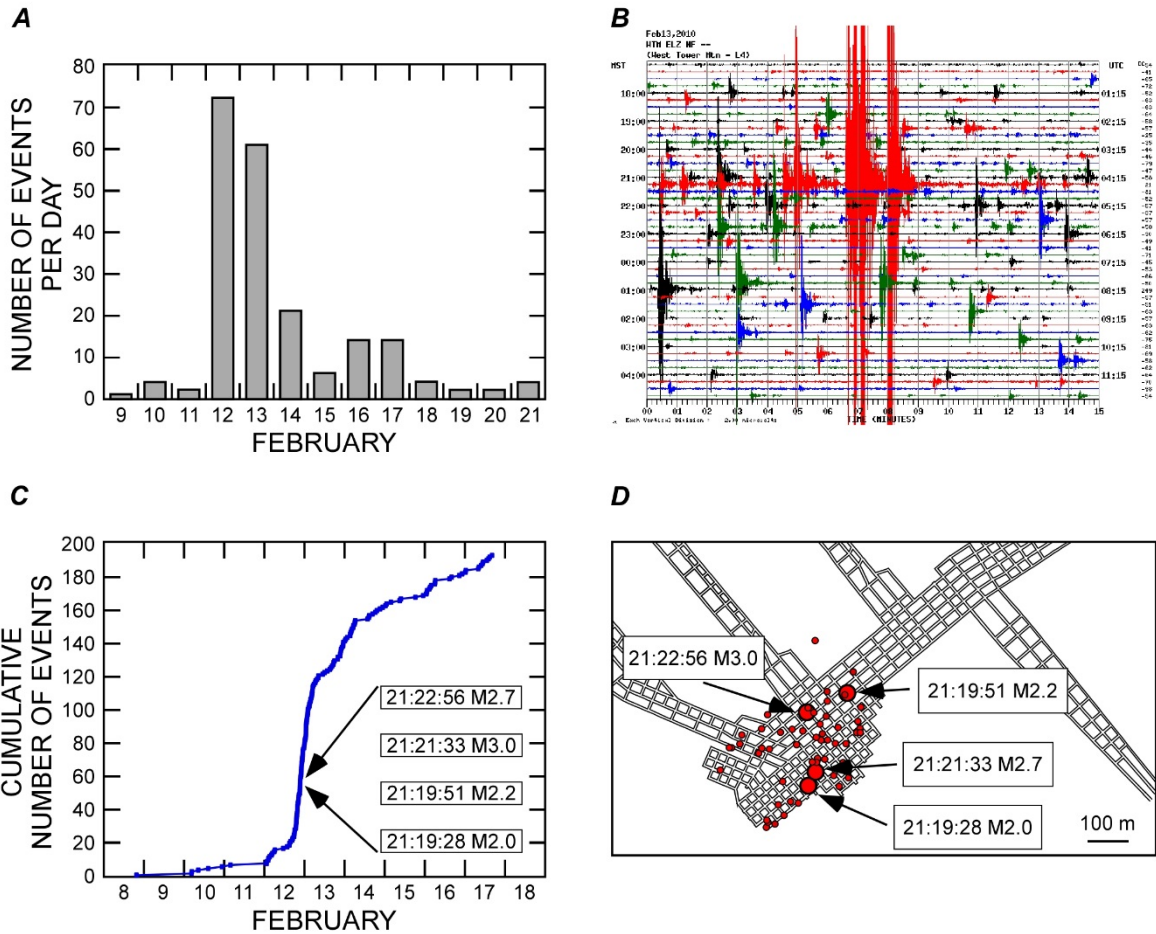


Figure 27. Seismic response to progressive failure. (A) number of events per day with $M \geq 1$, (B) helicorder plot from day with four events with $M \geq 2$, (C) cumulative number of events during progressive failure, (D) map view of manually processed event locations.

Monitoring the seismic response of the progressive failure with the district-wide system provided documentation of the: (1) extent of the disturbed area generating seismic activity, (2) magnitudes of the events, and (3) times at which activity accelerated and then abated. The latter provides information to help identify the return of the ground to a stable state, which is useful for making decisions regarding the progress of an accident investigation and plans for mine recovery.

Seismic Event Sequence in an Inaccessible Area

The second example illustrates a period of elevated seismic activity that coincided with the extraction of the last panel in a five-panel longwall sequence. Depth of cover over panel 5 ranged from 350 to 575 m (1,150 to 1,900 ft) and had steadily increased from 150 m (500 ft) as panels 1 through 5 were mined (Figure 28). Numerous steeply dipping fault structures cut across the panels.



Figure 28. Map showing a five-panel longwall section traversed by several steeply dipping faults (blue lines).

As extraction began on the fifth panel, the seismicity rate, reflected in the slope of the cumulative number of events as a function of time (Figure 29), increased substantially (months 31–39) and remained quite constant as the panel was mined at a nearly constant rate—the average retreat rate over all panels was 7.2 ± 0.5 m/day (24 ± 2 ft/day). Observations made in an investigation of manually processed events with $M \geq 1.5$ include: (1) rapid increase in the seismicity rate with the mining of the fifth panel was not accompanied by any notable, or unusual, change in ground response in the working areas, (2) most of the activity (Figure 30) was confined to inaccessible areas behind the longwall face, occurring up to 500 m (1,600 ft) back, (3) events along the tailgate had a larger average magnitude than the events along the headgate, and (4) seismic activity did not appear to be dominantly affected by the presence of faulting. These observations are consistent with our qualitative understanding of how the rock mass should respond to a growing number of adjacent panels under increasing overburden conditions. The increasing rate of seismicity (56, 63, 340, 728, and 2,608 events with $M > 1.0$, respectively, for panels 1–5) is a reflection of the combination of increasing span of the overall excavation—which reduces the stiffness of the global rock mass loading environment—and increasing depth of cover. Studies that use such data sets to evaluate how well numerical modeling predictions match field observations are currently underway.

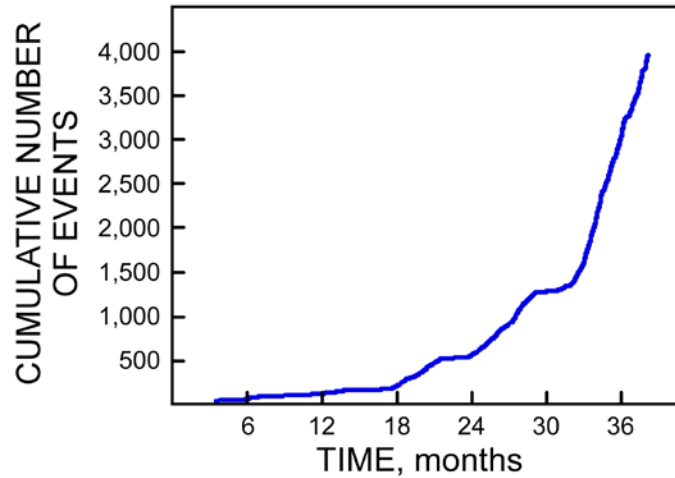


Figure 29. Cumulative number of seismic events with $M \geq 1.0$ during a 5-panel extraction sequence, showing a significant increase in activity during mining of the fifth panel (months 31–39).

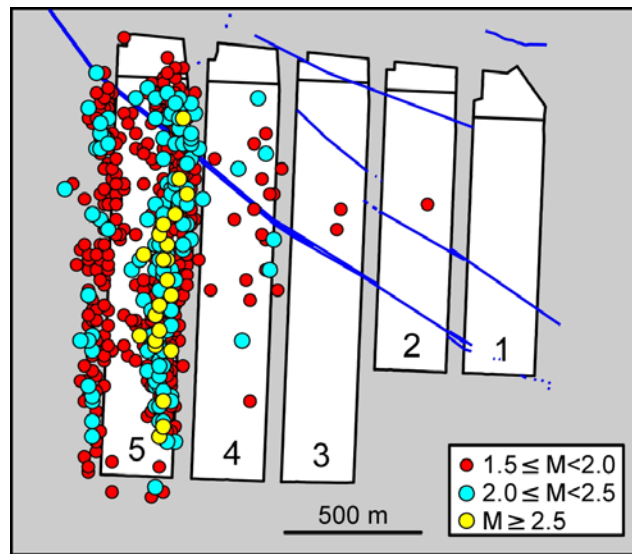


Figure 30. Seismic event locations during mining of fifth panel in 5-panel sequence.

Summary

A district-wide seismic network with software-automated processing provides: (1) a real-time monitoring tool to bring awareness and documentation of seismic activity, (2) automated event locations that differentiate sources between mines or locations within an individual mine, and (3) an automated communication tool for distributing information on the occurrence of events and levels of observed peak ground motion. With additional effort expended in manual processing and analysis, dynamic failure processes on the scale of individual longwall panels, or smaller areas, can be better scrutinized.

Microseismic Monitoring Network Option

A microseismic monitoring network uses a focused, dense sensor array to target a limited area of mine workings. As described herein, our emphasis is on active longwall panels or a series of adjacent panels under deep cover. These types of networks are known variously as panel-scale, face-centered, or close-in networks [Arabasz and McCarter 2009]. They are intended to provide detailed coverage of seismically related deformation in active mine workings as opposed to a mine-wide or district-wide system that monitors only the largest events over a broad region without focusing in any one area. Compared to the latter systems, a microseismic network offers higher event detection sensitivity and better spatial resolution of event locations.

In a production environment, the only practical way for a mine operator to implement this scale of a network is to secure the services of a commercial vendor that provides microseismic monitoring in underground mines. With the voluminous amount of event data possible, the additional advantage of the commercial vendor is the availability of 24/7/365 support and the possibility of conducting all processing, analysis, and report generation externally via a service contract. A microseismic network also requires the greatest amount of upfront, and annual, cost and participation by mine personnel. Only a few highly specialized companies provide these networks to the mining industry as a day-to-day production tool.

A commercial microseismic system was evaluated by NIOSH in a joint effort with a coal operator in one of the North Fork Valley coal mines. The system was deployed while extracting longwall panels under depths of cover ranging from 460 to 800 m (1,500 to 2,600 ft) and is described in the sections that follow.

Stations

To minimize the distance between the expected event locations and the seismic stations, eight geophones were installed underground and 10 to 12 were placed on the surface (Figure 31). Due to the limited areas where underground stations could be placed, raypaths to many of the surface stations were often shorter than those to the more distant underground stations; signals to surface stations frequently appeared among the first five P-wave arrivals, despite the thick overburden.

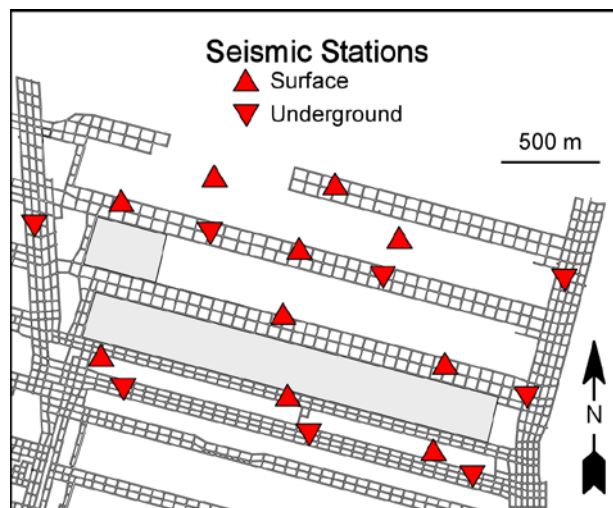


Figure 31. Surface and underground geophone stations of microseismic array covering one or more adjacent longwall panels.

Stations installed in the mains and headgate were confined to fresh-air entries. Geophones were periodically removed in the headgate and relocated ahead of the face to remain in fresh air. Although recommended use in hardrock mines is to install the 14-Hz triaxial geophones in 10-m-deep boreholes, in this example the geophones were mounted on the roof to facilitate easy removal and relocation. Circuitry to extend the low-frequency range was used with all geophones to enhance measurements of corner frequencies of the large magnitude events. Low-power digitizing units were located adjacent to the geophones and, at the end of long cables, the current-limiting receiving electronics were located in fresh air with other mine control and communications electronics. A fiber-optic cable provided timing and network communications with the surface where the system server merged surface and underground data streams into the processing system.

Surface geophones were located 450 to 800 m (1,500 to 2,600 ft) above the coal seam. The 4.5-Hz triaxial sensors were mounted on concrete pads (Figure 32A), positioned to take advantage of any near-surface bedrock, avoiding where possible direct placement over underground areas that were to be fully excavated. Remote photovoltaic systems (Figure 32B) powered each station's digitizing and communications electronics with a digital radio telemetry link back to the Internet-connected data acquisition and processing server. Station timing is provided through GPS receivers. A temporary mounting platform for the power, data acquisition, and communications infrastructure allows for periodic relocation of the surface stations to maintain an appropriate distance to the active panels as panels are excavated, and as gob-vent borehole access roads are reclaimed.

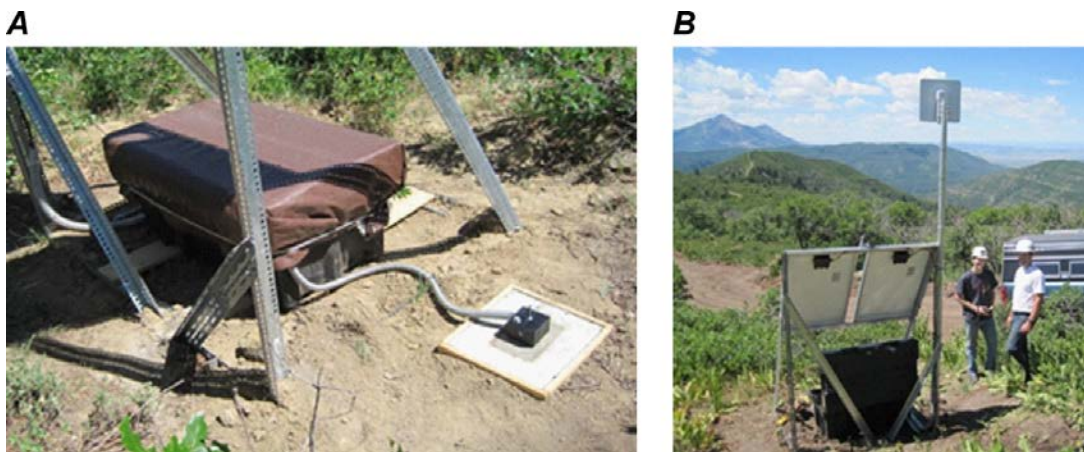


Figure 32. Surface station of microseismic network, showing: (a) triaxial surface geophone prior to burial and (b) station infrastructure platform.

During monitoring of the first two panels, the array footprint measured approximately 2,600 by 1,500 m (8,500 by 5,000 ft), which then expanded northward as additional panels were mined. The average three-dimensional distance between a seismic source and a geophone for the first five arrivals was ~550 m (~1,800 ft) with a maximum distance of ~1,800 m (~5,900 ft). Such sensor spacing would qualify this system as a mine-wide system under the sensor density specifications outlined by Mendecki et al. [1999] for hardrock mines (5 sensors within 1 km (3,300 ft)) instead of a microseismic monitoring system (5 sensors within 300 m (1,000 ft)). Nevertheless, we retain the term “microseismic” with our emphasis on focused monitoring in the vicinity of a rapidly moving face over a region that is considerably smaller than the overall areal extent of the mine.

Data Processing

Sampling rates for underground and surface stations were 5,000 and 1,000 samples per second, respectively. Local data screening takes place at each station to determine candidate events rather than transmitting a continuous data stream to a main system computer. Apparent event triggers from each station are associated into coherent events at the main data collection computer where further processing occurs (event locations and source parameter estimates). Event files are then saved to disk and manually processed. Moment magnitudes are calculated based on a combination of event moment and energy measures. Magnitude ranges observed during the monitoring period extended from 3.4 down to -3, with as many as 3,500 triggered event files recorded each day during active periods. As the smallest events were not of great interest in this study, a threshold of 10 station triggers was set as the minimum required for processing an event. Such a large number of reporting stations ensured that the event was big enough to provide adequate signal-to-noise ratio to place reasonably good constraint on solutions of event locations.

The main data collection and processing PC was located in a deeply incised canyon where there was no conventional commercial Internet access available. Consequently, a satellite receiver was used to provide connectivity. In addition to remote access and control, triggered event files, summary event parameters, etc., were continually copied to a remote data analysis platform at NIOSH for viewing, archiving, analysis, and manual reprocessing.

Event locations were calculated using a dipping, layered velocity model. Two- and three-layer simplified models were developed through a simultaneous inversion of arrival times for both event locations and velocity model [King 2012]. This procedure was developed to provide the ability to periodically update the velocity model as mining progressed. A two-layer model with the interface between the layers positioned at the coal seam was used in the event locations presented herein. The P-wave velocities of the upper and lower layers were 2,771 m/s (9,091 ft/s) and 3,880 m/s (12,467 ft/s), respectively. While the two-layer model provided a more realistic event distribution than a homogeneous isotropic model, the results shown in the next section, Example Results, indicate the need for a three-dimensional velocity model to adequately account for the impact of voids, gob, and fracture zones resulting from the excavation.

Resolution of the vertical location coordinate is difficult with the sensor geometry, as in Figure 31, coupled with the uncertainties in the velocity model. Additional processing effort is required to place confidence in the vertical positions of the activity, as small perturbations in the rapidly changing velocity in the vertical direction can have significant changes in the calculated vertical location coordinate.

S-phases are ordinarily used to increase the constraint on event locations in hardrock mines with homogeneous isotropic velocity structure, especially for systems with few stations. Using S-phases in the location process in this coal mine environment, however, had the opposite effect. Several factors are thought to contribute to this behavior: (1) anisotropy in the layers between the coal seam and the surface, (2) violation of assumption of constant V_p / V_s ratio, (3) shear-wave splitting, and (4) the presence of high-amplitude trapped and interface phases, which are mistaken for the S-phase on underground stations. The inconsistent, or misinterpreted, picking of the S-wave arrival resulted in event locations that were generally degraded; thus, use of the shear-wave arrival for locations was minimized.

Example Results

Microseismic activity observed over a seven-day period while mining the second panel of a longwall section is shown in Figure 33. The 4,331 events occurred as the face retreated 42 m (137 ft) during nine longwall production shifts (excavated area shown in yellow rectangle). Several features in this example highlight the types of information that are potentially available through scrutiny of seismic activity recorded by this scale of a network. The heaviest concentration of activity occurs in a broad band along the 250-m-wide (825-ft-wide) longwall face. Activity also concentrates along the tailgate (gateroad 2) behind the face with a light concentration of events ahead of the immediate face activity on the tailgate side. Similarly, there is a light concentration of seismicity on the pillars to the south of the first excavated panel (vicinity of gateroad 1). Both of these areas of activity might be a response to the increases in abutment stress from the extraction of the second panel, which are superimposed on stresses emplaced after the first panel is mined. There is also a notable concentration of activity behind the face on the headgate side (gateroad 3), but instead of concentrating on the headgate pillars themselves, they locate to the north of the headgate pillars in the solid coal of the next panel. The absence of activity in the headgate pillars and the presence, at a greater distance, of significant activity in the solid coal panel suggests systematic mislocation of the headgate pillar events to the north. Such systematic offsets are commonly observed in close-in network data with the mislocations generally occurring in a direction away from a low-velocity zone such as a longwall gob area. This effect arises because travel times are slower through the gob than are assumed with a uniform layered velocity model (e.g., Figure A46 in Appendix A).

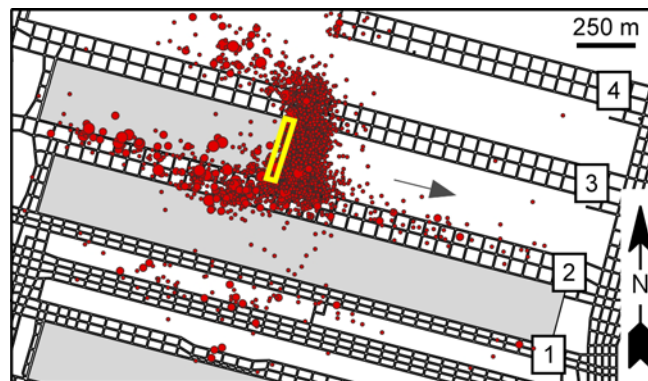


Figure 33. Seven days of seismic activity (red circles) located by the microseismic network during 42 m (137 ft) of longwall retreat (yellow rectangle). Completed longwall panels are shaded gray and unmined panels are white.

Despite the current uncertainties in event locations, it is clear that the data can be used to delineate temporal and spatial trends of deformation processes in a way that is not possible with visual observations. The pattern of deformation illuminated by the larger events is somewhat different from that inferred from the smaller-magnitude events of the microseismic data. To emphasize the larger events (shown in Figure 34), events with magnitudes in the ranges $0 \leq M < 1.5$ and $1.5 \leq M \leq 2.7$ (as confirmed with the district-wide network) are highlighted with blue and yellow symbols, respectively. Although the heaviest concentration of events located by the microseismic system cluster around the longwall face, the larger events occur more in the

gateroads and panel edge at the tailgate. The pattern of large-event seismic deformation is similar to the pattern observed with the district-wide network at the mine in Figure 30, where events with $M \geq 1.5$ were distributed along both gateroads behind the face.

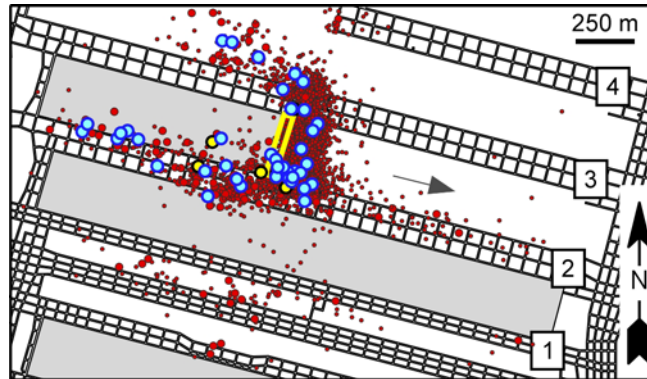


Figure 34. Large magnitude events during 42 m (137 ft) of longwall retreat ($0 \leq M < 1.5$, blue; $1.5 \leq M \leq 2.7$, yellow).

One of the clear benefits of the microseismic system is its ability to delineate finer-scale details of mine response not evident with arrays that are less dense and less sensitive. Even in the absence of active longwall mining, a time-dependent rock-mass deformation response becomes highlighted when tracking small-magnitude activity through time. Figure 35 shows events ($-2.7 \leq M \leq 1.2$) occurring over a one-month period several weeks after the first panel was completed. This one-month period of time coincided with the delayed resumption of longwall retreat as development of the second-panel headgate (gateroad 3) was finished. The concentration of activity midway along gateroad 3 in Figure 35 was produced during completion of this headgate. When viewed over similar periods of time, concentrations of low-level activity in areas without active mining were sometimes reported by the mine operator to be areas that ultimately required additional support. The concentrated activity along gateroad 2 is an example of an area that had such a time-dependent deformation response.

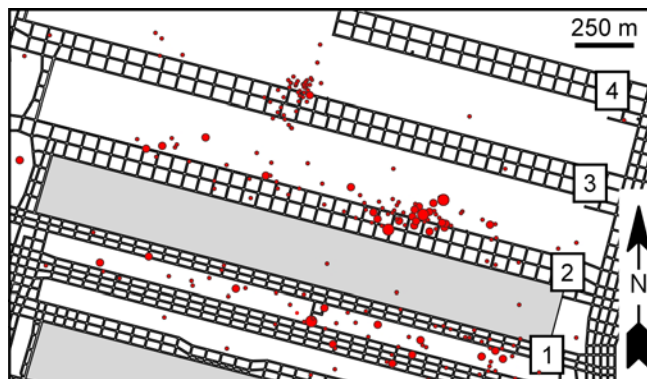


Figure 35. Microseismic activity observed during 30-day period of no mining.

On the time scale of individual mining shifts, or days of mining, a clear time-dependent response in microseismic activity was observed. Figure 36 shows the number of events located in each hour of the day over the course of one month of mining during two shifts a day (day and swing shifts). Longwall operation starts around 8 a.m. and generally continues at a steady rate until an hour or so before midnight (hour 24). Following the peak of activity between 9 and 10 p.m. (hours 21 and 22), the rate declines until the day shift resumes the next day.

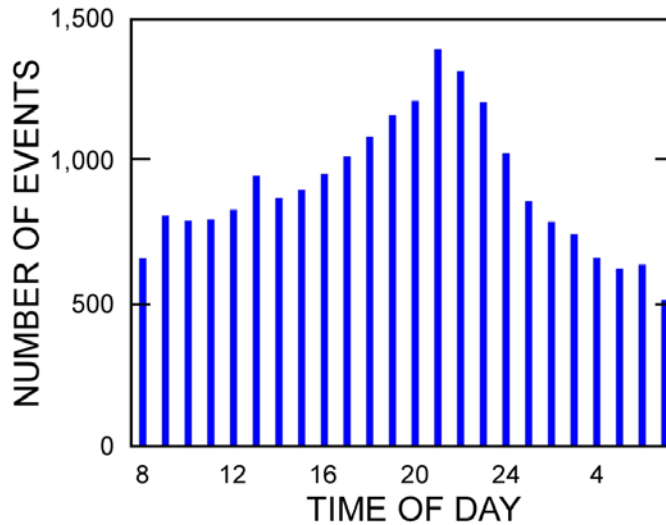


Figure 36. Number of seismic events detected during each hour of the day during a 30-day period with longwall production on both day and swing shifts. Peak activity occurs between 9 and 10 p.m. (hours 21 and 22).

Finally, in order to contrast the difference between the microseismic network and that of a mine-, or district-wide network, we compare the event detection sensitivity of each over a common recording period in Figure 37. The number of events recorded, processed, and located by each network, as well as longwall face-retreat distance, are shown for each day in this 10-day period. Approximately 32 times more events were detected and located by the microseismic (panel-scale) network than the district-wide network. An even larger number of microseismic events could have been processed with a reduction of the minimum number of station triggers specified for manual processing, which was purposefully set high to guarantee a high signal-to-noise ratio. On average, four triggered event files were recorded for every event that was manually processed with the minimum 10-station triggers criterion. If activity rates continued as observed in this 10-day period for one year, the district-wide network would have reported 972 events for this mine, while the microseismic network would have located 30,945 events and recorded 118,100 waveform files.

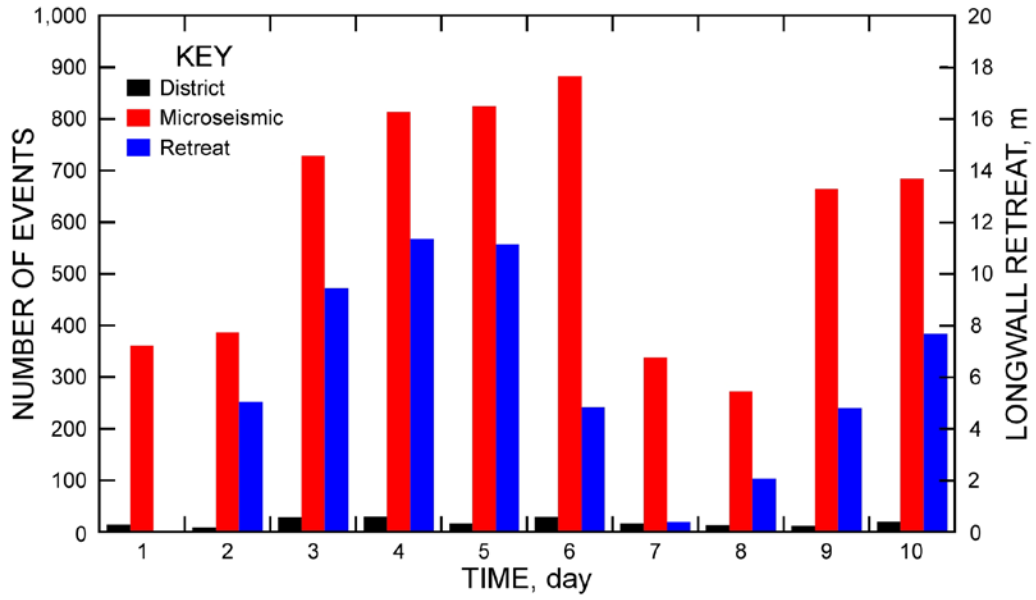


Figure 37. Seismic activity per day detected by microseismic-scale (panel-scale) and district-wide networks and daily longwall retreat distances.

Discussion

Many of the objectives for seismic monitoring in deep coal mines can be met by more than one monitoring strategy. Monitoring objectives and appropriate strategies to meet various objectives are identified in Table 3.

Table 3. Seismic monitoring objectives matched to monitoring strategies

Objective	Single station monitoring	Augment regional network monitoring	Temporary deployment monitoring	District-/ mine-wide monitoring	Micro-seismic monitoring
Awareness	X	X	X	X	X
Documentation for external sources		X	X	X	
Documentation for in-mine sources			X	X	X
Vibration levels	X		X	X	X
Rescue response, damage assessment			X	X	X
Resolve mine and geologic structures			X	X	X
Post-event analysis			X	X	X
Evaluation/verification of mine design			X	X	X
Hazard assessment			X	X	X

Factors Guiding Strategy Selection

Required location accuracy and anticipated event magnitude guide the selection of which monitoring strategy is most appropriate. In general, event location errors are reduced and smaller events are detected by increasing sensor density as in the progression from regional- to district- to mine-wide to microseismic-scale networks. If the goal is to evaluate the progression of failure that culminates in periodic caving of a massive cantilevering roof layer above a longwall face, a microseismic network may be desired. The high sensitivity and sensor density of a microseismic network provides the ability to detect and locate small-scale fractures attending macroscopic failure progression (e.g., [Hayes 2000]). If the objective is to provide documentation of the absence of activity in a mining operation that expects none, a single station with continuous monitoring can provide information to satisfy this objective. Alternatively, if it is desired to be able to differentiate between modest-sized events occurring in old workings and the adjacent current active workings, then a system with appropriate event location accuracy must be selected.

Pre-installation Estimates of Event Location Accuracy

Based on experience in hardrock mines, recommendations have been made for minimum source-to-receiver distances in different types of monitoring networks (e.g., [Mendecki et al. 1999]). Table 4 identifies recommended minimum source-to-receiver distances, or sensor densities, associated with district-wide, mine-wide (or shaft-wide), and microseismic-scale networks in deep South African hardrock mines. The networks are assumed to contain five triaxial sensors, yielding 15 total components reporting either P or S phase arrivals. If shear-wave arrivals are not used, a higher sensor density than is shown in Table 4 is required to provide the same constraint on event locations. Sensor densities are specified as average source-to-receiver distances for the first five sensors reporting arrivals. Sensor densities listed in Table 4 are suggested minimum values, and much higher sensor densities are found in many hardrock mines.

Table 4. Minimum sensor densities for different scale networks (after [Mendecki et al. 1999])

Network	Scale (km)	Minimum Magnitude	Minimum sensor density
District/Regional	1–30	0	5 sites within 5 km of source
Mine-wide	0.3–5	-1	5 sites within 1 km of source
Microseismic	0.1–1	-3	5 sites within 0.30 km (300 m) of source

For comparison, the coal mine district-wide and microseismic-scale network examples have sensor density distances of five sites within 3.0 km (1.9 mi) and 550 m (1,800 ft), respectively. Although network labels do not directly carry over between hardrock and coal mines, the important parameter guiding implementation of seismic monitoring is event location accuracy, so that station density is of first-order concern.

One rule-of-thumb estimate for event location accuracy is that, with a suitable velocity model, the uncertainty in the location can approach as small as ~3% of the average source-to-receiver distance. Thus, the shorter the source-to-receiver distances are, the smaller the location uncertainties. Implicit in this estimate is that errors in station coordinates, arrival-time measurements, and velocity represent random fluctuations. For velocity variations of 3% or higher, Durrheim et al. [2007] recommend either omitting arrival picks from certain stations or implementing a more detailed velocity model (i.e., something other than homogeneous isotropic). Applying the 3% rule-of-thumb to the average source-to-receiver distances of Table 4 yields location errors of 150 m (500 ft) for district-wide, 30 m (100 ft) for mine-wide, and 9 m (30 ft) for microseismic networks. Even for hardrock mines, these values should be considered to be minimum location uncertainty values obtained under idealized conditions.

In coal mining environments, the spatial variation in seismic velocity clearly varies with the lithology, and to a far greater degree than 3%. As a result, a much greater effort is needed to establish realistic layered velocity models to achieve the same constraint on event locations.

Effects of Heterogeneous Velocity Structure

Standard location methods using homogeneous layered velocity models appear satisfactory for accomplishing objectives where the demands on location accuracy are not stringent, including: awareness, documentation, vibration measurement, and rescue response (Table 5). Improvements in event locations do appear necessary when the objective is to resolve microseismic activity on particular mining or geological structures. Such is the case with post-event analysis, mine design evaluation, and hazard assessment. Generally, in order to achieve the necessary location improvements to adequately meet these objectives, a 3D heterogeneous model is required. However, there are some nontrivial techniques that may increase event location accuracy sufficiently (two such techniques are presented in Appendix D) to allow for some of these objectives to be at least partially met with a homogenous layered model. Moreover, progress could be made in some areas with slightly less stringent location accuracy requirements (e.g., a mine-wide system can detect and locate large magnitude events to aid in long-term coal burst risk mitigation).

Table 5. Velocity model requirements for specific monitoring objectives

Objective	Homogenous layered velocity model	Heterogeneous velocity model
Awareness	X	X
Documentation for external sources	X	X
Documentation for in-mine sources	X	X
Vibration levels	X	X
Rescue response, damage assessment	X	X
Resolve mine and geologic structures		X
Post-event analysis		X
Evaluation/verification of mine design		X
Hazard assessment		X

As examples relevant to using microseismic networks to mitigate coal burst hazards, recent field measurements and modeling work have focused on load-transfer distance as an important measure of deep longwall mine performance [Larson et al. 2015]. Stress and deformation distributions revealed through three-dimensional spatial and temporal trends in microseismic event locations and source parameters can provide a much higher degree of constraint in measuring load-transfer distance than static rock mechanics measurements taken in limited, accessible areas of a mine. Similarly, assessment of the performance of different combinations of yield, abutment, and interpanel barrier pillars in mitigating burst hazards [Gilbride and Hardy 2004] could also benefit by comparing model projections with observations of seismic response.

Unfortunately, systematic errors in event locations (i.e., Figure 33) have the potential to skew such results. Therefore, improvements are necessary before these techniques can effectively satisfy these objectives.

There are two obvious approaches to increasing event location accuracy—increasing sensor density and implementing a more realistic velocity model. As described earlier, deploying sensors in the working areas at a much higher sensor density is not considered practical for many applications relevant over the scale of deep longwall coal panels. In addition, increasing sensor density does not eliminate the need for a more realistic velocity model. Use of three-dimensional velocity models to account for the influence of voids, pillar deformation, stress heterogeneity, and gob and fracture zone formation attending excavation can reduce systematic errors that stand in the way of accomplishing these objectives.

To aid in the construction of 3D velocity models, NIOSH has developed a prototype seismic calibration source for use in return-air entries [Swanson et al. 2014]. Initial tests under 600 m (2,000 ft) of cover indicate that the prototype has the range to provide repeatable P-wave first-arrival measurements to stations on the surface out to a horizontal distance of 800 m (2,600 ft) or more. Controlled sources provide the opportunity to refine, and gain confidence in, the velocity model and to reduce the disparity between known and calculated source locations. Efforts to incorporate three-dimensional velocity structures that evolve with longwall mining into microseismic event location algorithms are in progress [Boltz et al. 2016].

Hazard Assessment and Risk Management for Rockbursts

Seismic monitoring, analysis, and interpretation are key components of the hazard assessment and risk management system used in rockburst-prone hardrock mines. As we consider the application of these methods to address issues related to coal bursts, it is useful to reflect on the experience gained in hardrock mines. In 2007, Durrheim et al. reported on a major effort to review the seismic monitoring component of rockburst risk management practice in South African mines, and “to formulate standards, guidelines, and descriptions of best practice.” Although it was possible to set standards for some areas of mine seismology practice such as network design and emergency response, in other areas of practice, such as seismic hazard assessment and risk management, it was acknowledged by Durrheim et al. [2007] that “most methods currently in use have not been rigorously evaluated and validated.” To a greater or lesser extent, “many methods were found to rely on local experience and subjective judgment.” As a result, it was “deemed premature to set standards, or even firm guidelines,” because this knowledge and experience had not yet been translated into explicit guidelines.

Thus, although the monitoring technology has been widely implemented for satisfying numerous objectives, including hazard assessment and risk management, the knowledge and experience in these areas have not been readily translated into explicit guidelines. This was particularly so for short-term hazard assessments (SHA). As concluded by Durrheim et al. [2007]:

“Long- and medium-term seismic hazard assessments are widely used when designing mine layouts and sequences. However, there is unanimous agreement that the short-term SHA is not reliable enough to be used for routine rockburst risk management, despite considerable research effort. Although this has proven to be a difficult, and perhaps intractable problem, it is believed to be worthwhile to persevere

with efforts to improve SHA procedures. There are several promising avenues of research. For example, the forecasting of rockbursts might be improved through real-time integration of seismic and rock deformation data . . . mining data, and numerical models of rock mass behaviour.”

Implementation

Estimates of the levels of complexity, staff time, and expense associated with implementing each of the five different monitoring strategies are shown in Table 6. The deployment of a single station can readily be accomplished by tech-savvy members of the engineering/geology staff. In contemplating applying seismic monitoring to any ground control problem, it is strongly advisable to acquire some preliminary, or sample, data to inform the network selection and design process. For the small amount of expense and effort, deployment of a single station offers a wealth of information concerning the character of signals, and the frequency and amplitude of vibrations. If the mine is located within, or near, the coverage area of a regional seismic network—which are mostly operated by universities—mine staff are likely to find a welcome response to an offer to host a station of the network. Adding stations to such networks improves the event detection sensitivity and location accuracy all across the array. Deployment of a temporary network can involve installation of stations in any of the configurations and station densities of the other approaches, with more staff time required for underground installations. Although it may be possible to find a university or other research group to team up with for development of a mine-wide or district-wide network, one is more likely to find a vendor that specializes in conventional earthquake or mining seismology. Microseismic monitoring in hardrock mines is a mature business, and at least two vendors with worldwide experience in installing, servicing, and providing data processing services for underground mining provide services in the United States.

Table 6. Levels of complexity, staff time, and expense for different seismic monitoring strategies

Seismic Monitoring Strategy	Level of Complexity	Mine Staff Involvement	Expense
Single station	Low	Medium	Low (\$1–10k)
Augment regional network	Low	Low	Moderately low
Temporary network deployment	Low to medium (contract out)	Low to medium	Moderate (no on-going expense)
District- and mine-wide networks	High	Low to medium	Moderately high
Microseismic network	High	High	High (\$100k+)

Each monitoring option is amenable to providing real-time data display and distribution over a computer network, although this can be difficult with some forms of temporary networks. All options allow the collected seismic data to remain private. The only exception may be augmenting a regional seismic network, where data are often made public, but this would depend on the particular agreement with, and requirements of, the regional network.

It is evident that seismic monitoring can play a role in addressing coal mine ground control issues and other monitoring objectives. Adoption by industry, though, can only come through monitoring experience with attendant demonstration of its utility. The monitoring strategies reported herein provide several avenues for acquiring knowledge and experience that can be applied toward meeting varied objectives.

Conclusion

Deployment of seismic monitoring systems in the vicinity of deep longwall coal mines reveals a variety of seismic rock mass responses. These responses range from nearly aseismic to high-magnitude yet non-damaging activity to coal bursting. This report identifies numerous potential objectives for seismic monitoring, ranging from providing simple awareness of the ground response to mapping out the details of seismic deformation at the face on a real-time basis and over a wide range of magnitude scales. Several strategies for accomplishing desired objectives are described, along with examples of their deployments and potential avenues for their implementation.

Mapping spatial and temporal distributions of microseismic activity has the potential to improve mine safety through recognition of atypical rock mass response, evaluation of mine stability, and improved understanding of dynamic failures. Variations in the seismic velocity structure accompanying coal extraction pose a challenge for accurately locating seismic events.

In order to relate deformation on specific mine and geologic structures to microseismic activity, improvements in event location methodologies are needed. Significant progress in using microseismic data to achieve some of the ground control hazard assessment and risk management objectives will likely ensue with the implementation of realistic time-variable, three-dimensional velocity models.

Demonstration and independent validation of the utility of seismic monitoring in improving safety in deep U.S. coal mines is a prerequisite to acceptance and use of the technology by the mining industry. It is hoped that by offering five different approaches with a wide range in expense and complexity, we have identified several possible paths to explore and adopt the use of seismic monitoring as one of the tools in a mine's safety toolbox.

Acknowledgments

Special acknowledgment is given to the staff of all of the mining companies that participated in the field studies described in this report, and the numerous employees of the National Institute for Occupational Safety and Health (NIOSH), both in the field and office, all of whom contributed to the success of the field studies.

References

- ANSS [2014]. Advanced national seismic system. Performance standards Version 2.8. http://earthquake.usgs.gov/monitoring/anss/docs/ANSS_Perf_Standards.pdf.
- ANSS [2016]. Backbone seismic stations. Advanced National Seismic System (ANSS). <http://earthquake.usgs.gov/monitoring/operations/network.php?network=ANSS>.
- Arabasz WJ, Nava SJ, Phelps WT [1997]. Mining seismicity in the Wasatch Plateau and Book Cliffs coal mining districts, Utah, USA. In: Gibowicz SJ, Lasocki S, eds. Rockbursts and Seismicity in Mines, Rotterdam, A. A. Balkema Publishers, pp. 111-116.
- Arabasz WJ, Pechmann JC [2001]. Seismic characterization of coal-mining seismicity in Utah for CTBT monitoring. Lawrence Livermore National Laboratory internal report UCRL-CR-143772, Mar. 2001, 122 pp.
- Arabasz WJ, Nava SJ, McCarter MK, Pankow KL, Pechmann JC, Ake J, McGarr A [2005]. Coal-mining seismicity and groundshaking hazard: A case study in the Trail Mountain area, Emery County, Utah. *Bulletin of the Seismological Society of America* 95(1):18–30. doi:10.1785/0120040045
- Arabasz WJ, McCarter MK, [2009]. Task no. 1 seismic monitoring applicable to deep coal mines. University of Utah summary report NIOSH Contract No. 200-2008-25438. Studies to

Promote Development of Recommendations for Deep Retreat Coal Mine Safety, June 2009, 60 pp.

Baltz R, Hucke A [2008]. Rockburst prevention in the German coal industry. In: Proceedings of the 27th International Conference on Ground Control in Mining, July 29–31. Morgantown, WV: pp. 46-50.

Bischoff M, Cete A, Fritschen R, Meier T [2010a]. Coal mining induced seismicity in the Ruhr area, Germany. *Pure Appl Geophys* 167:63–75.

Bischoff M, Fischer L, Wehling-Benatelli S, Fritschen R, Meier T, Friederich W [2010b]. Source mechanisms of mining-induced seismic events in Hamm, eastern Ruhr area, Germany. In Proceedings 32nd European Seismology Commission General Assembly, Montpellier, France, September 6-10, 2010.

Boltz MS, Pankow KL, McCarter MK [2014]. Fine details of mining-induced seismicity at the Trail Mountain coal mine using modified hypocentral relocation techniques. *Bulletin of the Seismological Society of America* 104(1):193–203. doi:10.1785/0120130011.

Boltz MS, Chambers D, Swanson P [2016]. Effects of a three-dimensional velocity structure on the locations of coal mining-induced seismicity. In: Proceedings of the 50th US Rock Mechanics / Geomechanics Symposium, June 26–29. San Francisco, CA: 10 pp.

Bourbié T, Coussy O, Zinszner B [1987]. Acoustics of porous media. Édition Technip, Paris.

Brady BHG, Brown EH [1985]. Rock mechanics for underground mining. Kluwer Academic Publishers. 527 pp.

Brune JN [1970]. Tectonic stress and the spectra of seismic shear waves from earthquakes. *Journal of Geophysical Research* 75(26):4997–5009.

Castagna J, Batzle M, Eastwood R [1985]. Relationships between compressional-wave and shear-wave velocities in clastic silicate rocks. *Geophysics* 50(4):571–581.

Chambers DJ, Koper KD, Pankow KL, McCarter MK [2015]. Detecting and characterizing coal mine related seismicity in the Western US using subspace methods. *Geophysical Journal International* 203(2):1388–1399.

Cichowicz A [1993]. An automatic S-phase picker. *Bulletin of the Seismological Society of America* 83(1):180–189.

CDC [2012]. Map of locations of active underground coal mining operations, 2012. <http://www.cdc.gov/niosh/mining/UserFiles/statistics/12m1luoc.svg>.

Dehn K, Knoll S [2013]. Expansion, performance, and improvement of the Caladay Mines, Wallace, ID. In: Proceedings of the 47th US Rock Mechanics / Geomechanics Symposium, June 23–26. San Francisco, CA: 8 pp.

Dresen L, Rüter H [1994]. Seismic coal exploration part B: In-Seam Seismics. Pergamon Press, 446 pp.

Durrheim RJ, Anderson RL, Cichowicz A, Ebrahim-Trollope R, Hubert G, Kijko A, McGarr A, Ortlepp WD, Van der Merwe N [2006]. The risks to miners, mines, and the public posed by large seismic events in the gold mining districts of South Africa. In: Hadjigeorgiou J, Grenon, M, eds. Proceedings of the Third International Seminar on Deep and High Stress Mining. Université Laval, Canada, Section 30.

Durrheim RJ, Cichowicz A, Ebrahim-Trollope R, Essrich F, Goldbach O, Linzer LM, Spottiswoode SM, Stankiewicz T [2007]. Guidelines, standards and best practice for seismic hazard assessment and rockburst risk management in South African mines. In: Potvin Y, ed. Deep Mining. Perth: Australian Centre for Geomechanics, pp. 249–261.

Durrheim R [2010]. Mitigating the risk of rockbursts in the deep hard rock mines of South Africa: 100 years of research. In: Brune J, ed. Extracting the science: a century of mining research. Society for Mining, Metallurgy, and Exploration, Inc., ISBN 978-0-87335-322-9, pp. 156–171.

Earle P, Bittenbinder A, Bogaert B, Johnson C [2003]. Tune to the worm: Seismic network operation using the USGS Earthworm system. Observations and Research Facilities for European Seismology, Orfeus Newsletter 5(1).

Eisermann AS, Ziv A, Wust-Bloch GH [2015]. Real-time back azimuth for earthquake early warning. Bulletin of the Seismological Society of America 105(4):2274–2285. doi: 10.1785/0120140298

Ellenberger J, Heasley K, Swanson P, Mercier J, [2001]. Three-dimensional microseismic monitoring of a Utah longwall. In: Elsworth D, Tinucci JP, Heasley KA, eds. Rock Mechanics in the Public Interest. Proceedings of the 38th U.S. Rock Mechanics Symposium, July 7–10, Washington, D.C.:D.C. Rocks, Balkema, pp. 1321–1326.

Fletcher JB, McGarr A [2005]. Moment tensor inversion of ground motion from mining-induced earthquakes, Trail Mountain, Utah. Bulletin of the Seismological Society of America, 95(1):48–57. doi:10.1785/0120040047.

Friberg P, Lisowski S, Dricker I, Hellman S [2010]. Earthworm in the 21st century. In: European Geosciences Union General Assembly, 2–7 May 2010, Vienna, Austria, p. 12,654.

Fritschen R [2015]. DMT Group, Essen, Germany. Personal communication with Peter Swanson, December 2015.

Gates R, Guana M, Morley T, O'Donnell J, Smith G, Watkins T, Weaver C, Zelanko J [2008]. Fatal underground coal burst accidents, August 6 and 16, 2007, Mine Safety and Health Administration, coal mine safety and health report of investigation, CAI-2007-15-17, 19-24. 472 pp.

Gibowicz SJ, Niewiadomski J, Wiejacz P, Domański B [1989]. Source study of the Lubin, Poland, mine tremor of 20 June 1987. Acta Geophysica Polonica 37(2):111–132.

Gibowicz SJ, Young RP, Talebi S, Rawlence DJ [1991]. Source parameters of seismic events at the underground research laboratory in Manitoba, Canada: Scaling relations for events with moment magnitude smaller than -2. *Bulletin of the Seismological Society of America* 81(4): 1157–82.

Gibowicz SJ, Kijko A [1994]. *An introduction to mining seismology*, Academic Press, 396 pp.

Gilbride LJ, Hardy MP [2004]. Interpanel barriers for deep western U.S. longwall mining. In: *Proceedings of the 23rd International Conference on Ground Control in Mining*, August 3–5, Morgantown, WV, pp. 35–41.

Goodfellow SD, Young RP [2014]. A laboratory acoustic emission experiment under in situ conditions. *Geophys Res Lett* 41: 3422–3430, doi:10.1002/2014GL059965.

Gregory AR [1976]. Fluid saturation effects on dynamic elastic properties of sedimentary rocks. *Geophys* 41:895–921.

Hanks T, Kanamori H [1979]. A moment magnitude scale. *Journal of Geophysical Research* 84: 2,348–2,350.

Hatherly P, Luo X, Dixon R, McKavanagh B [1997]. Seismic monitoring of ground caving processes associated with longwall mining of coal. In Gibowicz SJ, Lasocki S, eds. *Rockbursts and Seismicity in Mines*, Rotterdam, A. A. Balkema Publishers, pp. 121–124.

Hayes P [2000]. Moonee Colliery: Renewing the economic viability of a mine using microseismic and hydraulic fracturing techniques in massive roof conditions. In: *Proceedings of the 19th International Conference on Ground Control in Mining*, August 8–10, Morgantown, WV, pp. 38–44.

Hudyma MR, Brummer RK [2007]. Seismic monitoring in mines – Design, operation, tricks and traps, in *Rock Mechanics: Meeting Society’s Challenges and Demands*. In: Eberhardt E, Stead D, Morrison T, eds. *Proceedings of the First Canada-US Rock Mechanics Symposium*. May 27–31, 2007. Vancouver, Canada, vol. 2 Case Histories, pp. 1,423–1,430.

Iannacchione AT, Zelanko JC [1995]. Occurrence and remediation of coal mine bumps: A historical review. In: *Proceedings of the Mechanics and Mitigation of Violent Failure in Coal and Hard-Rock Mines*, U.S. Bureau of Mines Special Publication 01-95, pp. 27–68.

Jones RE [1994]. Investigation of sandstone escarpment stability in the vicinity of longwall mining operations [MS thesis] Salt Lake City, UT: University of Utah, Department of Mining Engineering.

King AR [2005]. Source-parameter estimation in a coal environment. In: *Proceedings of the Sixth International Symposium on Rockburst and Seismicity in Mines*. March 9–11, 2005. Australia.

King AR, Talebi S [2007]. Anisotropy effects on microseismic event location. *Pure and Applied Geophysics* 164(11):2,141–2,156.

King AR [2012]. Velocity model determination for accurate location of mining-induced seismic events. In: Proceedings of the 22nd International Geophysical Conference and Exhibition. Feb. 26–29, 2012. Brisbane, Australia. Australian Society of Exploration Geophysicists (ASEG).

King MS [1966]. Wave velocities in rocks as a function of changes in overburden pressure and pore fluid saturants. *Geophysics* 31(1):50–73.

Klein F [2014]. User's Guide to HYPOINVERSE-2000, A Fortran Program to solve for earthquake locations and magnitudes. USGS Open-File Report 02-171, version 1.4, 123 pp.

Kubacki T, Koper KD, Pankow KL, McCarter MK [2014]. Changes in mining-induced seismicity before and after the 2007 Crandall Canyon Mine collapse. *Journal of Geophysical Research*, 119(6):4,876–4,889. doi:10.1002/2014JB011037.

Larson MK, Lawson HE, Tesarik DR [2015]. Load transfer distance measurements at two mines in the western U.S. In: Proceedings of the 34th International Conference on Ground Control in Mining. Barczak T, et al. eds. Morgantown, WV: West Virginia University, pp. 1–8.

Leighton F, Steblay BJ [1977]. Application of microseismics in coal mines. In: Hardy, Leighton, eds. Proceedings of the First Conference on Acoustic Emissions/Microseismic Activity in Geologic Structures and Materials. Pennsylvania State University, June 9–11, 1975, pp. 205–229.

Lin FC, Li D, Clayton RW, Hollis D [2013]. High-resolution 3D shallow crustal structure in Long Beach, California: Application of ambient noise tomography on a dense seismic array. *Geophysics* 78(4):Q45–Q56.

Luo X, Hatherly P [1998]. Application of microseismic monitoring to characterize geomechanical conditions in longwall mining. *Exploration Geophysics* 29, pp. 489–493.

Lurka A [2015]. Central Mining Institute, Katowice, Poland, personal communication, P. Swanson, December 2015.

Lynch R, Mendecki AJ [2001]. High-resolution seismic monitoring in mines. In: van Aswegen G, Durrheim RJ, Ortlepp WD, eds. Proceedings of the Fifth International Symposium on Rockbursts and Seismicity in Mines, Johannesburg, South Africa. South African Institute of Mining and Metallurgy, pp. 19–24.

Mark C, Gadde M [2008]. Global trends in coal mine horizontal stress measurements. In: Peng SS, Tadolini SC, Mark C, Finfinger GL, Heasley KA, Khair AW, Luo Y, eds. In: Proceedings of the 27th International Conference on Ground Control in Mining. Morgantown, WV, pp. 319–331.

Mark C, Phillipson S, Tyrna P, Gauna M [2012]. Characteristics of coal bursts in the North Fork Valley of the Gunnison River Valley, Colorado. In: Proceedings of the 31st International Conference on Ground Control in Mining. Morgantown, WV.

- McGarr A, Bicknell J, Sembera E, Green RWE [1989]. Analysis of exceptionally large tremors in two gold mining districts of South Africa. *Pure and Applied Geophysics*, *129*(3/4):295–307.
- McGarr A, Bicknell J, Churcher J, Spottiswoode S [1990]. Comparison of ground motion from tremors and explosions in deep gold mines. *Journal of Geophysical Research: Solid Earth*, *95*:21,777–792.
- McGarr AD, Simpson D, Seeber L [2002]. 40 Case histories of induced and triggered seismicity. *International Geophysics* *81*(A):647–661.
- McLaskey GC, Lockner DA [2014]. Preslip and cascade processes initiating laboratory stick slip. *Journal of Geophysical Research: Solid Earth* *119*:6,323–6,336. doi: 10.1002/2014JB011220.
- Megies T, Beyreuther M, Barsch R, Krischer L, Wassermann J [2011]. ObsPy – What can it do for data centers and observatories? *Annals of Geophysics* *54*(1): 47–58.
- Mendecki AJ [1993]. Keynote address: Real-time quantitative seismology in mines. In: Young RP, ed. *Balkema, Rotterdam. Rockbursts and Seismicity in Mines*, pp. 287–295.
- Mendecki A, van Aswegen G, Mountfort P [1999]. A guide to routine seismic monitoring in mines. In: Jager AJ, Ryder JA, eds. *A Handbook on Rock Engineering Practice for Tabular Hard Rock Mines. The Safety in Mines Research Advisory Committee, Johannesburg*, pp. 287–309.
- Minney D, Kotze G, van Aswegen G [1997]. Seismic monitoring of the caving process above a retreating longwall at New Denmark Colliery, South Africa. In: *Rockbursts and Seismicity in Mines, Proceedings of the Fourth Symposium on Rockburst and Mine Seismicity*, Balkema, Rotterdam. pp. 125–130.
- NAP [2001]. Review of EarthScope integrated science. National Academies Pres. Committee on the review of EarthScope science objectives and implementation planning. Board on Earth Sciences and Resources, National Research Council. ISBN: 0-309-07644-7, 76 pp. <http://www.nap.edu/catalog/10271.html>.
- Nicholson C, Simpson D [1985]. Changes in V_p/V_s with depth: Implications for appropriate velocity models, improved earthquake locations, and material properties of the upper crust. *Bulletin of the Seismological Society of America*, *75*(4):1,105–1,123.
- NIOSH [2010]. Research report on coal pillar recovery under deep cover. http://www.cdc.gov/niosh/mining/UserFiles/works/pdfs/Report_on_Coal_Pillar_Recovery_under_Deep_Cover_02-10.pdf.
- NRC [2012]. Induced seismicity potential in energy technologies. National Research Council. Washington, D.C.: The National Academies Press. http://www.nap.edu/catalog.php?record_id=13355.

- Oye V, Bungum H, Roth M [2005]. Source parameters and scaling relations for mining-related seismicity within the Pyhäsalmi ore mine, Finland. *Bulletin of the Seismological Society of America*. 95(3):1,101–1,126.
- Pechmann JC, Arabasz WJ, Pankow KL, Burlacu R, McCarter M K [2008]. Seismological report on the 6 August 2007 Crandall Canyon Mine collapse in Utah. *Seismological Research Letters*, 79(5):620–636. doi:10.1785/gssrl.79.5.620.
- Qi Q, Li J, Ning Y, Ouyang Z, Zhao S, Wei L [2015]. The technology and practice of rockburst prevention in Chinese deep coal mines. In: *Proceeding of the Forty-ninth US Rock Mechanics/Geomechanics Symposium*. American Rock Mechanics Association.
- Riemer K, Durrheim R [2011]. Mining seismicity in the Witwatersrand Basin: Monitoring, mechanisms and mitigation strategies in perspective. *Journal of Rock Mechanics and Geotechnical Engineering* 3(3):250–259.
- Rowell GA [1989]. Microseismic monitoring in coal. In: *Proceedings of the 23rd International Conference on Safety in Mines Research Institutes*, Washington DC, Sept. 11–15. pp. 645-655.
- Rowell GA, Lemons JS [1991]. Microseismic analysis of a mountain bump. In: *Proceedings of the Fifth Conference on Acoustic Emission/Microseismic Activity in Geologic Structures and Materials*. June 11–13. Pennsylvania State University.
- Sen AT, Cesca S, Bischoff M, Meier T, Dahm T [2013]. Automated full moment tensor inversion of coal mining-induced seismicity. *Geophysical Journal International* 195:1,267–1,281.
- Shearer PM [2011]. *Introduction to seismology*. 2nd ed. Cambridge University Press. 396 pp.
- Siskind DE [1983]. Structure response and damage produced by ground vibration from surface mine blasting. U.S. Bureau of Mines Report of Investigations, RI 8507.
- Spottiswoode S [1984]. Source mechanisms of mine tremors at Blyvooruitzicht gold mine. In: Gay NC, Wainwright EH, eds. *Proceedings of the First International Symposium on Rockbursts and Seismicity in Mines*, Johannesburg, South Africa. South African Institute of Mining and Metallurgy, pp. 29–37.
- Spottiswoode S, McGarr A [1975]. Source parameters of tremors in a deep-level gold mine. *Bulletin of the Seismological Society of America*. 65(3):93–112.
- Stein S, Wysession M [2009]. *An introduction to seismology, earthquakes, and earth structure*. John Wiley & Sons, 498 pp.
- Su D, Hasenfus G, Stull L [2014]. Ground control design considerations for reducing longwall-induced stress and seismicity associated with massive sandstone under deep cover. In: *Proceedings of the 33rd International Conference on Ground Control in Mining*, Morgantown WV, pp. 54–62.

- Swanson PL [2001]. Development of an automated PC-network-based seismic monitoring system. In: Rockbursts and Seismicity in Mines, Proceedings of the Fifth Symposium on Rockburst and Mine Seismicity, South African Institute of Mining and Metallurgy. pp. 11–17.
- Swanson P, Stewart C, Koontz W [2008]. Monitoring coal mine seismicity with an automated wireless digital strong-motion network. In: Peng SS, Mark C, Finfinger GL, Tadolini SC, Khair AW, Heasley KA, Luo-Y, eds. Proceedings of the 27th International Conference on Ground Control in Mining. July 29–31. Morgantown, WV.
- Swanson P, Clark C, Richardson J, Martin L, Zahl E, Etter A [2014]. Stress-release seismic source for seismic velocity measurement in mines. American Geophysical Union Fall meeting. San Francisco, CA. Paper S23C-4508.
- Talebi S, Côté M [2005]. Implosional focal mechanisms in a hard-rock mine. In: Potvin Y, Hudyma M, eds. Proceedings of the Sixth International Symposium on Rockbursts and Seismicity in Mines. Perth, Australia. pp. 113–121.
- Uhrig LF, van Melle FA [1955]. Velocity anisotropy in stratified media. *Geophysics* 42:774–779.
- USARRAY [2015]. U.S. Array component of Earthscope. <http://www.usarray.org/ceusn>.
- USGS [2016]. Earthquake magnitude policy (implemented on January 18, 2002). http://earthquake.usgs.gov/aboutus/docs/020204mag_policy.php.
- van Aswegen G, Butler AG [1993]. Applications of quantitative seismology in South African gold mines. In: Young RP, ed. Proceedings of the Third International Symposium on Rockbursts and Seismicity in Mines. Kingston, Ontario, Canada. pp. 261–266.
- Waldhauser F, Ellsworth WL [2000]. A double-difference earthquake location algorithm: Method and application to the northern Hayward fault, California. *Bulletin of the Seismological Society of America*. 90(6), pp. 1,353–1,368.
- Whyatt J, Varley F [2008]. Catastrophic failures of underground evaporite mines. In: Peng SS, ed. Proceedings of the 27th International Conference on Ground Control in Mining. Morgantown, WV, pp. 29–31.
- Williams DJ, Arabasz WJ [1989]. Mining-related and tectonic seismicity in the East Mountain Area Wasatch Plateau, Utah, U.S.A. *Pure and Applied Geophysics* 129(1):345–368.
- Wilson PE, Lemons JS [1992]. Continuous microseismic monitoring in a deep longwall coal mine. In: Proceedings of the Fourth Conference on Ground Control for Midwestern U.S. Coal Mines. Mt. Vernon, IL, pp. 227–133.
- Wong IG, Humphrey JR, Adams JA, Silva WJ [1989]. Observations of mine seismicity in the Eastern Wasatch Plateau, Utah, U.S.A.: A possible case of implosional failure. *Pure and Applied Geophysics* 129:369–405.

Appendix A: Wave Propagation Medium Effects

Seismic rays, or raypaths, describe trajectories of seismic waves that are similar to light rays in optics. The geometrical construct of a raypath arrow that is perpendicular to and pointing in the direction of the moving wavefront provides a mathematical simplification, allowing ready solutions for many problems in seismology. In the context of geometric ray theory, this appendix explores several complications related to waveform interaction with common elements of coal mine geology, and discusses strategies that can partially account for geological deviations from simple velocity models.

Layer-specific Properties

The sudden variation in elastic properties across sedimentary layers results in raypaths that are not straight but are reflected, refracted, and mode converted. Seismic energy can also get trapped in low-velocity layers such as coal seams. Refracted rays are deflected at boundaries between layers with different seismic velocities, V_i , according to Snell's law (Figure A1). The general trend is for seismic velocities to increase with depth. Critically refracted rays produce head waves that travel along the interface between layers where there is a sudden increase in seismic velocity. Ultimately, these waves, travelling at the velocity of the faster layer, propagate upward on a refracted wavepath that leads to the surface. At a certain distance from the source, the refracted waves arrive ahead of the slower direct wave.

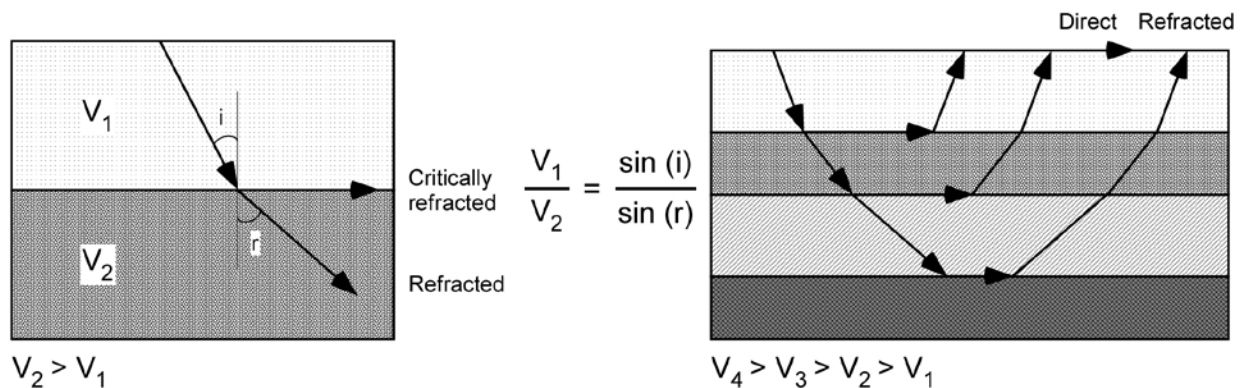


Figure A1. Snell's law governing seismic wave refraction in layered media.

In order to use the arrival times of the first arriving phase to locate events, one must be able to reconstruct the path that the seismic energy traveled. This is only possible with a realistic model of the seismic velocity structure. Locating events in a hardrock mine with a uniform seismic velocity and, consequently, straight raypaths is quite simple by comparison.

Wave reflections at interface boundaries are governed by the mismatch in the acoustic impedance (velocity times density, $V^*\rho$) of the layers comprising the boundary. Amplitudes of reflections increase with higher contrasts in the bounding layers' acoustic impedance (Figure A2). The combination of coal's low velocity and low density gives it a low impedance and large contrast (up to a factor of ~ 4) with contacting layers. This produces an environment where

seismic energy can undergo complete internal reflection at each boundary of the coal seam, which essentially traps the energy within the seam [Dresen and Rüter 1994]. Large contrasts in acoustic impedance can also cause mode conversion—the conversion of one seismic phase into another [Stein and Wysession 2009]. For example, in addition to reflected and refracted P-waves, a P-wave incident on a high-impedance contrast boundary partially converts to reflected and refracted S-phases (Figure A3). Similar mode conversions occur with incident shear waves.

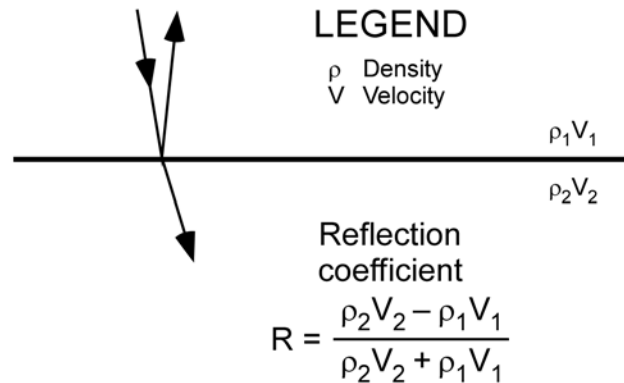


Figure A2. Reflection at layer boundaries controlled by acoustic impedance.

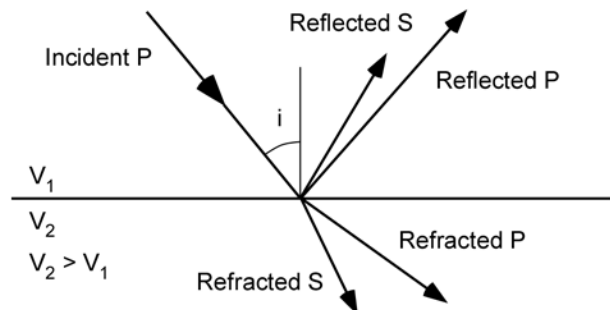


Figure A3. Conversion of incident P-wave into reflected P- and S-waves in the upper layer and refracted P- and S-waves in the lower layer.

As noted by King [2005], processing algorithms used in hardrock mines for source parameter inversion are often not directly applicable to the coal environment. The presence of strong reflections from coal seams, near-field effects, and anisotropy needs to be taken into account in order to be able to determine accurate source parameters of seismic events.

In addition to the P and S body waves, surface waves are generated when body waves interact with a free surface. Surface waves have large amplitudes, propagate with speeds slightly less than shear waves, and are dispersive—meaning that waves travel at a speed dependent upon the wave frequency.

Waveform Character

The complexities associated with wave propagation through stratified layers can significantly influence the waveform character in comparison to many hardrock mines where propagation conditions are more uniform and isotropic. As an example, waveforms generated by a M2.9 coal bump and observed at distances ranging from 0.5 to 16.9 km (0.3 to 10.5 mi) are shown in Figure A4. The surface sensors were vertical 1-Hz seismometers. As the distance between source and receiver grows, there is an increasing number of distinct paths of variable lengths that waves can travel to reach the receiver; the varied travel times along the paths is one reason why the signal duration increases with distance traveled. Another factor is the existence of multiple wave types (P, S, surface waves, trapped modes, etc.) that travel at different speeds, so they arrive increasingly separated in time at farther distances.

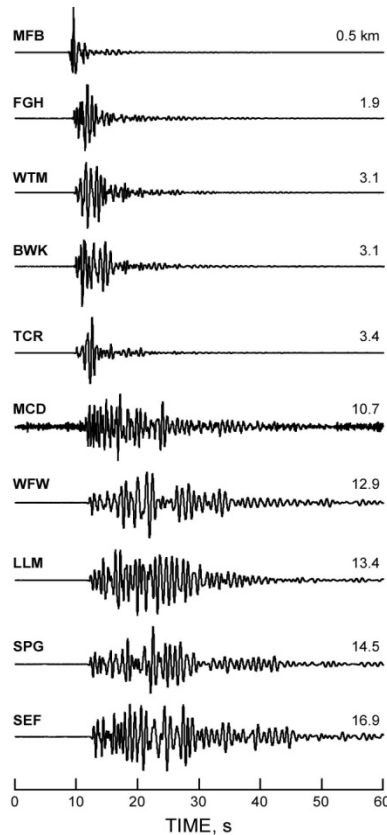


Figure A4. Effect of propagation path on waveform character as observed at ten seismic stations at increasing distance.

The impact of near-surface layers on waveform character becomes more evident when contrasted with signals spending a shorter amount of time in the near-surface layers. Signatures from two different events with similar magnitudes and total propagation distances, but different paths, are compared in Figure A5. The traces are three-component acceleration waveforms (vertical, north, and east) recorded at one station for both a mining-related event and a natural earthquake (after [Swanson et al. 2008]). By comparing signals at the same seismic station, the influences of differing instrument characteristics and local site conditions are eliminated. The upper three traces were produced by a magnitude 2.2 nondamaging event in the vicinity of an

active longwall under 600 m (2,000 ft) of cover. The lower three traces, recorded at the same station, were produced by a natural earthquake with magnitude 2.4. The distances between the sources and station for these two events are approximately 14 and 19 km (8.7 and 11.8 mi), respectively.

There are several notable differences in waveform character of the two events in Figure A5. The natural event exhibits a classic earthquake-like signature with abrupt P-wave arrival on the vertical component Z, followed by a sharp S-wave pulse on the horizontal components N and E. The waveform signature of the mining-related event appears quite different. The demarcation of P- and S-phases is not nearly as well defined, and there appear to be several additional phases present, or complexity that is absent in the earthquake seismogram. In addition, the duration of shaking of the mining event appears to be longer despite the slightly smaller magnitude (2.2 versus 2.4), and the frequency content across the entire waveform is lower for the mining event than for the natural earthquake.

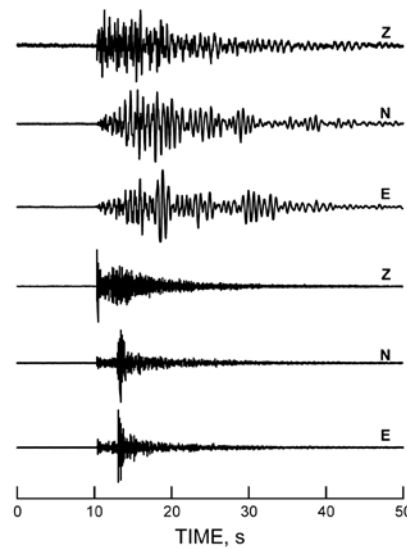


Figure A5. Two sets of three-component seismograms (vertical Z, north N, and east E) recorded on a common station comparing signals generated from a mining-induced event (top) and a natural earthquake (bottom).

The calculated depth of the natural earthquake is approximately 4 km (2.5 mi), whereas the depth of the mining-related event is less than ~1 km (0.6 mi). Consequently, waves from the natural event spent only a small fraction of their propagation time in the complex, attenuating, low-velocity structure of the upper 1 km. Waves from the mining-induced event spent much, if not all, of their propagation time within this near-surface region, largely traveling parallel to the layering. The propagation path effects account for much of the difference in waveform appearance and result in complications when processing the data.

Velocity-model Development

Accurate seismic event locations are not only important in their own right, but they are also the starting point for determination of other seismic source parameters. While a simple homogeneous isotropic velocity model is adequate for routine event locations in the vast

majority of hardrock mines, a layered model is a minimum requirement to capture the first-order velocity characteristics in a coal mine. Calibration blasts are typically used to measure travel times in hardrock mines, and velocities from different stations are averaged with the assumption of straight raypaths. As most U.S. coal mines do not blast as part of day-to-day operations, calibration blasts are not always possible, and when they are, the propagation distances achieved with a few sticks of powder are not sufficient to deliver adequate signals across the larger-sized arrays in attenuating coal measure rocks.

In the case of a district-wide network with propagation distances exceeding 10 km (6.3 mi), the fastest raypaths between source and receiver are refracted waves that travel via the faster deeper layers. For the deeper layers, it is necessary to seek out seismic velocity models that have been developed for regional seismic networks or for other geophysical efforts. These models can serve as a base model for the lower layers, and then upper layers can be estimated on the basis of any borehole sonic logs available from local exploration work and/or knowledge of strata properties. Unfortunately, exploration geophysics efforts often concentrate only in the vicinity of the coal seam or seams, so sonic logs are not always available to characterize the velocity structure between the seam or seams and the surface.

An example sonic log collected from a borehole penetrating just below a coal seam at 500 m (1,600 ft) depth is shown in Figure A6. Seismic velocities are calculated from measurements of the travel time along the borehole wall between points on the sonic probe spaced 60 cm (24 in) apart. An attempt is then made to fit a suitable number of layers with variable widths to the data as an estimation for a velocity model. Where available, information on geologic structures may help constrain the model layers. Geologic information may also provide a starting point for the model in the absence of any sonic logs or direct measurements. Results from multiple boreholes provide a sense of spatial variation in seismic velocity. Sonic logs from two boreholes offset by 900 m (3,000 ft) are shown in Figure A7. There can be significant uncertainty in assigning layer position, thickness, and velocity values to the entire mining region when large variability exists.

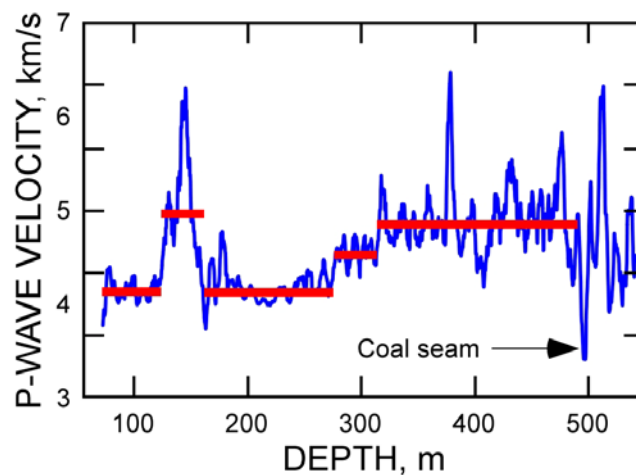


Figure A6. Sonic log in strata above the coal seam with model velocity values and layer thicknesses assigned to individual layers (red horizontal bars).

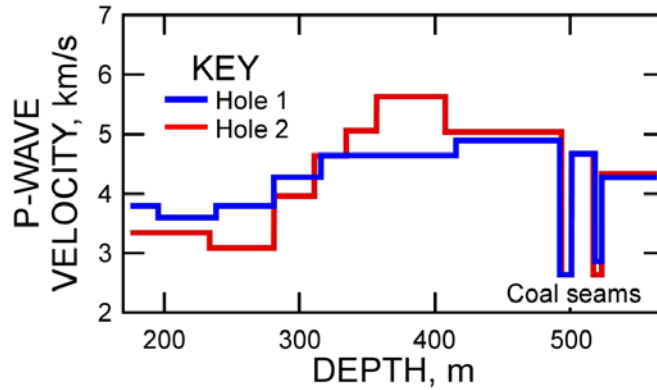


Figure A7. Comparison of velocity structures in two nearby boreholes.

In addition, layered media often have anisotropic mechanical properties. Field measurements indicate that wave speeds can be as much as 20%–40% higher in the horizontal than vertical direction [Uhrig and van Melle 1955]. Accounting for such anisotropy in velocity models improves event locations in sedimentary environments (e.g. [King and Talebi 2007]).

Another effect on seismic velocity that is relevant to certain coal mining districts is variation in overburden thickness. Calibration blasts were used in one deep western coal mine to place constraint on the seismic velocity in the layers immediately above the coal seam (Figure A8). Blasts were performed at the edges of the panel near both gateroads and mains containing roof-mounted geophones. While the geology of near-seam strata was nominally the same in each location, a repeatable systematic variation in velocity was found to be associated with depth of cover. An increase of P-wave velocity of approximately 10% was found as depth of cover varied from 300 to 750 m (1,000 to 2,500 ft). Assuming a density of $2,500 \text{ kg/m}^3$, the pressure increases from 7.4 MPa to 18.4 MPa. Similar velocity changes and greater are often observed in laboratory measurements under similar pressure conditions (e.g. [King 1966; Bourbié et al. 1987]). Overburden stress thus represents another factor contributing to systematic variations in local seismic velocity structure. Although pressure certainly affects P-velocity measurements, the magnitude of the effect observed in Figure A8 is less than the variation observed in sonic logs from one hole to another within a similar span of distance (Figure A7). Nonetheless, it is a source of variability, especially for near-surface sedimentary rocks in canyon-mesa terrain. Additionally, fluids, such as ground water, affect P-wave velocity significantly (e.g. [Gregory 1976]), especially at the (comparatively) low confining conditions of underground coal environments. Seasonal ground water fluctuations can also impose a potentially time-variable influence on the velocity structure.

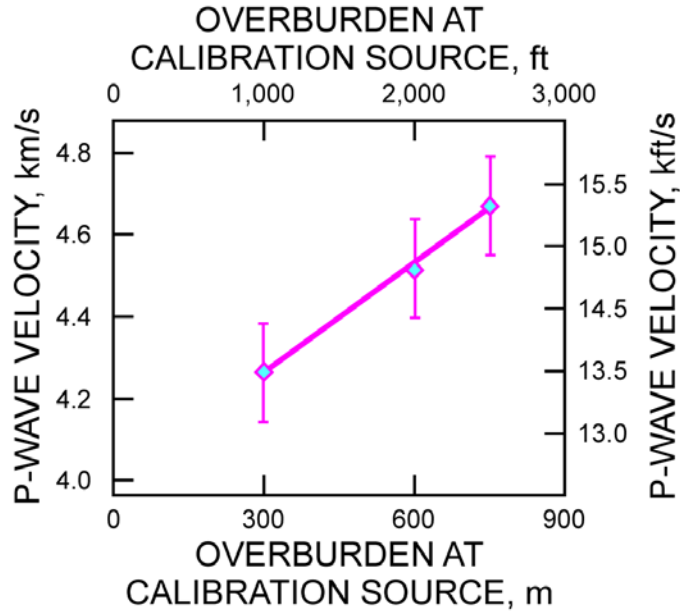


Figure A8. Variation of P-wave velocity with overburden.

An initial model of the seismic velocity structure is constructed on the basis of undisturbed geologic layers. Once excavation proceeds, especially where large rock volumes are perturbed with subsidence attending full-extraction mining, changes in seismic velocity occur. The effect of neglecting systematic discrepancies between actual and modeled velocities is illustrated by considering raypaths traversing a low-velocity zone such as a longwall gob area. As mentioned in reference to the systematic event mislocations observed in Figure 33, such offsets are commonly observed in close-in network data with mislocations generally occurring in a direction away from regions of low velocity. This effect arises because travel times are slower through the gob than are assumed with a uniform isotropic velocity model. A simple graphical depiction of travel-time vectors in Figure A9 illustrates the principle. In frame A, travel-time vectors emanating from two seismometers (red triangles) have lengths that connect with the actual source location (circle symbol) when the seismic velocity is known and uniform (i.e., the longwall panel has not yet been mined). In frame B, a modest 10% reduction in seismic velocity is imposed upon the extracted longwall panel to simulate the effect of mining, resulting in travel times that are 10% longer than in the unmined panel. Travel-time vectors, as shown, no longer meet at the actual event location. Frame C shows the resultant change of the position where travel-time observations from both sensors can be satisfied simultaneously. This is the effect of event mislocation that can happen when raypaths encounter a low-velocity zone that is not incorporated into the seismic velocity model used in the location calculations. The magnitude and direction of the event mislocation depends strongly upon the position(s) of the low-velocity zones with respect to the raypaths that participate in the solution [Boltz et al. 2016].

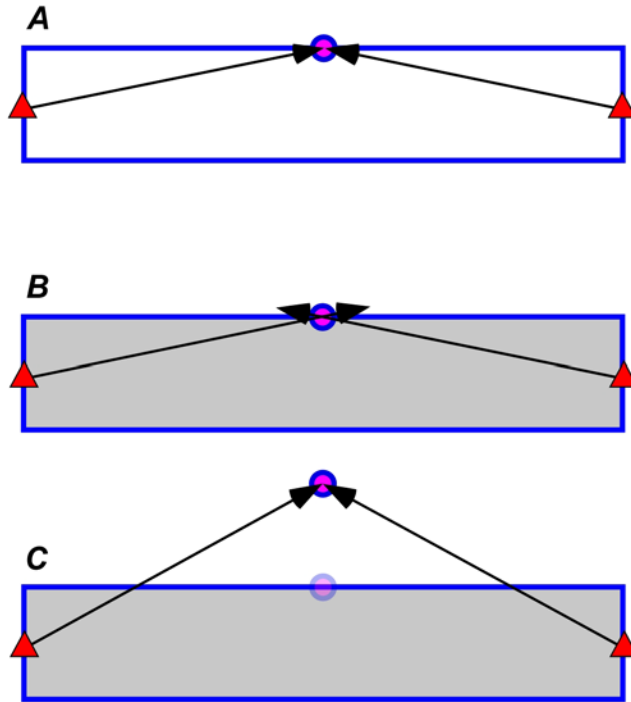


Figure A9. Shift in calculated event locations when seismic velocity model fails to match actual velocity. Frame A shows raypath lengths calculated for an unmined coal panel with known seismic velocity. Frame B shows the effect of a modest 10% reduction in seismic velocity. Frame C shows the resultant change of the calculated event location where travel-time observations from both sensors can be satisfied simultaneously.

Appendix B: Seismic Source Characteristics Derived from Waveform Measurements

Waveform Measurements

Analysis of emitted seismic waves allows certain characteristics of the source to be estimated. Measurements made on seismic waveforms that have been corrected for the influences of the propagation medium, geometric spreading, and instrument response allow determination of seismic moment, M_o , corner frequency f_c , and radiated seismic energy, E_s . From these basic measurements other source parameters can be derived: rupture area A , source dimension r , stress drop, $\Delta\sigma$, apparent stress, σ_a , averaged shear slip, \bar{d} , apparent volume, V_a , energy index, EI , etc. [e.g., Gibowicz and Kijko 1994].

In the frequency domain, M_o can be obtained from the wave displacement amplitude at the low-frequency limit, Ω_o , and r is inversely proportional to the corner frequency, f_c . f_c marks the point of departure of the amplitude spectrum from the flat low-frequency limit to smaller values at higher frequencies (Figure B1).

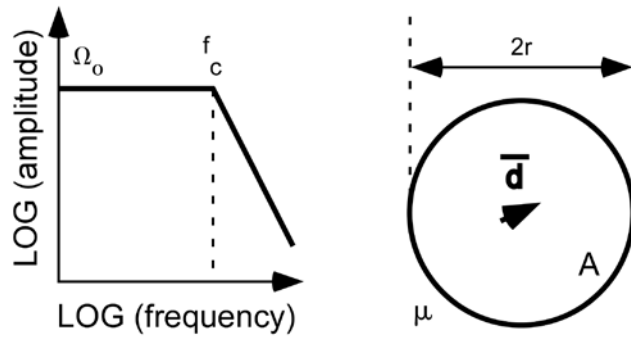


**Figure B1. Theoretical displacement amplitude spectrum (graph on left)
for shear slip on circular crack (illustration on right).**

Seismic wave energy, E_s , is computed by integrating the square of the particle velocity measured in the far field over all frequencies and incidence angles.

Source Parameters

In this section, seismic moment and the other source parameters are defined. Seismic moment is defined as follows:

$$M_o = \mu A \bar{d} \tag{B1}$$

where μ is the shear modulus of the source rocks, A is rupture area, and \bar{d} is the averaged shear displacement across the rupture surface (Figure B1).

Moment magnitude is based on the logarithm of the seismic moment [Hanks and Kanamori 1979] with moment specified in units of dyne cm.

$$M = (\log M_o)/1.5 - 10.7 \quad (\text{B2})$$

The characteristic source dimension,

$$r \sim 1/f_c \quad (\text{B3})$$

is inversely proportional to the corner frequency, f_c , (for P- and/or S-waves).

Values of stress drop, $\Delta\sigma$, are calculated for specific geometrical rupture models. For a circular crack model [Brune 1970] of radius r :

$$\Delta\sigma = (7/16)*M_o/r^3 \sim M_o(f_c)^3 \quad (\text{B4})$$

A more model-independent measure of stress is given by the apparent stress,

$$\sigma_a = \eta\bar{\sigma} = \eta(\sigma_f + \sigma_i)/2 = \mu(E_s/M_o) \quad (\text{B5})$$

where $\bar{\sigma}$ is the mean stress acting during the dynamic stress drop, σ_i and σ_f are the initial and final static stresses in the source zone, respectively, η is the seismic efficiency (< 10%), and E_s is the radiated seismic energy.

This last equation indicates the direct relation between stress in the source region and radiated energy. Examining how the ratio of E_s/M_o varies throughout the rock mass for events with similar moments gives a probe of the local stresses acting in the vicinity of those events [e.g., Mendecki et al. 1999]. In other words, if a map is created of the locations of events with similar moments and the event symbol is scaled according to radiated energy, then this map is equivalent to a map showing the relative values of stress. Areas of high radiated energies are associated with areas of high stress.

Apparent volume,

$$V_a = M_o/2\sigma_a = (M_o)^2/2\mu E_s \quad (\text{B6})$$

is a measure of the rock volume undergoing dynamic inelastic strain [Mendecki 1993].

Energy index is a ratio that identifies how energetic a particular event is, given that radiated energy for a set moment has been observed to range over a factor of 1,000 [van Aswegen and Butler 1993]. The energy index is given by:

$$EI = E(M_o)/E(M_o)_{ave} \quad (\text{B7})$$

where the radiated seismic energy measured for one event $E(M_o)$ is normalized to the energy expected for an average event of the same moment $E(M_o)_{ave}$. $E(M_o)_{ave}$ is the value of energy expected for an event of moment M_o on the basis of a fit to $\log E_s$ versus $\log M_o$ of all events in the region of evaluation. Values of energy index greater than and less than 1 indicate, respectively, higher or lower values of energy radiated than the average for that value of moment.

Energy Index and Cumulative Apparent Volume Plots

A short- to medium-term hazard assessment method used in some hardrock mines involves plotting the time histories of the energy index and cumulative apparent volume. Field data has been presented to suggest that when a mine or geologic structure is taking on increased loads, the energy index for events starts to increase, meaning that events are getting more energetic than they were previously. After such a structure starts to fail, or soften, the average radiated energy drops, putting the energy index below 1. Similarly, a plot of cumulative apparent volume [Minney et al. 1997] reflects the volume of inelastic strain, or relaxation, in the source region. Plotting the cumulative volume allows one to discern changes in the rate of volume changes from the slope of the curve. A number of examples in the literature [Lynch and Mendecki 2001] suggest that, in certain cases, the energy index drops and the cumulative apparent volume rises in advance of larger seismic events.

Seismic Moment Tensor

The source parameters presented above describe a simple two-dimensional, shear-slip source, also known as a double-couple source, which involves no volume change. This can be shown to be a special case of a more general moment tensor description of a seismic source that includes volumetric components [Gibowicz and Kijko 1994]. Implosional components are often needed to describe the closure of mine openings that attend mining-induced seismic events [Fletcher and McGarr 2005]. The procedure for extracting the full moment tensor requires clean, high-quality seismic waveforms and is not generally as well-suited to software-automated processing as are some of the other source parameters, although progress is apparently being made in this area [Sen et al. 2013].

Seismic Magnitudes, Moments, and Energies

As a way to attach physical significance to seismic events of different magnitudes, the seismic energy radiated from events of a given magnitude/moment is converted to the change in the potential energy of falling objects in Table B1 below. Self-similar earthquake energy scaling is assumed. In this manner the difference, for example, between a magnitude 0 and -2 event can be placed into context. For clarification, the energy associated with the falling objects would not produce a seismic event of the given magnitude. It merely represents the amount of radiated seismic energy for an event of that magnitude. The radiated energy is only a small fraction of the total energy associated with earthquake sources [e.g., Fletcher and McGarr 2005] with estimates ranging from less than 1% to 10%. Ranges of rupture dimensions and fault slip, for stress drops ranging from 0.1 to 10 MPa, are also given in Table B1 for comparison.

Table B1. Relations between seismic magnitude, moment, radiated energy, rupture dimension, and potential energy equivalent

Moment magnitude	Seismic moment (J)	Seismic energy	Rupture dimension	Amount of slip	Potential energy equivalent to seismic energy
6	1.1×10^{18}	63 TJ	20–80 km	0.05–1 m	
5	3.5×10^{16}	2 TJ	2–10 km		
4	1.1×10^{15}	63 GJ	0.7–4 km	0.5–10 cm	
3	3.5×10^{13}	2 GJ	0.2–1 km		
2	1.1×10^{12}	63 MJ	70–300 m	0.05–1 cm	1-m-thick football field size chunk of coal falling 1.6 m
1	3.5×10^{10}	2 MJ	20–100 m		D9 dozer falling 4.5 m
0	1.1×10^9	63 kJ	7–30 m	0.05–1 mm	4x4 pickup falling 3 m
-1	3.5×10^7	2 kJ	2–10 m		100-kg person falling 2 m
-2	1.1×10^6	63 J	0.8–4 m	5–100 mm	six pack of soda falling 3 m
-3	3.5×10^4	2 J	0.2–1 m		1 can of soda falling 0.5 m
-4	1.1×10^3	0.06 J	0.08–0.4 m	0.5–10 mm	1 penny falling 2.5 m

Appendix C: Single-Station Monitoring Implementation Options

As implementing a single-station monitoring strategy is often a prudent step before moving to more complicated strategies, a number of options are discussed in this appendix. The first option is especially tailored as a do-it-yourself project for individuals without direct experience in seismology and is described in some detail here.

Low-cost hardware and software are available through the Public Seismic Network (PSN). PSN develops hardware and software to facilitate the recording of earthquakes for the worldwide amateur seismology community. Two basic data acquisition platforms are available. The 4-channel, strong-motion accelerometer unit has a built-in three-component accelerometer and provision for using an optional 4.5-Hz or 1-Hz geophone for the fourth channel. The second 4-channel digitizing board is oriented toward seismometers but does not come with any sensors. New and used geophones are often available through PSN. In both data acquisition units, the maximum sample rate is 200 samples per second (i.e., suitable for far-field awareness monitoring in district- and mine-wide scale use), there is a choice between a USB or RS-232 interface, there is an option for GPS timing, and the data can be streamed into an Earthworm monitoring system.

The WinSDR software for instrument configuration and data acquisition comes with the hardware (and is capable of running on Raspberry Pi in order to stream data to Earthworm). The WinQuake software is the free Windows software package for displaying and manipulating the waveform data from the hardware with provision for picking phase arrivals, filtering, calculating spectra, and outputting time series data into a few different formats. Additionally, for the more advanced users, there is a popular open-source python package called ObsPy [Megies et al. 2011] which is a very powerful tool for performing data processing and visualization tasks.

The following are possible hardware and software options for implementing a single-station approach:

- PSN hardware and software (<http://psn.quake.net/>)
- Swarm—open-source software allowing virtual seismometers to produce desktop helicorder records from on-line local/regional stations (<http://volcanoes.usgs.gov/software/swarm/index.php>)
- Earthworm open-source software with Earthworm-compatible hardware (<http://www.earthwormcentral.org/>)
- Microseismic system vendors
- Blast vibration monitor equipment
- Broadband seismometer (commercial sources with hardware-specific software)

Appendix D: Station Corrections and Multi-event Location Techniques

Travel-time Station Corrections

Event location errors are produced by both random and systematic factors. Random errors are associated with slight mispicks of arrival times and errors in the measurement of station locations. Random variations in the seismic velocity along raypaths to each station, even in a medium well characterized by an isotropic homogeneous velocity model, also contribute random fluctuations in arrival times. Most estimates of event location error derived from a location calculation assume that these are the sources of error and that they are random, not systematic. Station correction factors and multi-event location techniques are calculational methods to address small systematic errors in the velocity model.

A fundamental error statistic is the travel-time residual, which is the difference between the arrival time predicted by the velocity model and the observed arrival time. Most location algorithms seek to minimize the sum, or the sum of the squares, of the individual stations' travel-time residuals. At a given station, truly random errors should produce travel-time residuals approaching zero when averaging over a large number of events. In practice, when viewing results from locating many events, a trend toward a consistent residual value, either positive or negative, is often observed for each station. This is frequently assumed to be associated with systematic variations of velocity near the stations due to local differences in the weathering of near-surface rocks. A station-correction factor is a fixed travel-time delay, or advance, that is added to the arrival times at each station in order to bring the resulting travel-time residuals closer, on average, to zero. Small travel-time residuals are usually interpreted to mean lower location error, provided a sufficient number of stations were used in the event's location.

If the monitored region encompasses a range of geological and geographical conditions, multiple velocity models can be incorporated into the location algorithm. Alternatively, if the velocity changes are not too major, a different set of station correction factors may be applied when locating events in different regions (e.g., the different mines in Figure 24). In this manner, systematic variations in the seismic velocity that are not accounted for in the model can be ameliorated somewhat by applying these station-correction factors, producing event locations relative to those events used to determine the corrections. An example of how a station-correction factor can mitigate the impact of a systematic error in velocity is shown in Figure D1.

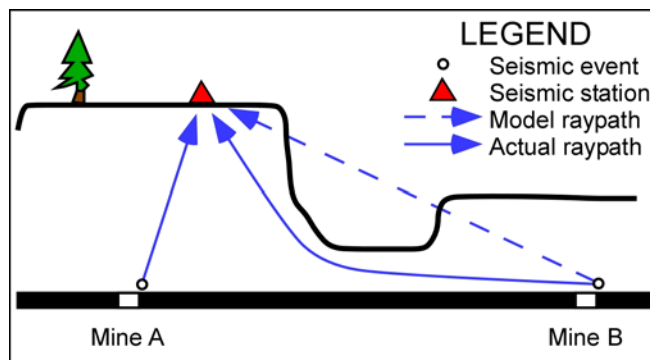


Figure D1. Velocity model errors partially compensated by travel-time station correction factors. Raypaths from mine B are affected by topographic features unaccounted for in the velocity model.

One station in a network of stations is shown in the vicinity of two mines in Figure D1. Raypaths from seismic events generated in the mine on the left travel directly, or straight, to the surface station above. For purposes of illustration, it is assumed that the velocity is constant between the coal seam and the surface. For an event occurring in the vicinity of Mine B, the location procedure, with its homogeneous isotropic velocity model, calculates the travel time as if there were no mesa-canyon topography present as indicated by the straight dashed-line raypath. The actual, longer raypath takes more time than that assumed by the model. As a result, all event locations at Mine B are biased by this systematic deviation from the assumed velocity model. Applying a station correction factor, equal to the average residual value, which compensates for the additional travel time effectively, but only partially, counteracts the systematic error in the velocity model. A more accurate model would be a heterogeneous, three-dimensional model, with a P-wave velocity of the speed of sound in air in the canyon.

Since many deep coal mines occur under steep rugged terrain, situations like that depicted in Figure D1 can be expected at various positions throughout the extensive underground workings of a single mine. Thus, when there is a particular area experiencing a notable event or sequence of activity in an area that fails to match the assumed velocity model, (e.g., at the edge of a steep side of a canyon in Figure D1), systematic shifts in event locations will occur. Developing a new set of station-correction factors for this particular region and this set of events is one way of forcing the systematically mislocated events back into an area of known activity without having to deal with the complexity of a three-dimensional heterogeneous model.

Multi-event Location Techniques

Master-event location techniques [Gibowicz and Kijko 1994] and double-difference techniques [Waldhauser and Ellsworth 2000] provide a way of achieving event locations that are accurate relative to the locations of other events. These techniques work by cancelling out the effect of spatial variation in velocity along raypaths to a given station and require that all of the events that are being located share a largely common path between the source region and each sensor. In these methods, travel-time residuals between pairs of events are minimized while linking together all other event-station pairs. This only works effectively for certain geometrical configurations of stations and events, specifically when the distance between pairs of events is small relative to both the distance to the stations and the spatial variations in velocity. Figure D2 shows two identical 6-station networks with two different distributions of activity. In the left-hand side of the figure, raypaths from all of the events back to each of the stations share common paths where the unknown deviations from the velocity model are the same. In this geometrical configuration, the double-difference location technique cancels out the deviations of the velocity model from the actual velocity structure along each raypath [Waldhauser and Ellsworth 2000]. The result is a tight clustering of event locations that is often obscured without such processing. The absolute location of the cluster, however, is still subject to systematic errors resulting from inadequacies of the velocity model.

With the distribution of activity in the network on the right-hand side of Figure D2, the range of azimuths at all of the stations is far greater than in the left-hand side. As the raypaths to the stations are not the same for all of the events throughout the mine, the double-differencing strategy does not work for the area of activity as a whole. Use of the double-difference technique in this situation is limited to those sub-volumes producing similar raypaths back to the stations.

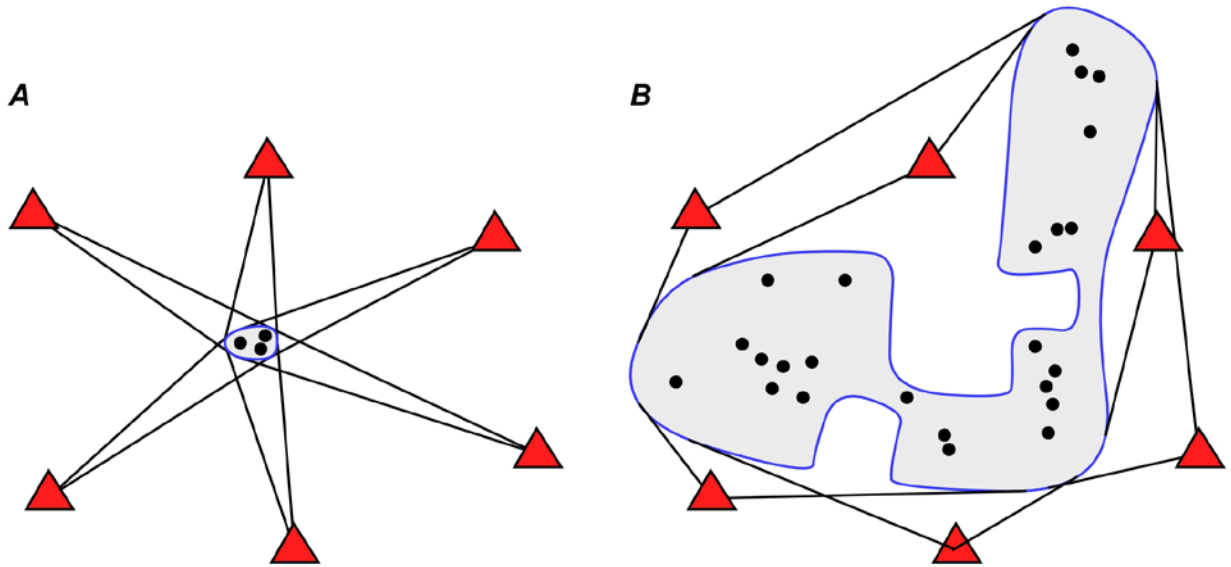


Figure D2. Raypaths between stations (red triangles) and event clusters (black dots) affect suitability of double-difference location scheme. (a) suitable array configuration, (b) unsuitable array configuration.

Thus, this technique is better suited to improving relative locations when the area of activity is small and unchanging in comparison to the scale of the array. Its application to a microseismic-scale network, as in the network on the right, is not as straightforward. Although it could be used to tighten up multiple clusters of activity—e.g., activity associated within limited portions of the longwall face, headgate, and tailgate—the positions of clusters relative to each other will still exhibit systematic mislocations. A calibration event would be needed to anchor the calculated location of each cluster group. Master-event location techniques work by examining differences in arrival times for pairs of events where one of the events is a calibration blast or other event of known location.

Boltz et al. [2014] used double differencing to account for the temporal-spatial variations in the velocity as a result of the gob formation as mining advanced in a single longwall panel. Prior to applying the double-difference technique, the depths of the events migrated toward the surface and located above the topography at the end of the panel in an unrealistic pattern. Tightly linking the events pulled the resulting event depths down to where they followed the approximate dip of the coal seam.

Glossary of Seismic Terms

Acceleration. The second derivative of displacement and common measure of ground motion.

Acoustic impedance. A property that describes the opposition of a material to acoustic wave transmission, which is determined by multiplying the density of the material and the velocity of the wave traveling through the material.

Apparent stress. A failure-model-independent estimate of the average stress state around a seismic source region.

Apparent volume. The volume of the failed rock mass near the source of a seismic event.

Arrival time. The time at which seismic energy of an event reaches a station.

Attenuation. The decrease in seismic energy intensity observed over time and distance.

Averaged shear slip. The particle displacement averaged over a fault-slip failure area.

Back azimuth. The angle from north to a line originating at a station and terminating at a seismic event.

Body waves. The elastic energy radiated from a seismic event that does not require a free-surface to persist (i.e., travels through the interior of the earth). Consists of P-waves (pressure) and S-waves (shear).

Broadband seismometer. An instrument for recording seismic events that is able to adequately record a wide range of frequencies (e.g., 1/30 Hz to 100 Hz).

Coda-wave magnitude. A magnitude scale based on the duration of an event waveform. Larger events tend to produce longer duration waveforms for a given source-receiver distance.

Corner frequency. The frequency (in Hz) at which the spectra amplitudes of an observed waveform begin to drop off.

Critically refracted wave. A raypath with an incidence angle to a material boundary that will cause the wave to travel, as a head wave, along the boundary and eventually reflect to the surface.

Direct wave. The energy that travels from the seismic source to the receiver without reflection.

Displacement amplitude spectrum. Amplitudes as a function of frequency for seismic waveforms recorded as, or transformed to, displacement.

District-wide network. A seismic network which monitors a group of mines (a district).

Double-difference location method. A multi-event relocation method that locates events relative to other events based on the differences in their travel times.

Energy index. The ratio of radiated seismic energy for a given event over the average radiated energy for events of comparable seismic moments.

Exploration seismic array. The typical instrumentation used for reflection and/or refraction surveys, which consists of several geophones connected via cables to an acquisition system that are deployed on a temporary basis.

Frequency range. The range of frequencies that are best recorded by a given seismic instrument.

Geophone. A common instrument for measuring ground motion (in velocity).

Head wave. Raypath that travels along the interface between two materials at the speed of the material with the faster seismic velocity.

Helicorder record. A plot of continuous data recorded by a single seismic instrument, which usually shows multiple hours of data.

Hodogram. A two- or three-dimensional plot of ground motion over time.

Homogeneous isotropic velocity model. A seismic velocity model characterizing the velocity as a single value that does not vary based on the propagation direction of the seismic energy.

Incidence angle. Angle between a raypath and a direction perpendicular to the material into which the seismic energy is being transmitted.

Induced seismic event. A seismic event that is caused by human activity.

Local magnitude. A magnitude scale based on the amplitude of seismic energy at a station and its distance from the event. A subset of local magnitude is the Richter magnitude, which requires amplitudes to be measured on a real, or simulated, Wood-Anderson seismograph.

Low-pass filter. A filter for attenuating energy above the cutoff frequency.

Magnitude. A measure of the size of a seismic event, which can be based on a number of observed features of the event waveforms. Because there are several magnitude scales, care must be taken when comparing magnitudes calculated by different sources.

Microseismic event. A small, typically induced, seismic event—not to be confused with microseism, which refers to faint earth tremors caused by natural phenomena (e.g., ocean waves).

Microseismic network. A group of seismic instruments designed to record small, typically induced, events originating from a concentrated region. Generally, station density is much smaller than regional networks designed to monitor tectonic earthquakes.

Mine-wide network. A group of seismic instruments monitoring seismic activity at a single mine.

Mode conversion. A waveform phenomena wherein seismic energy is converted from one phase to another (e.g., P-waves to S-waves on a material boundary).

Moment magnitude. The generally preferred magnitude scale based on seismic moment, which relates to physical properties of the seismic source.

Particle-motion diagram. See Hodogram.

Particle velocity. The velocity (or speed) of a single particle in a media.

Polarization. The direction of a wave's oscillation with respect to the wave's direction of propagation.

P-wave. Pressure or compressional wave. Particle motion occurs in a direction parallel to the direction of wave propagation. Typically, the first phase that is observed in a waveform for a seismic event.

Radiated seismic energy. The seismic energy released by an event. Radiated seismic energy only accounts for a small amount of the total energy released at the event source region (< 10%).

Raypath. The physical path taken by seismic energy traveling from the source to the receiver.

Reflection. A change of propagation direction for a raypath upon reaching a material boundary such that it returns to the material from which it originated.

Reflection coefficient. The ratio of the amplitudes of a reflected and an incident wave.

Refraction. A change of propagation direction for a raypath as it passes through a material boundary into a material with a different acoustic impedance.

Rockburst. A seismic event that causes damage to active mine workings.

Rupture area. The failed area at the source of a seismic event, often idealized with simple geometries.

Seismic efficiency. The percentage of energy released by a seismic event that is radiated by seismic waves.

Seismic event. A dynamic failure that radiates seismic energy.

Seismic moment. A quantity used to measure the size of an earthquake.

Seismic network. A group of instruments used to record ground motion induced by seismic events.

Seismic phase. A characterization of seismic energy based on particle motion and raypath.

Seismic velocity. A material property that describes the speed at which seismic energy travels through the material.

Seismometer. An instrument for recording ground motion caused by seismic events.

Short-period seismometer. A seismic instrument designed to record high-frequency energy (e.g., 1 to 100 Hz).

Signal-to-noise ratio. The ratio of the amplitude of a seismic signal to the amplitude of background noise.

Single-station location. A calculated location of a seismic event that is obtained using data from only one station.

Snell's law. The law governing the bending of seismic (and other) waves traveling through material boundaries.

Sonic log. A log detailing the seismic velocity along a borehole perimeter.

Source dimension. The physical dimensions of a seismic source.

S-P time. The arrival time of the first observed S-wave minus the arrival time of the first observed P-wave. Can be used to estimate the source-receiver distance.

Station correction. An empirical correction applied to travel times at a seismic station to help account for un-modeled heterogeneity in the velocity structure.

Stress drop. The decrease in stress experienced around a seismic source region after an event occurs.

Strong-motion seismometer. A seismic instrument designed to record high-amplitude ground motions without exceeding the instrument's dynamic range.

Surface waves. Seismic waves that require a free surface to exist.

S-wave. Shear wave. Particle motion occurs in a direction perpendicular to the direction of wave propagation. Arrives at a station after the P-wave.

Travel time. The time required for seismic energy to travel from the source to a receiver.

Triaxial sensor. Seismic instrument with three perpendicular sensors that record ground motion. The sensors are often oriented in the vertical, north-south, and east-west directions.

Uniaxial sensor. Seismic instrument with a single sensor that records ground motion in a single direction.



*Delivering on the Nation's promise:
safety and health at work for all people
through research and prevention*

To receive NIOSH documents or more information about occupational safety and health topics, please contact NIOSH: :

Telephone: 1-800-CDC-INFO

TTY: 1-888-232-6348

CDC INFO: www.cdc.gov/info

or visit the NIOSH Web site at **www.cdc.gov/niosh**

For a monthly update on news at NIOSH, subscribe to NIOSH eNews by visiting **www.cdc.gov/niosh/eNews..**

DHHS (NIOSH) Publication No. 2017-102

SAFER • HEALTHIER • PEOPLE™